

Proteomic analysis reveals distinct cerebrospinal fluid signatures across genetic frontotemporal dementia subtypes

Authors: Aitana Sogorb-Esteve^{1,2*}, Sophia Weiner^{3*}, Joel Simrén^{3*}, Imogen J Swift^{1,2}, Martina Bocchetta^{2,4}, Emily G. Todd², David M. Cash^{1,2}, Arabella Bouzigues², Lucy L. Russell², Phoebe H. Foster², Eve Ferry-Bolder², John C. van Swieten⁵, Lize C. Jiskoot⁵, Harro Seelaar⁵, Raquel Sanchez-Valle⁶, Robert Laforce⁷, Caroline Graff^{8,9}, Daniela Galimberti^{10,11}, Rik Vandenberghe^{12,13,14}, Alexandre de Mendonça¹⁵, Pietro Tiraboschi¹⁶, Isabel Santana^{17,18}, Alexander Gerhard^{19,20}, Johannes Levin^{21,22,23}, Sandro Sorbi^{24,25}, Markus Otto^{26,27}, Florence Pasquier^{28,29,30}, Simon Ducharme^{31,32}, Chris R. Butler^{33,34}, Isabelle Le Ber^{35,36,37}, Elizabeth Finger³⁸, Maria Carmela Tartaglia³⁹, Mario Masellis⁴⁰, James B. Rowe⁴¹, Matthias Synofzik^{42,43}, Fermin Moreno^{44,45}, Barbara Borroni^{46,47}, GENFI consortium, Kaj Blennow^{3,48,49,50}, Henrik Zetterberg^{1,3,48,51,52,53*}, Jonathan D. Rohrer^{2*}, Johan Gobom^{3,48*}.

*The authors have contributed equally to the work.

[†]Consortium author list shown in Appendix

Affiliations:

¹UK Dementia Research Institute at University College London; WC1N 3BG, London, UK

²Dementia Research Centre, UCL Queen Square Institute of Neurology, University College London; WC1N 3BG, London, UK

³Department of Psychiatry and Neurochemistry, Institute of Neuroscience and Physiology, the Sahlgrenska Academy at the University of Gothenburg; 431 39, Mölndal, Sweden

⁴Centre for Cognitive and Clinical Neuroscience, Division of Psychology, Department of Life Sciences, College of Health, Medicine and Life Sciences, Brunel University, UB8 3PH, London, UK

⁵Department of Neurology, Erasmus Medical Centre; 3015 GD, Rotterdam, Netherlands

⁶Alzheimer's disease and Other Cognitive Disorders Unit, Neurology Service, Hospital Clínic, Institut d'Investigacions Biomèdiques August Pi I Sunyer, University of Barcelona; 08036, Barcelona, Spain

⁷Clinique Interdisciplinaire de Mémoire, Département des Sciences Neurologiques, CHU de Québec, and Faculté de Médecine, Université Laval; G1V 0A6, Québec, QC, Canada

⁸Center for Alzheimer Research, Division of Neurogeriatrics, Department of Neurobiology, Care Sciences and Society, Bioclinicum, Karolinska Institutet; 171 64, Solna, Sweden

⁹Unit for Hereditary Dementias, Theme Aging, Karolinska University Hospital; 171 77, Solna, Sweden

¹⁰Fondazione Ca' Granda, IRCCS Ospedale Policlinico; 20122, Milan, Italy

¹¹University of Milan, Centro Dino Ferrari; 20122, Milan, Italy

37 ¹²Laboratory for Cognitive Neurology, Department of Neurosciences, KU Leuven; 3000, Leuven, Belgium
38 ¹³Neurology Service, University Hospitals Leuven; 3000, Leuven, Belgium
39 ¹⁴Leuven Brain Institute, KU Leuven; 3000, Leuven, Belgium
40 ¹⁵Faculty of Medicine, University of Lisbon; 1649-028, Lisbon, Portugal
41 ¹⁶Fondazione IRCCS Istituto Neurologico Carlo Besta; 20133, Milano, Italy
42 ¹⁷University Hospital of Coimbra (HUC), Neurology Service, Faculty of Medicine, University of Coimbra;
43 3004-531, Coimbra, Portugal
44 ¹⁸Center for Neuroscience and Cell Biology, Faculty of Medicine, University of Coimbra; 3004-531,
45 Coimbra, Portugal
46 ¹⁹Division of Neuroscience and Experimental Psychology, Wolfson Molecular Imaging Centre, University
47 of Manchester; M20 3LJ, Manchester, UK
48 ²⁰Departments of Geriatric Medicine and Nuclear Medicine, University of Duisburg-Essen; 4514,
49 Germany
50 ²¹Department of Neurology, Ludwig-Maximilians Universität München; 80539, Munich, Germany
51 ²²German Center for Neurodegenerative Diseases (DZNE); 81377, Munich, Germany
52 ²³Munich Cluster of Systems Neurology (SyNergy); 81377, Munich, Germany
53 ²⁴Department of Neurofarba, University of Florence; 50139, Florence, Italy
54 ²⁵IRCCS Fondazione Don Carlo Gnocchi; 50143, Florence, Italy
55 ²⁶Department of Neurology, University of Ulm; 89081, Ulm, Germany
56 ²⁷Martin-Luther-University Hospital of Halle-Wittenberg, Department of Neurology, 06120, Halle (Saale),
57 Germany
58 ²⁸University of Lille; 59000 France
59 ²⁹Inserm 1172, Lille; 59000 France
60 ³⁰CHU, CNR-MAJ, Labex Distalz, LiCEND Lille; France
61 ³¹Department of Psychiatry, McGill University Health Centre, McGill University; H4A 3J1, Montreal,
62 Québec, Canada
63 ³²McConnell Brain Imaging Centre, Montreal Neurological Institute, McGill University; H3A 0G4,
64 Montreal, Québec, Canada
65 ³³Nuffield Department of Clinical Neurosciences, Medical Sciences Division, University of Oxford; OX3
66 9DU, Oxford, UK
67 ³⁴Department of Brain Sciences, Imperial College London; W12 0NN, London, UK
68 ³⁵Sorbonne Université, Paris Brain Institute – Institut du Cerveau – ICM, Inserm U1127, CNRS UMR
69 7225, AP-HP - Hôpital Pitié-Salpêtrière; 75013, Paris, France
70 ³⁶Centre de référence des démences rares ou précoces, IM2A, Département de Neurologie, AP-HP -
71 Hôpital Pitié-Salpêtrière; 75013, Paris, France
72 ³⁷Département de Neurologie, AP-HP - Hôpital Pitié-Salpêtrière ; Paris, France
73 ³⁸Department of Clinical Neurological Sciences, University of Western Ontario; N6A 5A5, London, ON,
74 Canada

³⁹Tanz Centre for Research in Neurodegenerative Diseases, University of Toronto; M5S 1A8, Toronto, ON, Canada

⁴⁰Sunnybrook Health Sciences Centre, Sunnybrook Research Institute, University of Toronto; M4N 3M5, Toronto, Canada

⁴¹Department of Clinical Neurosciences, University of Cambridge; CB2 3EB, Cambridge, UK

⁴²Division Translational Genomics of Neurodegenerative Diseases, Hertie-Institute for Clinical Brain Research and Center of Neurology, University of Tübingen; 72076, Tübingen, Germany

⁴³Center for Neurodegenerative Diseases (DZNE); 72076, Tübingen, Germany

⁴⁴Cognitive Disorders Unit, Department of Neurology, Donostia University Hospital; 20014, San Sebastian, Spain

⁴⁵Neuroscience Area, Biodonostia Health Research Institute; 20014, San Sebastian, Gipuzkoa, Spain

⁴⁶Department of Clinical and Experimental Sciences, University of Brescia; 25123, Italy

⁴⁷Department of Continuity of Care and Frialty, ASST Spedali Civili Brescia; 25123, Italy

⁴⁸Clinical Neurochemistry Laboratory, Sahlgrenska University Hospital; SE-43180, Mölndal, Sweden

⁴⁹Institut du Cerveau et de la Moelle épinière (ICM), Pitié-Salpêtrière Hospital, Sorbonne Université, 75013, Paris, France

⁵⁰University of Science and Technology of China and First Affiliated Hospital of USTC, Hefei, Anhui, P.R. China

⁵¹Department of Neurodegenerative Disease, UCL Institute of Neurology, Queen Square; WC1N 3BG, London, UK

⁵²Hong Kong Center for Neurodegenerative Diseases, Clear Water Bay; Hong Kong, China

⁵³Wisconsin Alzheimer's Disease Research Center, University of Wisconsin School of Medicine and Public Health, University of Wisconsin-Madison; 53792, Madison, WI, USA

Corresponding author: Aitana Sogorb-Esteve a.sogorb-estev@ucl.ac.uk

Abstract

We used an untargeted mass spectrometric approach, tandem mass tag (TMT) proteomics, for the identification of proteomic signatures in genetic frontotemporal dementia (FTD). A total of 238 cerebrospinal fluid (CSF) samples from the Genetic FTD Initiative (GENFI) were analysed, including 107 presymptomatic (44 *C9orf72*, 38 *GRN*, 25 *MAPT*) and 55 symptomatic (27 *C9orf72*, 17 *GRN*, 11 *MAPT*) mutation carriers as well as 76 mutation-negative controls ('non-carriers'). We found shared and distinct proteomic alterations in each genetic form of FTD. Among the proteins significantly altered in symptomatic mutation carriers compared to non-carriers, we found a set of proteins including neuronal pentraxin 2 (NPTX2) and fatty acid binding protein 3 (FABP3) shared across all three genetic forms, as well as in patients with Alzheimer's disease from previously published datasets. We observed differential changes in lysosomal proteins among symptomatic mutation carriers with marked abundance decreases in *MAPT* carriers, but not other carriers. Further, we identified mutation-associated proteomic changes already evident in presymptomatic mutation carriers. Weighted gene co-expression network analysis combined with gene ontology annotation revealed clusters of proteins enriched in neurodegeneration and glial responses, as well as synapse-, or lysosome-related proteins indicating that these are the central biological processes affected in genetic FTD. These clusters correlated with measures of disease severity and associated with cognitive decline. This study revealed distinct proteomic changes in the CSF of patients with genetic FTD, providing insights into the pathological processes involved in the disease. Additionally, we identified proteins that warrant further exploration as diagnostic and prognostic biomarker candidates.

One sentence summary: Both distinct and common cerebrospinal fluid proteomic signatures were observed in the different genetic forms of frontotemporal dementia.

Main Text:

INTRODUCTION

Frontotemporal dementia (FTD) is an umbrella term referring to a group of progressive neurodegenerative disorders, which typically present with behavioral changes (behavioral variant, (bvFTD), language problems (primary progressive aphasia, PPA), or motor impairment (either FTD with amyotrophic lateral sclerosis or FTD with parkinsonism)) (1). Although less common than Alzheimer's disease (AD), dementia with Lewy bodies and vascular dementia, FTD is a leading cause of early onset dementia (2). The underlying molecular basis of FTD is complex, but most cases can be attributed to a frontotemporal lobar degeneration (FTLD) pathology, with cellular inclusions of tau, TAR DNA-binding protein 43 (TDP-43) or FET proteins (FUS (Fused in sarcoma), EWS (Ewing sarcoma) and TAF15 (TATA-binding associated factor 15)) (3). Unlike AD, around a third of FTD cases have a genetic cause, with the most common mutations occurring in three genes: *GRN* (progranulin) and *C9orf72* (chromosome 9 open reading frame 72), both of which are typically accompanied by an underlying TDP-43 proteinopathy, as well as *MAPT* (microtubule-associated protein tau), manifesting as tauopathy (1, 4).

In FTD, the complex relationship between clinical presentations and underlying molecular pathology poses a challenge for its diagnosis and treatment. AD can be viewed as a successful example of how the introduction of cerebrospinal fluid (CSF) biomarker-assisted diagnosis has led to recent therapeutic advances (5) with the potential to revolutionise its treatment. In the case of FTD, however, the historic lack of biomarkers, as well as the complex relationship between clinical symptomatology and underlying pathophysiology have so far hampered such advancements. Nonetheless, there are biomarkers that show promise also in the context of FTD. Neurofilament light chain (NfL) has emerged as a promising, although disease-nonspecific, biomarker in differentiating FTD from primary psychiatric causes of behavioral symptoms (6) and, due to plasma NfL increasing in concentration in the presymptomatic phase of genetic FTD, also as a biomarker to detect neurodegeneration onset and disease intensity (7). Although there are indications that group-level concentrations of NfL are highest (at least in plasma) in *GRN* carriers (8), NfL cannot be used to identify the underlying pathology. For

this purpose, mutation- or pathology-specific biomarkers are needed, with current examples being limited, such as low plasma/CSF progranulin as indication of an underlying *GRN* mutation resulting in haploinsufficiency (9, 10); or promising new results on TDP-43 or 3R/4R tau protein in plasma-derived extracellular vesicles (11), that need further replication. Due to the lack of an *antemortem* gold standard for FTLT-tau and TDP-43 pathologies, sporadic FTD is likely not an ideal model to develop novel biomarkers at present. In familial FTD, however, the clear relationship between genetic mutation and resulting pathology may provide a context that allows the identification of such markers.

Previous studies using antibody-based methods (12–14) or mass spectrometric techniques (15, 16) have identified several FTD biomarker candidates, including neurofilament light, medium (NfM), and heavy (NfH), neuronal pentraxins, chitinase-3-like protein 1 (CHI3L1, also known as YKL-40), and ubiquitin carboxy-terminal hydrolase L1 (UCHL1). However, none of these proteins have proven specific for either FTLT or its subtypes, with similar alterations being seen in other neurodegenerative disorders, such as AD, Creutzfeldt-Jakob disease or ALS (14, 17–21).

In this study, we adopted an untargeted proteomics approach, using high-resolution mass spectrometry combined with tandem mass tag (TMT), to measure CSF proteins in a large, well-characterised genetic FTD cohort: the Genetic FTD Initiative (GENFI) study. We aimed to measure changes in low-abundant proteins not previously implicated in FTD to identify proteomic signatures of symptomatic groups carrying the most common genetic mutations causing FTD and therefore potentially distinguish specific underlying pathologies. Furthermore, we explored CSF proteomic changes that may identify mutation carriers at the presymptomatic stage of the disease, as has been done previously in autosomal dominant AD (22). Lastly, we investigated alterations of biological pathways in FTD, as mirrored in the CSF proteome, and their association with relevant clinical parameters and cognitive decline.

RESULTS

We analyzed a total of 238 CSF samples from 71 *C9orf72* expansion carriers, 55 *GRN* mutation carriers, and 36 *MAPT* mutation carriers, including both presymptomatic and symptomatic carriers in each group, as well as 76 asymptomatic non-carriers (Table 1).

Key methodological information of this study is summarized in Fig. 1, and specific descriptions for each analysis are detailed in the Materials and Methods and Supplementary Methods sections. Having prepared and analyzed all study samples using protocols previously described and developed by our laboratory (23–25), we initially explored differential protein abundances among symptomatic groups to assess wide-spread CSF proteomic changes in the context of different underlying pathologies and compared those to AD. Next, we utilised linear models to discern mutation-associated proteins already changed at the presymptomatic disease stage. Furthermore, employing weighted gene co-expression network analysis (WGCNA), we aimed to elucidate pathophysiological features associated with genetic mutations, as well as the cross-sectional correlations of protein networks with measures of cognitive function and brain volume. Finally, to investigate the prognostic properties of protein networks, we assessed their association with cognitive decline.

After outlier exclusion and removal of proteins with high missingness, we identified and obtained quantitative information for 1981 CSF proteins. First, we compared our TMT dataset to existing biomarker data from the same sample cohort. TMT CSF neurofilament light chain (NEFL; henceforth used interchangeably with protein abbreviation, NfL) measurements strongly correlated with plasma NfL measurements acquired on the Single molecule array (Simoa, Quanterix) platform ($R=0.62$, $P<0.001$; fig. S1A). The relative protein abundances of 14-3-3 epsilon (referred to as YWHAE) ($R=0.39$, $P<0.001$; fig. S1B), neuronal pentraxin 2 (NPTX2) ($R=0.8$, $P<0.001$; fig. S1C), and neuronal pentraxin receptor (NPTXR) ($R=0.68$, $P<0.001$; fig. S1D) also correlated significantly with previous data from the same cohort, acquired using targeted mass spectrometric analysis (26). The strong correlations of TMT relative protein abundances with measures acquired on two independent platforms indicate good analytical precision of our results.

Cerebrospinal fluid proteomes differ across symptomatic FTD mutation carrier groups

Linear regression analysis, including age and sex as covariates, was used to perform group comparisons between non-carriers and symptomatic mutation carriers. In the case of symptomatic *MAPT* mutation carriers, 58 proteins significantly differed in abundance compared with non-carriers (Fig. 2A; Table S1A), whereas the abundance of 138 and 385 proteins was significantly altered in symptomatic *GRN* (Fig. 2B; Table S1B) and *C9orf72* mutation carriers (Fig. 2C; Table S1C) compared to non-carriers, respectively ($P_{adjust} < 0.05$).

Next, to strengthen our findings, we compared our results to those from an external cohort consisting of symptomatic *GRN* carriers (n=11) and healthy non-carriers (n=12) (27) whose CSF proteome was measured with label-free mass spectrometry. Most proteins were commonly quantified in both studies, of which 73 proteins were significantly changed in both datasets ($P_{unadjusted} < 0.05$) (fig. S2, Table S2), with log₂ fold changes being strongly correlated between the studies ($R=0.87$, $P < 0.001$) (fig. S2).

From the 25 hits that presented the largest log₂ fold changes in each symptomatic mutation group (Table S3), a list of proteins was compiled (excluding overlap between groups) denoting corresponding protein abundance fold changes compared with non-carriers in a heatmap (Fig. 2D; Table S3). As expected, the three neurofilaments, NfL, NfM and NfH, alongside YKL-40 (CHI3L1), exhibited the greatest fold change in abundance across most symptomatic groups when compared to non-carriers, with NfL abundances being up to 7.4-times higher in symptomatic *GRN* carriers in comparison to non-carriers. Other proteins showing a notable positive fold change in symptomatic mutation carriers included the spectrins (SPTBN1, SPTAN1) as well as UCHL1 (ubiquitin C-terminal hydrolase 1), FABP3 (fatty acid binding protein 3), PEA15 (Proliferation and apoptosis adaptor protein 15) and several 14-3-3 proteins (YWHAZ, YWHAG, YWHAЕ). Proteins that were lower in abundance across symptomatic mutation carriers compared with non-carriers included the synaptic proteins NPTXR, NPTX2 and NPTX1, as well as PCSK2 (proprotein convertase subtilisin/kexin type 2) and PENK (proenkephalin). Furthermore, *GRN* relative abundance levels was lower in *GRN*

mutation carriers. Most proteins showed the same directionality of abundance fold change across the three mutation carrier groups except for a few proteins. These include GRN, which showed opposite direction of change in symptomatic *C9orf72* and *GRN* carriers (both $P_{adjust} < 0.05$), and the lysosomal proteins deoxyribonuclease 2 (DNASE2) and phospholipase B domain containing 2 (PLBD2), which were selectively decreased in symptomatic *MAPT* carriers.

Proteomic similarities and differences between genetic FTD and sporadic AD

Since some of the proteins quantified in this study are expected to change also in other neurodegenerative disorders, we compared the summary statistics of our differential abundance analyses of symptomatic FTD mutation carrier groups with summary statistics of previously published TMT proteomics datasets from two distinct AD studies: the European Medical Information Framework (EMIF) CSF study (25) and a CSF proteomics study performed by Higginbotham and colleagues (28). Of the about 1192 proteins quantifiable in all three studies, (Fig. 3A; Table S4A, Table S4B and Table S5), only 6 were significantly changed in all groups ($P_{adjust} < 0.05$) (YWHAZ, YWHAG, UCHL1, NPTXR, NPTX2 and FABP3, Fig. 3, B and C; Table S5). Conversely, many proteins were distinctly changed in each FTD mutation carrier group (Fig. 3, B and C, Table S5), with more widespread changes being found in symptomatic *C9orf72* carriers (calretinin [CALB2], sortilin 1 [SORT1] and roundabout guidance receptor 1 [ROBO1]) compared with *GRN* (transmembrane protein 132A [TMEM132A], ring finger protein [RNF13] and chitinase 3 like 2 [CHI3L2]) and *MAPT* (hexosaminidase subunit alpha [HEXA], semaphorin 6A [SEMA6A] and cathepsin D [CTSD]) carriers. Proteins shared between *C9orf72* and *GRN* carriers included many proteins involved in lysosomal processes (GRN, cathepsin S [CTSS], lysosomal-associated membrane protein 1 [LAMP1]). Proteins uniquely changed in both AD studies included neurogranin (NRGN) and SPARC related modular calcium binding 1 (SMOC1), both previously shown to increase in response to amyloid pathology (29). Only two proteins were distinctly changed in all symptomatic FTD mutation carrier groups (CD44 and follistatin like 4 [FSTL4]), likely reflecting the different processes involved in these disease-causing mutations.

Mutation-associated proteomic changes are evident in presymptomatic disease mutation carriers

Having compared proteomic alterations of symptomatic FTD subtypes and their overlap with AD, we next set out to determine changes in protein abundances associated with a specific genetic background, regardless of affectation (presence or absence of symptoms). The presence of symptoms is expected to coincide with diverse neurodegenerative processes impacting the CSF proteome and obscuring potential mutation-related changes. Thus, to investigate proteomic alterations attributable to each underlying pathogenic mutation, we (i) fitted linear models combining all study participants, testing the effect of genetic mutation on protein abundances while adjusting for affectation (Fig. 4, Table S6) and (ii) compared CSF proteomes of presymptomatic individuals with non-carriers for each genetic group separately (fig. S3-S8, Table S7A-S7C). This approach yielded several proteins strongly associated with either *C9orf72* (Fig. 4A), *GRN* (Fig. 4B) or *MAPT* (Fig. 4C) mutation status, of which the top five proteins for each association were chosen for visual display. Standardised β coefficients indicate the strength of the association respectively and are depicted in a forest plot for ease of comparison. The protein most strongly associated with *C9orf72* mutation status was CALB2 (Fig. 4A, standardised $\beta=0.77$, $P_{\text{adjust}} < 0.01$), which could also be found among the top changed proteins in the analysis of presymptomatic *C9orf72* carriers vs. non-carriers (Fig. S5 and S8). Numerous proteins found to be associated with *C9orf72*, such as glucose-6-phosphate isomerase (GPI), hexokinase 1 (HK1) (Fig. 4A, fig. S8), and phosphoglycerate kinase 1 (PGK1) (fig. S8) are key enzymes of the glycolysis pathway, hinting at early metabolic disturbances. The proteins CALB2, HK1, and PGK1 demonstrated a stepwise increase in abundance from non-carriers over presymptomatic to symptomatic *C9orf72* carriers (fig. S8), further underlining their implication in *C9orf72*-related disease processes.

Reflecting the GRN haploinsufficiency, the protein most strongly associated with *GRN* mutation status was GRN itself, (Fig. 4B, fig. S4 and S7, standardised $\beta=-1.59$, $P_{\text{adjust}} < 0.01$), followed by NAGA (alpha-N-acetylgalactosaminidase) (standardised $\beta=0.71$, $P_{\text{adjust}}=0.04$) and RNF13 (standardised $\beta=0.64$, $P_{\text{adjust}}=0.09$). RNF13, though narrowly failing to reach the significance threshold of 0.05 after multiple testing correction in the combined analysis, was found to be

significantly changed in the presymptomatic *GRN* carrier vs. non-carrier analysis (fig. S4, $P_{\text{adjust}}=0.03$) and increased in abundance across the *GRN* disease continuum (fig. S7). The proteins most strongly associated with *MAPT* mutation status were PEA15 (Fig. 4C, standardised $\beta=0.9$, $P_{\text{adjust}}<0.01$) and SEMA6A (standardised $\beta=-0.82$, $P_{\text{adjust}}<0.05$). PEA15 was also significantly altered in the comparison between presymptomatic *MAPT* carriers vs. non-carriers (fig. S3, $P_{\text{adjust}}=0.02$) and increased in abundance from the presymptomatic to symptomatic disease stage (fig. S6). Due to concerns of family membership adversely affecting our results, we conducted sensitivity analyses adopting the same linear models as in the main analysis but including one member from each family. These analyses presented similar results (Table S8, A to E).

Protein networks reveal pathology-specific pathophysiological alterations and correlate with clinical parameters

Having studied the proteomic signatures of each genetic group, we further explored the biological processes implicated in these proteomic changes by performing WGCNA (fig. S9 to S23). WGCNA is an analysis tool aimed at reducing the complexity of a proteomics dataset by breaking it down into gene ontology (GO)-annotated protein clusters. These protein modules consist of highly co-correlated proteins likely reflecting similar biological processes. We identified a total of 14 protein modules, including a group of 645 proteins that could not be assigned to any of the modules and a module containing contaminants from the laboratory environment. The modules varied in size from 14 to 349 proteins with a median module size of 52 proteins (Table S9). We determined the biological relevance of each protein module utilising GO analysis of its constituent proteins and selected the most representative term for module annotation (fig. S12 to S23). Furthermore, we identified the hub proteins of each module, indicating the proteins most strongly correlating ($R>0.7$) with the module's first principal component (Eigenprotein value), as most representative and important proteins of the respective module.

Figure 5A shows a selection of six protein modules and their corresponding Eigenprotein values (representative abundance values) plotted across all genetic groups as well as non-carriers. One module, which we termed 'Core markers' of neurodegenerative disease, consisted of 15 proteins and

was most strongly increased in abundance in each genetic group at the symptomatic stages when compared to non-carriers. The strong difference between non-carriers and presymptomatic *MAPT* carriers is largely influenced by age. It included YWHAG, NEFL, CHI3L1, NEFM and YWHAZ as hub proteins. These proteins were also among the top hits in the differential abundance analysis and had the highest fold change in symptomatic mutation carriers compared with non-carriers (Fig. 2D). As expected, many proteins belonging to the ‘Core markers’ module were also seen among the proteins overlapping between the three genetic forms and were found to be altered in the CSF of AD patients in the EMIF and Higginbotham studies (Fig. 3B and 3C).

Correlating the ‘Core marker’ Eigenprotein values with clinical parameters in both presymptomatic and symptomatic mutation carriers (Fig. 5B) revealed a strong positive association of the module with both plasma NfL ($R=0.86$, $P_{\text{adjust}} < 0.0001$) and the National Alzheimer's Coordinating Center's Frontotemporal Lobar Degeneration plus clinical dementia rating sum of boxes (FTLD-CDR-SOB) disease severity scores ($R=0.67$, $P_{\text{adjust}} < 0.0001$) as well as a negative association with MMSE scores ($R=-0.53$, $P_{\text{adjust}} < 0.0001$) and regional brain volumes. The ‘Core markers’ module also positively correlated with estimated years until disease onset (EYO) in presymptomatic individuals ($R=0.68$, $P_{\text{adjust}} < 0.0001$).

Besides the ‘Core markers’ module, Eigenprotein values for both the ‘Actin binding’ module and the ‘Stress response’ module were higher across symptomatic mutation carrier groups (albeit not statistically significant), suggesting common pathophysiological alterations in these processes (Fig. 5A). Both modules, along with the ‘Glycosaminoglycan processing’ module (Fig. S24D), showed a similar correlation pattern to the ‘Core markers’ module.

Conversely, the ‘Synapse’ module, containing proteins such as CHGB, SHISA6, CADM3, CADM1 and GPR158 showed lower Eigenprotein values in all symptomatic mutation carrier groups compared with non-carriers, although changes were not significant. Its correlation pattern with clinical parameters was inverse compared to the ‘Core markers’ module, exhibiting negative correlations with

age, plasma NfL and FTLN-CDR-SOB scores, and positive correlations with MMSE scores and brain volumes (Fig. 5B), similarly to the 'Neuronal development' and the 'Extracellular matrix 1' modules (fig. S24B and E). The 'Neuronal development' module contained several proteins considered to be markers of synaptic loss (NPTX2 and NPTXR, among others) and was significantly lower in symptomatic *C9orf72* carriers ($P_{\text{adjust}} < 0.05$).

We also identified a module associated with lysosomal proteins ('Lysosome' module), for which Eigenprotein values were selectively decreased in symptomatic *MAPT* mutation carriers compared to non-carriers ($P_{\text{adjust}} < 0.05$). They were also slightly decreased in presymptomatic *MAPT* individuals, albeit without statistical significance ($P = 0.79$). The hub proteins were determined to be SIAE (sialic acid acetyltransferase), hexosaminidase subunit beta (HEXB), HEXA, DNASE2 and PLBD2, all of which are implicated in lysosomal processes. These specific changes in *MAPT* mutation carriers in DNASE2 and PLBD2 were already evident in the heatmap (Fig. 2D) contrasting symptomatic mutation carrier groups. Other lysosomal proteins found to be commonly changed in *GRN* and *C9orf72* carriers (LAMP1 and CTSS, Fig. 3) were not part of the 'Lysosome' module, suggesting different subpopulations of lysosomal proteins, which might be reflective of distinct biological processes. The 'Lysosome' module did not correlate with markers of neurodegeneration, cognitive decline or brain atrophy.

The 'Immune response' module contained proteins related to the complement pathway and the immune system. For all symptomatic groups, there was a visible trend of increase in these clusters when compared to non-carriers, however, these differences were not statistically significant ($P > 0.05$). This module showed similar correlation patterns with clinical features to the 'Core markers' module.

Protein networks associate with cognitive decline in mutation carriers

To evaluate the prognostic properties of protein networks, the module Eigenprotein values of mutation carriers with cognitive evaluation at the time of lumbar puncture (LP) ($n = 146$, mean number of annual visits = 2.7, range 1-5) were modelled with FTLN-CDR-SOB score as outcome. In

agreement with analyses of cross-sectional cognitive scores, higher ‘Core markers’ Eigenprotein values were most strongly associated with higher FTLD-CDR-SOB scores, reflecting poorer cognitive outcomes (standardised $\beta=0.83$, $P<0.001$; Fig. 6A). A similar but less prominent pattern was seen for the ‘Actin binding’ module (standardised $\beta=0.50$, $P<0.001$; Fig. 6B). Conversely, lower Eigenvalues of the ‘Synapse’ module were associated with increasing FTLD-CDR-SOB scores (standardised $\beta=-0.49$, $P<0.001$; Fig. 6C). This indicated that lower ‘Synapse’ Eigenprotein values were associated with worse cognitive outcomes. Further, ‘Semaphorin signalling’, ‘Neuronal development’, ‘Extracellular Matrix 1’, ‘Lysosome’ and ‘Immune response’ module Eigenprotein values were also significantly (all $P<0.05$) associated with cognitive decline (Fig. 6D; for full model output, see Table S10).

DISCUSSION

The present study offers a detailed and untargeted account of the CSF proteomic signatures in genetic FTD. By including participants from the well-characterised GENFI cohort, with presymptomatic and symptomatic carriers of pathogenic mutations in the three genes comprising the overwhelming majority of genetic FTD, we covered most of the clinical continuum as well as its underlying genetic causes. Our analytical approach allowed us to uncover proteomic changes beyond known CSF and blood biomarkers, such as NfL, GFAP, and progranulin, suggesting potential pathology- and FTD-specific biomarkers.

To assess both differences and similarities across the FTD spectrum, we explored the proteome of each genetic group through separate analyses. Employing differential protein abundance analysis, we found several proteins that were altered in all symptomatic mutation carriers. Among these proteins, many of the top hits were neuronal proteins known to be increased in CSF in several neurodegenerative diseases, including neurofilaments (NfL, NfM and NfH), and 14-3-3 proteins (YWHAZ, YWHAG) (17, 18, 30). NfL (both when measured in CSF and plasma) has especially been suggested to be of diagnostic, prognostic and theragnostic value in FTD, as both this and other studies find large fold changes (seemingly most pronounced in *GRN* carriers) compared with healthy controls and even other brain-related conditions, which bears important implications for differential diagnoses (7, 30, 31). The decreased relative abundances of neuronal pentraxins (NPTX1, NPTX2) and their receptor (NPTXR), previously reported to be decreased in genetic FTD (15, 26, 32) and other neurodegenerative diseases (18, 33), further emphasises the presence of synaptic changes in FTD. These markers displayed a similar fold change in the study of FTD-*GRN* by Pesämaa et al. (27), which we used to validate our findings. In addition, changes shared between groups included proteins recently suggested to be associated with astrocytic and microglial responses in AD as well as FTD-TDP brains, such as rab GDP dissociation inhibitor alpha (GDI1), FABP3, and CD44 (34). Although not significantly changed in either the EMIF or Higginbotham study, CD44 antigen has been shown to play a role in neuroinflammation in AD, in relation to disease associated microglia (DAM) (34, 35) and their communication with astrocytes (36), as well as in *GRN* deficient animal models (37).

Despite not being specific to glial responses in FTD, the clear increases seen in symptomatic FTD suggest that CD44 may be a promising fluid-based marker to index such glial changes in future trials. Of note, GDI1, FABP3, and CD44 were also identified as microglial activation-dependent markers in the study by Pesämaa et al. (27).

Many of the proteins found to be clearly altered in all groups of symptomatic carriers were assigned to the ‘Core markers’ module in the protein network analysis (YWHAG, NfL, UCHL-1, FABP3, CHI3L1, CD44). Several of these ‘Core marker’ proteins (FABP3, UCHL1 and YWHAG, among others) were also shown to be changed in abundance in the CSF of AD patients, as evident by the EMIF and Higginbotham studies (25, 28). Together, these findings support the strong neurodegenerative and glial component of both diseases and highlight that, despite AD and FTD being separate disease entities, they appear to share common downstream pathophysiological features. Of note, the ‘Core markers’ also reflected disease severity and imaging measures of neurodegeneration and proved to be the protein network most closely linked to cognitive decline and estimated years until disease onset highlighting the prognostic value of markers reflecting neurodegenerative and neuroinflammatory processes.

Besides the ‘Core markers’ module, we identified several other protein modules seemingly altered across several groups in the FTD spectrum compared with non-carriers, with constituent proteins relating to the synapse (‘Synapse’ module), in line with results shown in the heatmap (Fig. 2), actin binding and stress response. Lower relative abundances of the ‘Synapse’ Eigenprotein values also predicted cognitive decline in mutation carriers. Although these protein networks strongly correlated with clinical and neuroimaging features, abundance differences compared with non-carriers were rendered non-significant, likely due to their association with age. Of note, the synaptic protein neurogranin (NRGN) as well as the extracellular matrix protein SMOC1 were not altered in any of the groups of symptomatic genetic FTD mutation carriers but altered in both AD studies. This is in line with previous research (29) and suggests their specificity for amyloid-related changes in AD. Conversely, the protein FSTL4 was found to be changed in all groups of symptomatic FTD mutation

carriers but not AD, hinting at its potential specificity for FTD. Knowledge is still limited on the extent to which this protein is associated with neurodegenerative disorders, although one small study reported lower protein abundances of FSTL4 in patients with ALS (38).

As this study aimed to look beyond proteomic alterations shared between FTD subtypes as well as AD, we also investigated the differences across genetic forms of FTD and their expected underlying pathologies. We identified lysosomal proteins with the potential to separate processes implicated in *MAPT* mutation carriers but not the other two groups. Decreased DNSAE2 and PLBD2 (which show divergent patterns in symptomatic *GRN* and *C9orf72* carriers as shown in Fig. 2B) appear to be specifically related to the presence of tau pathology, without the amyloid background observed in AD (as evident in Fig. 3). This was further supported by PLBD2 and DNASE2 being among the hub proteins in the ‘lysosome’ module, driving the marked Eigenprotein value decrease in *MAPT* mutation carriers (Fig. 5G). Indeed, evidence suggests that PLBD2 and DNASE2 play a role in lysosomal processes (39–42). These results were unexpected, given the evidence of lysosomal dysfunction in *GRN* mutation carriers, but not in *MAPT* mutation carriers, due to the role of progranulin in the endolysosomal pathway (43, 44). Nonetheless, tau protein has been previously implicated in the trafficking of autophagic vesicles and autolysosome fusion (45–47), suggesting that a reduction of proteins related to the endolysosomal pathway in *MAPT* may indicate a potential dysregulation in this system. Lysosomal acid phosphatase 2 (ACP2) (48), a member of the ‘lysosome’ module, was found to be downregulated in presymptomatic *MAPT* carriers, which aligns with the changes seen in the protein networks found in symptomatic carriers. This dysregulation might be different from that observed in *C9orf72* and *GRN* carriers, in which there was a selective increase for some lysosomal proteins (LAMP1 and CTSS) not belonging to the ‘Lysosome’ module and thus displaying a different correlation pattern.

In analyses stratifying groups by mutation irrespective of symptomatology, we observed a stepwise abundance increase across the disease continuum in PEA15, an astroglial protein associated with glial responses (34), being more strongly associated with *MAPT* mutation carriership than with *GRN* and

C9orf72. In *GRN* carriers, the expected decrease in *GRN* concentrations was observed (10) in both presymptomatic and symptomatic *GRN* carriers. Further, we found increased concentrations of *RNF13* in both presymptomatic and symptomatic *GRN* carriers, which might be reflecting an underlying alteration in the ubiquitin system (49), not as well captured in *MAPT* and *C9orf72* carriers. Further, we discovered several proteins that were changed in *C9orf72* expansion carriers, including *PGK1* which was elevated not only in presymptomatic carriers in comparison with non-carriers but also showed a stepwise increase across the disease continuum. In addition, *CALB2* as well as *HK1* were elevated in presymptomatic *C9orf72* carriers and, like *PGK1*, their relative abundances appeared to increase with disease progression. Both *HK1* and *PGK1* are key enzymes of the glycolysis pathway suggesting that a dysregulation of the glucose metabolism might be an early feature of *C9orf72*-related FTD (50). *HK1* and *CALB2* were also selected as two of the top proteins in analyses comparing mutation carriers irrespective of underlying symptomatology, indicating their stronger association with a *C9orf72* mutation.

This study has limitations. The identification of a lower number of proteins that were changed in *MAPT* mutation carriers in comparison with *GRN* and *C9orf72* mutation carriers may be biased due to the lower number of participants in this group. *C9orf72* seems to be the most common genetic cause of FTD worldwide, followed by *GRN* and then *MAPT* (1), and this trend is reflected in the recruitment of the GENFI study. Due to the structure of participant recruitment in the GENFI cohort, some participants from the same family were included in the study. Family members may share genetic and environmental factors to a greater degree than the general population, which may bias the results. However, we conducted sensitivity analyses that included only one member from each family, with comparable results.

Although genetic FTD offers the unique advantage of linking proteomic changes to pathological alterations *antemortem*, specifically distinguishing between tau and TDP-43 pathology, it cannot be excluded that observed proteomic changes are, in fact, specific to the underlying genetic mutation and not necessarily transferable to the resulting pathology in sporadic FTD.

Further, although both the EMIF and Higginbotham *et al.* studies employed similar statistical and mass spectrometric methods, it is likely that some of the differences seen between studies are due to varying power to detect proteomic alterations. Finally, the age-difference between symptomatic carriers and non-carriers may have resulted in age influencing the interpretation of results. However, including age as a covariate in all relevant analyses is likely to mostly mitigate this potential issue.

To conclude, this study explored the CSF proteome in genetic FTD and found distinct changes occurring already in presymptomatic mutation carriers indicating early lysosomal dysfunction and alterations in proteins involved in glucose metabolism, with more widespread proteomic differences during the symptomatic stage of the disease. We found that proteomic profiles largely overlapped between the different causes of FTD as well as with AD, especially with respect to synaptic loss, glial responses and neurodegenerative processes. Furthermore, we discovered that certain lysosomal proteins are strongly associated with *MAPT*-mutation carriers, hinting at their potential value in distinguishing underlying FTD pathologies. Taken together, our results can inform the development of targeted assays that could be of value in clinical scenarios as well as in research aiming to better understand these diseases.

MATERIALS AND METHODS

Study design

The objective of this study was to explore the CSF proteomic signatures of the three most common genetic pathogenic mutations in FTD. To this end, 238 CSF samples from an ongoing case-control study cohort of genetic FTD, the GENFI cohort, were employed. Participants of the GENFI cohort were recruited from 14 GENFI centres, distributed across Europe and Canada, since 2012. One CSF sample per participant, generally obtained upon the first (baseline) visit, was included in the present cross-sectional study. The samples were randomised for measurement and the researchers were blinded for genetic status and genetic mutations at the time of the experiment. No prior calculations were performed to determine cohort size; all available samples were included in the study. The presence of batch effects and sample outliers were investigated using hierarchical clustering and principal component analysis before and after normalization. The proteomic experiments were conducted in one replicate. No participants were excluded. London Queen Square Ethics committee as well as local ethics committees at each site approved the study. The study complies with the Declaration of Helsinki. All participants provided written informed consent at enrolment including consent to publication. This study adhered to the STROBE reporting guidelines for observational studies.

Participants and sample collection

Participants were recruited from the GENFI study, which includes individuals with a diagnosis of FTD due to a pathogenic mutation in *MAPT*, *GRN*, or *C9orf72* (symptomatic mutation carriers), at-risk first-degree relatives (presymptomatic mutation carriers), and non-carriers (mutation-negative first-degree relatives from the same families). Demographics of the cohort are described in Table 1. Participants were assessed using a standardised history and examination and were classified as symptomatic if they met consensus diagnostic criteria (51, 52). The CDR Dementia Staging Instrument with National Alzheimer Coordinating Centre Frontotemporal Lobar Degeneration component (CDR® plus NACC FTLD) was used to assess disease severity, and the CDR® plus NACC FTLD sum of boxes (SOB) was used for quantitative analyses in this paper. Participants

underwent Volumetric T1-weighted MRI scans. More details on clinical evaluation and imaging can be found in Supplementary Methods.

CSF collection and sample preparation

CSF was collected in polypropylene tubes through a lumbar puncture and centrifuged to remove insoluble material and cells. Supernatants were aliquoted and stored at -80 °C within 2 hours after collection. CSF samples (25 µL) were reduced by the addition of Tris(2)-carboxyethylphosphine (TCEP) in sodium deoxycholate (DOC), and triethylammonium bicarbonate (TEAB) to a final concentration of 5 mM TCEP (1% DOC, 100 mM TEAB). Following incubation at 55 °C for one hour, samples were equilibrated to room temperature (RT). Carbamidomethylation was performed by adding iodoacetamide to a concentration of 10 mM and subsequently incubating the reaction mixture in the dark for 30 min at RT. Trypsin (100 µg per vial; Promega) was dissolved in resuspension buffer (Promega) and 1.5 µg were added for overnight digestion at 37 °C. The following day, TMTpro reagents (TMT 18plex, Thermo Fisher, 5 mg) were dissolved in 200 µL acetonitrile (ACN) having been equilibrated to RT. Samples were randomised across TMT sets and TMT labelling was performed by adding 10 µL of TMT reagent to each sample. Per set, a global internal standard (GIS; pool of all cohort samples) was included as the last TMT channel (135N) for reference and normalisation. The reaction mixture was incubated for one hour under constant agitation and afterwards the labelling process was quenched by the addition of hydroxylamine to a final concentration of 0.2% (v/v). Following an incubation period of 30 min, samples were combined into 18-plex sets and subsequently acidified with 0.5 M hydrochloric acid to precipitate DOC as well as diluted with 0.1% trifluoroacetic acid (TFA). To remove DOC, TMT sets were centrifuged at 4000*g for 15 min at 4 °C and the resulting supernatant was subjected to desalting by solid phase extraction (SPE). Desalting was performed on reversed-phase C18 cartridges (Sep-Pak C18 light) with a vacuum manifold. The columns were first washed with 2*1000 µL 0.1% TFA in 80% ACN and then equilibrated with 2*1000 µL 0.1% TFA. After sample loading, the column was again washed twice with 1000 µL 0.1% TFA and finally peptides were eluted with 0.1% TFA, 80% ACN. The eluate was split into three aliquots of equal volume, dried by vacuum centrifugation, and stored at -20 °C.

Plasma NfL and other CSF marker measurements are detailed in Supplementary Methods.

Offline high-pH reverse phase HPLC sample fractionation

Offline high-pH HPLC fractionation was performed on an UltiMate™ 3000 Nano LC system. Each TMT set aliquot was dissolved in 22 µL of 2.5 mM NH₄OH of which 20 µL were injected to be separated on an XBridge BEH C18 column (pore size: 130 Å, inner diameter: 4.6 mm). Peptide elution was accomplished using the following gradient: Buffer B was increased from 1% to 45% over a 65-minute period (flow rate of 100 µL/min), while Buffer C was maintained at 10% (Buffer A: H₂O, Buffer B: 84% ACN, Buffer C: 25 mM NH₄OH). Resulting fractions were collected circling over two rows in a 96-well microtiter plate at 1 min intervals, yielding 24 concatenated fractions. Subsequent column cleaning was performed at 90% B and 10% C for 10 minutes followed by an equilibration at 1% B and 10% C for 10 minutes. All fractions were subjected to vacuum centrifugation and stored dry at -20 °C until subsequent LC-MS analysis.

Liquid chromatography-mass spectrometry (LC-MS)

Fractions were dissolved in 50 µL 0.05% TFA, 0.1% bovine serum albumin (loading buffer) and loaded on a nano-LC (Ultimate RSLC Nano, Thermo Scientific) equipped with a C18 trap column (PepMap Acclaim 300 µm mm * 5 mm, Thermo Scientific) and C18 separation column (PepMap Acclaim 75 µm * 500 mm, Thermo Scientific), connected to an Orbitrap Fusion™ Lumos™ Tribrid™ mass spectrometer (Thermo Scientific), fitted with an Easy Spray Source and a high-field asymmetric waveform ion mobility spectrometry (FAIMS) unit for spatial ion separation. Peptides were separated according to the following gradient: 5 min, 4% B; 6 min, 10% B; 74 min, 40% B; 75 min, 100% B (Buffer A: 0.1% FA; Buffer B: 84% ACN, 0.1% FA). In the positive ion mode, alternating MS/MS cycles (cycle time = 1.5 s) were performed at compensation voltages (CV) of CV=-70 V, CV = -50 V. A full Orbitrap MS scan was recorded with the parameters specified as follows: R = 120 k, AGC target = 100%, max injection time = 50 ms. The full MS scan was then followed by data dependent Orbitrap MS/MS scans set to the following parameters: R = 50 k, AGC target = 200%, max. injection time = 120 ms, isolation window = 0.7 m/z, activation type = HCD.

Statistical analysis

All statistical analyses were performed with R version 4.1.2. For basic demographic variables, Omnibus Kruskal-Wallis tests were performed for continuous variables, whereas Fisher's exact tests were used for categorical variables. Unless otherwise specified, Spearman correlations were used to test associations between continuous variables. To assess differentially abundant proteins across the diagnostic groups, linear regression models were built with the \log_2 -transformed value of the measured protein abundance as dependent variable, testing the effect of the diagnostic group, and adjusting for both age and sex as covariates. Resulting P -values were adjusted with the Benjamini-Hochberg procedure to account for multiple testing. Statistical significance (α) was set at a two-sided $P < 0.05$. To ensure a minimum number of observations per group, proteins with a high fraction of missing values ($>75\%$ of participants) were excluded from the regression analysis. Additionally, group-wise outlier removal of protein measurements ($\pm 1.5 \times \text{IQR}$) was performed prior to regression analysis as the presence of outliers can severely affect resulting test statistics potentially increasing the rate of false negatives in the initial biomarker discovery phase. For all subsequent statistical analyses as well as boxplots shown in this paper, outliers were not removed. Linear models (also adjusted for age and sex) including only one member from each family were performed in comparisons when more than 5 participants were available in both groups. To identify mutation-specific signatures, linear models were fitted including protein abundance as a dependent variable while evaluating the effect of each mutation group including affectation (absence/presence of symptoms) as well as age and sex as covariates. To identify subsets of co-correlated proteins relating to pathophysiological features of genetic FTD, we performed network analysis (WGCNA) followed by GO annotation of the output modules. The prognostic properties of protein networks were evaluated using linear mixed effects models. The specifics of each of these methods are described in Supplementary Methods.

628

629

630

631

632

633

634

635

636 **SUPPLEMENTARY MATERIALS**

637 Supplementary methods

638 Fig. S1 – S25

639 References (53-56)

640 Data File S1 (Table S1-S10)

641 MDAR Reproducibility checklist

642

643

644

645

646

647

648

649

650

651

652

653

654

655

656

657

658

659

660

661

662

663

664

665 REFERENCES and Notes

- 666 1. C. V. Greaves, J. D. Rohrer, An update on genetic frontotemporal dementia. *J Neurol* **266**, 2075–2086 (2019).
- 667 2. S. Hendriks, K. Peetoom, C. Bakker, W. M. Van Der Flier, J. M. Papma, R. Koopmans, F. R. J. Verhey, M. De Vugt, S.
668 Köhler, A. Withall, J. L. Parlevliet, Ö. Uysal-Bozkir, R. C. Gibson, S. M. Neita, T. R. Nielsen, L. C. Salem, J. Nyberg, M. A.
669 Lopes, J. C. Dominguez, M. F. De Guzman, A. Egeberg, K. Radford, T. Broe, M. Subramaniam, E. Abdin, A. C. Bruni, R.
670 Di Lorenzo, K. Smith, L. Flicker, M. O. Mol, M. Basta, D. Yu, G. Masika, M. S. Petersen, L. Ruano, Global Prevalence of
671 Young-Onset Dementia: A Systematic Review and Meta-analysis. *JAMA Neurol* **78**, 1080–1090 (2021).
- 672 3. I. R. A. Mackenzie, M. Neumann, Molecular neuropathology of frontotemporal dementia: insights into disease
673 mechanisms from postmortem studies. *J Neurochem* **138**, 54–70 (2016).
- 674 4. J. D. Rohrer, R. Guerreiro, J. Vandrovcsa, J. Uphill, D. Reiman, J. Beck, A. M. Isaacs, A. Authier, R. Ferrari, N. C. Fox,
675 I. R. A. MacKenzie, J. D. Warren, R. De Silva, J. Holton, T. Revesz, J. Hardy, S. Mead, M. N. Rossor, The heritability and
676 genetics of frontotemporal lobar degeneration. *Neurology* **73**, 1451–1456 (2009).
- 677 5. C. H. van Dyck, Anti-Amyloid- β Monoclonal Antibodies for Alzheimer’s Disease: Pitfalls and Promise. *Biol Psychiatry*
678 **83**(4), 311–319 (2017).
- 679 6. M. R. Al Shweiki, P. Steinacker, P. Oeckl, B. Hengerer, A. Danek, K. Fassbender, J. Diehl-Schmid, H. Jahn, S. Anderl-
680 Straub, A. C. Ludolph, C. Schönfeldt-Lecuona, M. Otto, Neurofilament light chain as a blood to differentiate psychiatric
681 disorders from behavioural variant frontotemporal dementia. *J Psychiatr Res* **113**, 137–140 (2019).
- 682 7. J. C. Rojas, P. Wang, A. M. Staffaroni, C. Heller, Y. Cobigo, A. Wolf, S. Y. M. Goh, P. A. Ljubenkova, H. W. Heuer, J. C.
683 Fong, J. B. Taylor, E. Veras, L. Song, A. Jeromin, D. Hanlon, L. Yu, A. Khinikar, R. Sivasankaran, A. Kieloch, M. A.
684 Valentin, A. M. Karydas, L. L. Mitic, R. Pearlman, J. Kornak, J. H. Kramer, B. L. Miller, K. Kantarci, D. S. Knopman, N.
685 Graff-Radford, L. Petrucelli, R. Rademakers, D. J. Irwin, M. Grossman, E. M. Ramos, G. Coppola, M. F. Mendez, Y.
686 Bordelon, B. C. Dickerson, N. Ghoshal, E. D. Huey, I. R. Mackenzie, B. S. Appleby, K. Domoto-Reilly, G. Y. R. Hsiung, A.
687 W. Toga, S. Weintraub, D. I. Kaufer, D. Kerwin, I. Litvan, C. U. Onyike, A. Pantelyat, E. D. Roberson, M. C. Tartaglia, T.
688 Foroud, W. Chen, J. Czerkowicz, D. L. Graham, J. C. van Swieten, B. Borroni, R. Sanchez-Valle, F. Moreno, R. Laforce, C.
689 Graff, M. Synofzik, D. Galimberti, J. B. Rowe, M. Masellis, E. Finger, R. Vandenberghe, A. de Mendonça, F. Tagliavini, I.
690 Santana, S. Ducharme, C. R. Butler, A. Gerhard, J. Levin, A. Danek, M. Otto, S. Sorbi, D. M. Cash, R. S. Convery, M.
691 Bocchetta, M. Foiani, C. V. Greaves, G. Peakman, L. Russell, I. Swift, E. Todd, J. D. Rohrer, B. F. Boeve, H. J. Rosen, A. L.
692 Boxer, Plasma Neurofilament Light for Prediction of Disease Progression in Familial Frontotemporal Lobar Degeneration.
693 *Neurology* **96**, e2296–e2312 (2021).
- 694 8. A. M. Staffaroni, M. Quintana, B. Wendelberger, H. W. Heuer, L. L. Russell, Y. Cobigo, A. Wolf, S. Y. M. Goh, L.
695 Petrucelli, T. F. Gendron, C. Heller, A. L. Clark, J. C. Taylor, A. Wise, E. Ong, L. Forsberg, D. Brushaber, J. C. Rojas, L.
696 VandeVrede, P. Ljubenkova, J. Kramer, K. B. Casaletto, B. Appleby, Y. Bordelon, H. Botha, B. C. Dickerson, K. Domoto-
697 Reilly, J. A. Fields, T. Foroud, R. Gavrilo, D. Geschwind, N. Ghoshal, J. Goldman, J. Graff-Radford, N. Graff-Radford,
698 M. Grossman, M. G. H. Hall, G. Y. Hsiung, E. D. Huey, D. Irwin, D. T. Jones, K. Kantarci, D. Kaufer, D. Knopman, W.
699 Kremers, A. L. Lago, M. I. Lapid, I. Litvan, D. Lucente, I. R. Mackenzie, M. F. Mendez, C. Mester, B. L. Miller, C. U.
700 Onyike, R. Rademakers, V. K. Ramanan, E. M. Ramos, M. Rao, K. Rascovsky, K. P. Rankin, E. D. Roberson, R. Savica, M.
701 C. Tartaglia, S. Weintraub, B. Wong, D. M. Cash, A. Bouzigues, I. J. Swift, G. Peakman, M. Bocchetta, E. G. Todd, R. S.
702 Convery, J. B. Rowe, B. Borroni, D. Galimberti, P. Tiraboschi, M. Masellis, E. Finger, J. C. van Swieten, H. Seelaar, L. C.
703 Jiskoot, S. Sorbi, C. R. Butler, C. Graff, A. Gerhard, T. Langheinrich, R. Laforce, R. Sanchez-Valle, A. de Mendonça, F.
704 Moreno, M. Synofzik, R. Vandenberghe, S. Ducharme, I. Le Ber, J. Levin, A. Danek, M. Otto, F. Pasquier, I. Santana, J.
705 Kornak, B. F. Boeve, H. J. Rosen, J. D. Rohrer, A. L. Boxer, Temporal order of clinical and biomarker changes in familial
706 frontotemporal dementia. *Nat Med* **28**, 2194–2206 (2022).
- 707 9. N. Finch, M. Baker, R. Crook, K. Swanson, K. Kuntz, R. Surtees, G. Bisceglia, A. Rovelet-Lecrux, B. Boeve, R. C.
708 Petersen, D. W. Dickson, S. G. Younkin, V. Deramecourt, J. Crook, N. R. Graff-Radford, R. Rademakers, Plasma
709 progranulin levels predict progranulin mutation status in frontotemporal dementia patients and asymptomatic family
710 members. *Brain* **132**, 583–591 (2009).

10. L. H. H. Meeter, H. Patzke, G. Loewen, E. G. P. Dopper, Y. A. L. Pijnenburg, R. Van Minkelen, J. C. Van Swieten, Progranulin Levels in Plasma and Cerebrospinal Fluid in Granulin Mutation Carriers. *Dement Geriatr Cogn Dis Extra* **6**, 330–340 (2016).
11. M. Chatterjee, S. Özdemir, C. Fritz, W. Möbius, L. Kleineidam, E. Mandelkow, J. Biernat, C. Doğdu, O. Peters, N. C. Cosma, X. Wang, L. S. Schneider, J. Priller, E. Spruth, A. A. Kühn, P. Krause, T. Klockgether, I. R. Vogt, O. Kimmich, A. Spotke, D. C. Hoffmann, K. Fliessbach, C. Miklitz, C. McCormick, P. Weydt, B. Falkenburger, M. Brandt, R. Guenther, E. Dinter, J. Wiltfang, N. Hansen, M. Bähr, I. Zerr, A. Flöel, P. J. Nestor, E. Düzel, W. Glanz, E. Incesoy, K. Bürger, D. Janowitz, R. Perneczky, B. S. Rauchmann, F. Hopfner, O. Wagemann, J. Levin, S. Teipel, I. Kilimann, D. Goerss, J. Prudlo, T. Gasser, K. Brockmann, D. Mengel, M. Zimmermann, M. Synofzik, C. Wilke, J. Selma-González, J. Turon-Sans, M. A. Santos-Santos, D. Alcolea, S. Rubio-Guerra, J. Fortea, Á. Carbayo, A. Lleó, R. Rojas-García, I. Illán-Gala, M. Wagner, I. Frommann, S. Roeske, L. Bertram, M. T. Heneka, F. Brosseron, A. Ramirez, M. Schmid, R. Beschoner, A. Halle, J. Herms, M. Neumann, N. R. Barthélemy, R. J. Bateman, P. Rizzu, P. Heutink, O. Dols-Icardo, G. Höglinger, A. Hermann, A. Schneider, Plasma extracellular vesicle tau and TDP-43 as diagnostic biomarkers in FTD and ALS. *Nature Medicine* **30**, 1771–1783 (2024).
12. S. Bergström, L. Öijerstedt, J. Remnestål, J. Olofsson, A. Ullgren, H. Seelaar, J. C. van Swieten, M. Synofzik, R. Sanchez-Valle, F. Moreno, E. Finger, M. Masellis, C. Tartaglia, R. Vandenberghe, R. Laforce, D. Galimberti, B. Borroni, C. R. Butler, A. Gerhard, S. Ducharme, J. D. Rohrer, A. Månberg, C. Graff, P. Nilsson, L. Jiskoot, J. B. Rowe, A. de Mendonça, F. Tagliavini, I. Santana, I. Le Ber, J. Levin, A. Danek, M. Otto, G. Frisoni, R. Ghidoni, S. Sorbi, F. Pasquier, V. Jelic, C. Andersson, S. Afonso, M. R. Almeida, S. Anderl-Straub, A. Antonell, S. Archetti, A. Arighi, M. Balasa, M. Barandiaran, N. Bargalló, R. Bartha, B. Bender, A. Benussi, L. Benussi, V. Bessi, G. Binetti, S. Black, M. Bocchetta, S. Borrego-Ecija, J. Bras, R. Bruffaerts, M. Cañada, V. Cantoni, P. Caroppo, D. Cash, M. Castelo-Branco, R. Convery, T. Cope, G. Di Fede, A. Díez, D. Duro, C. Fenoglio, C. Ferrari, C. B. Ferreira, N. Fox, M. Freedman, G. Fumagalli, A. Gabilondo, R. Gasparotti, S. Gauthier, S. Gazzina, G. Giaccone, A. Gorostidi, C. Greaves, R. Guerreiro, C. Heller, T. Hoegen, B. Indakoechea, L. Jiskoot, H. O. Karnath, R. Keren, T. Langheinrich, M. J. Leitão, A. Lladó, G. Lombardi, S. Loosli, C. Maruta, S. Mead, L. Meeter, G. Miltenberger, R. van Minkelen, S. Mitchell, K. Moore, B. Nacmias, J. Nicholas, J. Olives, S. Ourselin, A. Padovani, J. Panman, J. M. Papma, G. Peakman, M. Pievani, Y. Pijnenburg, C. Polito, E. Premi, S. Prioni, C. Prix, R. Rademakers, V. Redaelli, T. Rittman, E. Rogaeva, P. Rosa-Neto, G. Rossi, M. Rosser, B. Santiago, E. Scarpini, S. Schönecker, E. Semler, R. Shafei, C. Shoesmith, M. Tábuas-Pereira, M. Tainta, R. Taipa, D. Tang-Wai, D. L. Thomas, P. Thompson, H. Thonberg, C. Timberlake, P. Tiraboschi, E. Todd, P. Van Damme, M. Vandenbulcke, M. Veldsman, A. Verdelho, J. Villanua, J. Warren, C. Wilke, I. Woollacott, E. Wlasich, H. Zetterberg, M. Zulaica, A panel of CSF proteins separates genetic frontotemporal dementia from presymptomatic mutation carriers: a GENFI study. *Mol Neurodegener* **16**, 79 (2021).
13. J. Remnestål, L. Öijerstedt, A. Ullgren, J. Olofsson, S. Bergström, K. Kulima, M. Ingelsson, L. Kilander, M. Uhlén, A. Månberg, C. Graff, P. Nilsson, Altered levels of CSF proteins in patients with FTD, presymptomatic mutation carriers and non-carriers. *Transl Neurodegener* **9**, 27 (2020).
14. C. E. Teunissen, N. Elias, M. J. A. Koel-Simmelink, S. Durieux-Lu, A. Malekzadeh, T. V. Pham, S. R. Piersma, T. Beccari, L. H. H. Meeter, E. G. P. Dopper, J. C. van Swieten, C. R. Jimenez, Y. A. L. Pijnenburg, Novel diagnostic cerebrospinal fluid biomarkers for pathologic subtypes of frontotemporal dementia identified by proteomics. *Alzheimers Dement (Amst)* **2**, 86–94 (2016).
15. E. L. van der Ende, L. H. Meeter, C. Stingl, J. G. J. van Rooij, M. P. Stoop, D. A. T. Nijholt, R. Sanchez-Valle, C. Graff, L. Öijerstedt, M. Grossman, C. McMillan, Y. A. L. Pijnenburg, R. Laforce, G. Binetti, L. Benussi, R. Ghidoni, T. M. Luider, H. Seelaar, J. C. van Swieten, Novel CSF biomarkers in genetic frontotemporal dementia identified by proteomics. *Ann Clin Transl Neurol* **6**, 698–707 (2019).
16. N. Mattsson, U. Rüetschi, Y. A. L. Pijnenburg, M. A. Blankenstein, V. N. Podust, S. Li, I. Fagerberg, L. Rosengren, K. Blennow, H. Zetterberg, Novel cerebrospinal fluid biomarkers of axonal degeneration in frontotemporal dementia. *Mol Med Rep* **1**, 757–761 (2008).
17. P. Barschke, P. Oeckl, P. Steinacker, M. H. D. R. Al Shweiki, J. H. Weishaupt, G. B. Landwehrmeyer, S. Anderl-Straub, P. Weydt, J. Diehl-Schmid, A. Danek, J. Kornhuber, M. L. Schroeter, J. Prudlo, H. Jahn, K. Fassbender, M. Lauer, E. L. Van Der Ende, J. C. Van Swieten, A. E. Volk, A. C. Ludolph, M. Otto, Different CSF protein profiles in amyotrophic lateral sclerosis and frontotemporal dementia with C9orf72 hexanucleotide repeat expansion. *J Neurol Neurosurg Psychiatry* **91**, 503–511 (2020).

18. J. Nilsson, J. Gobom, S. Sjödin, G. Brinkmalm, N. J. Ashton, J. Svensson, P. Johansson, E. Portelius, H. Zetterberg, K. Blennow, A. Brinkmalm, Cerebrospinal fluid biomarker panel for synaptic dysfunction in Alzheimer's disease. *Alzheimer's & Dementia: Diagnosis, Assessment & Disease Monitoring* **13**, e12179 (2021).

19. F. Llorens, K. Thüne, W. Tahir, E. Kanata, D. Diaz-Lucena, K. Xanthopoulos, E. Kovatsi, C. Pleschka, P. Garcia-Esparcia, M. Schmitz, D. Ozbay, S. Correia, A. Correia, I. Milosevic, O. Andréoletti, N. Fernández-Borges, I. M. Vorberg, M. Glatzel, T. Sklaviadis, J. M. Torres, S. Krasemann, R. Sánchez-Valle, I. Ferrer, I. Zerr, YKL-40 in the brain and cerebrospinal fluid of neurodegenerative dementias. *Mol Neurodegener* **12**, 83 (2017).

20. P. Oeckl, P. Weydt, D. R. Thal, J. H. Weishaupt, A. C. Ludolph, M. Otto, Proteomics in cerebrospinal fluid and spinal cord suggests UCHL1, MAP2 and GPNMB as biomarkers and underpins importance of transcriptional pathways in amyotrophic lateral sclerosis. *Acta Neuropathol* **139**, 119–134 (2020).

21. G. Ary, H. Sich, C. Larence, J. G. Ibbs, E. H. L. Ee, G. H. Arrington, The 14-3-3 Brain Protein in Cerebrospinal Fluid as a Marker for Transmissible Spongiform Encephalopathies, *N Engl J Med*. **335**, 924–930 (1996).

22. S. Palmqvist, S. Janelidze, Y. T. Quiroz, H. Zetterberg, F. Lopera, E. Stomrud, Y. Su, Y. Chen, G. E. Serrano, A. Leuzy, N. Mattsson-Carlsson, O. Strandberg, R. Smith, A. Villegas, D. Sepulveda-Falla, X. Chai, N. K. Proctor, T. G. Beach, K. Blennow, J. L. Dage, E. M. Reiman, O. Hansson, Discriminative Accuracy of Plasma Phospho-tau217 for Alzheimer Disease vs Other Neurodegenerative Disorders. *JAMA* **324**, 772–781 (2020).

23. N. K. Magdalinos, A. J. Noyce, R. Pinto, E. Lindstrom, J. Holmén-Larsson, M. Holtta, K. Blennow, H. R. Morris, T. Skillbäck, T. T. Warner, A. J. Lees, I. Pike, M. Ward, H. Zetterberg, J. Gobom, Identification of candidate cerebrospinal fluid biomarkers in parkinsonism using quantitative proteomics. *Parkinsonism Relat Disord* **37**, 65–71 (2017).

24. S. Weiner, M. Sauer, P. J. Visser, B. M. Tijms, E. Vorontsov, K. Blennow, H. Zetterberg, J. Gobom, Optimized sample preparation and data analysis for TMT proteomic analysis of cerebrospinal fluid applied to the identification of Alzheimer's disease biomarkers. *Clin Proteomics* **19**, 13 (2022).

25. B. M. Tijms, J. Gobom, L. Reus, I. Jansen, S. Hong, V. Dobricic, F. Kilpert, M. Ten Kate, F. Barkhof, M. Tsolaki, F. R. J. Verhey, J. Popp, P. Martinez-Lage, R. Vandenbergh, A. Lleó, J. L. Molinuevo, S. Engelborghs, L. Bertram, S. Lovestone, J. Streffer, S. Vos, I. Bos, K. Blennow, P. Scheltens, C. E. Teunissen, H. Zetterberg, P. J. Visser, Pathophysiological subtypes of Alzheimer's disease based on cerebrospinal fluid proteomics. *Brain* **143**, 3776–3792 (2020).

26. A. Sogorb-Esteve, J. Nilsson, I. J. Swift, C. Heller, M. Bocchetta, L. L. Russell, G. Peakman, R. S. Convery, J. C. van Swieten, H. Seelaar, B. Borroni, D. Galimberti, R. Sanchez-Valle, R. Laforce, F. Moreno, M. Synofzik, C. Graff, M. Masellis, M. C. Tartaglia, J. B. Rowe, R. Vandenbergh, E. Finger, F. Tagliavini, I. Santana, C. R. Butler, S. Ducharme, A. Gerhard, A. Danek, J. Levin, M. Otto, S. Sorbi, I. Le Ber, F. Pasquier, J. Gobom, A. Brinkmalm, K. Blennow, H. Zetterberg, J. D. Rohrer, A. Nelson, A. Bouzigues, C. V. Greaves, D. Cash, D. L. Thomas, E. Todd, H. Benotmane, J. Nicholas, K. Samra, R. Shafei, C. Timberlake, T. Cope, T. Rittman, A. Benussi, E. Premi, R. Gasparotti, S. Archetti, S. Gazzina, V. Cantoni, A. Arighi, C. Fenoglio, E. Scarpini, G. Fumagalli, V. Borracchi, G. Rossi, G. Giaccone, G. Di Fede, P. Caroppo, P. Tiraboschi, S. Prioni, V. Redaelli, D. Tang-Wai, E. Rogaeva, M. Castelo-Branco, M. Freedman, R. Keren, S. Black, S. Mitchell, C. Shoesmith, R. Bartha, R. Rademakers, J. Poos, J. M. Papma, L. Giannini, R. van Minkelen, Y. Pijnenburg, B. Nacmias, C. Ferrari, C. Polito, G. Lombardi, V. Bessi, M. Veldsman, C. Andersson, H. Thonberg, L. Öijerstedt, V. Jelic, P. Thompson, T. Langheinrich, A. Lladó, A. Antonell, J. Olives, M. Balasa, N. Bargalló, S. Borrego-Ecija, A. de Mendonça, A. Verdelho, C. Maruta, C. B. Ferreira, G. Miltenberger, F. S. do Couto, A. Gabilondo, A. Gorostidi, J. Villanua, M. Cañada, M. Tainta, M. Zulaica, M. Barandiaran, P. Alves, B. Bender, C. Wilke, L. Graf, A. Vogels, M. Vandenbulcke, P. Van Damme, R. Bruffaerts, K. Poesen, P. Rosa-Neto, S. Gauthier, A. Camuzat, A. Brice, A. Bertrand, A. Funkiewiez, D. Rinaldi, D. Saracino, O. Colliot, S. Sayah, C. Prix, E. Wlasich, O. Wagemann, S. Loosli, S. Schönecker, T. Hoegen, J. Lombardi, S. Anderl-Straub, A. Rollin, G. Kuchinski, M. Bertoux, T. Lebouvier, V. Deramecourt, B. Santiago, D. Duro, M. J. Leitão, M. R. Almeida, M. Tábuas-Pereira, S. Afonso, Differential impairment of cerebrospinal fluid synaptic biomarkers in the genetic forms of frontotemporal dementia. *Alzheimers Res Ther* **14**, 118 (2022).

27. I. Pesāmaa, S. A. Müller, S. Robinson, A. Darcher, D. Paquet, H. Zetterberg, S. F. Lichtenthaler, C. Haass, A microglial activity state biomarker panel differentiates FTD-granulin and Alzheimer's disease patients from controls. *Mol Neurodegener* **18**, 1–18 (2023).

809 28. L. Higginbotham, L. Ping, E. B. Dammer, D. M. Duong, M. Zhou, M. Gearing, C. Hurst, J. D. Glass, S. A. Factor, E. C.
810 B. Johnson, I. Hajjar, J. J. Lah, A. I. Levey, N. T. Seyfried, Integrated proteomics reveals brain-based cerebrospinal fluid
811 biomarkers in asymptomatic and symptomatic. *Alzheimer's disease. Sci. Adv* **6**, eaaz9360 (2020).

812 29. E. Portelius, B. Olsson, K. Höglund, N. C. Cullen, H. Kvartsberg, U. Andreasson, H. Zetterberg, Å. Sandelius, L. M.
813 Shaw, V. M. Y. Lee, D. J. Irwin, M. Grossman, D. Weintraub, A. Chen-Plotkin, D. A. Wolk, L. McCluskey, L. Elman, J.
814 McBride, J. B. Toledo, J. Q. Trojanowski, K. Blennow, Cerebrospinal fluid neurogranin concentration in neurodegeneration:
815 relation to clinical phenotypes and neuropathology. *Acta Neuropathol* **136**, 363–376 (2018).

816 30. N. J. Ashton, S. Janelidze, A. Al Khleifat, A. Leuzy, E. L. van der Ende, T. K. Karikari, A. L. Benedet, T. A. Pascoal, A.
817 Lleó, L. Parnetti, D. Galimberti, L. Bonanni, A. Pilotto, A. Padovani, J. Lycke, L. Novakova, M. Axelsson, L. Velayudhan,
818 G. D. Rabinovici, B. Miller, C. Pariante, N. Nikkheslat, S. M. Resnick, M. Thambisetty, M. Schöll, G. Fernández-Eulate, F.
819 J. Gil-Bea, A. López de Munain, A. Al-Chalabi, P. Rosa-Neto, A. Strydom, P. Svenningsson, E. Stomrud, A. Santillo, D.
820 Aarsland, J. C. van Swieten, S. Palmqvist, H. Zetterberg, K. Blennow, A. Hye, O. Hansson, A multicentre validation study
821 of the diagnostic value of plasma neurofilament light. *Nat Commun* **12**, 3400 (2021).

822 31. Illán-Gala I, Alcolea D, Montal V, Dols-Icardo O, Muñoz L, de Luna N, Turón-Sans J, Cortés-Vicente E, Sánchez-
823 Saudinós MB, Subirana A, Sala I, Blesa R, Clarimón J, Fortea J, Rojas-García R, Lleó A. CSF sAPPβ, YKL-40, and NfL
824 along the ALS-FTD spectrum. *Neurology* **91**, e1619-e1628 (2018).

825 32. E. L. Van Der Ende, M. Xiao, D. Xu, J. M. Poos, J. L. Panman, L. C. Jiskoot, L. H. Meeter, E. G. P. Dopper, J. M.
826 Papma, C. Heller, R. Convery, K. Moore, M. Bocchetta, M. Neason, G. Peakman, D. M. Cash, C. E. Teunissen, C. Graff, M.
827 Synofzik, F. Moreno, E. Finger, R. Sánchez-Valle, R. Vandenbergh, R. Laforce, M. Masellis, M. C. Tartaglia, J. B. Rowe,
828 C. R. Butler, S. Ducharme, A. Gerhard, A. Danek, J. Levin, Y. A. L. Pijnenburg, M. Otto, B. Borroni, F. Tagliavini, A. De
829 Mendonca, I. Santana, D. Galimberti, H. Seelaar, J. D. Rohrer, P. F. Worley, J. C. Van Swieten, Neuronal pentraxin 2: A
830 synapse-derived CSF biomarker in genetic frontotemporal dementia. *J Neurol Neurosurg Psychiatry* **91**, 612-621 (2020).

831 33. J. Nilsson, J. Constantinescu, B. Nellgård, P. Jakobsson, W. S. Brum, J. Gobom, L. Forsgren, K. Dalla, R.
832 Constantinescu, H. Zetterberg, O. Hansson, K. Blennow, D. Bäckström, A. Brinkmalm, Cerebrospinal Fluid Biomarkers of
833 Synaptic Dysfunction are Altered in Parkinson's Disease and Related Disorders. *Mov Disord* **38**, 267–277 (2023).

834 34. E. C. B. Johnson, E. B. Dammer, D. M. Duong, L. Ping, M. Zhou, L. Yin, L. A. Higginbotham, A. Guajardo, B. White,
835 J. C. Troncoso, M. Thambisetty, T. J. Montine, E. B. Lee, J. Q. Trojanowski, T. G. Beach, E. M. Reiman, V. Haroutunian,
836 M. Wang, E. Schadt, B. Zhang, D. W. Dickson, N. Ertekin-Taner, T. E. Golde, V. A. Petyuk, P. L. De Jager, D. A. Bennett,
837 T. S. Wingo, S. Rangaraju, I. Hajjar, J. M. Shulman, J. J. Lah, A. I. Levey, N. T. Seyfried, Large-scale proteomic analysis of
838 Alzheimer's disease brain and cerebrospinal fluid reveals early changes in energy metabolism associated with microglia and
839 astrocyte activation. *Nat Med* **26**, 769-780 (2020).

840 35. S. Rangaraju, E. B. Dammer, S. A. Raza, P. Rathakrishnan, H. Xiao, T. Gao, D. M. Duong, M. W. Pennington, J. J. Lah,
841 N. T. Seyfried, A. I. Levey, Identification and therapeutic modulation of a pro-inflammatory subset of disease-associated-
842 microglia in Alzheimer's disease. *Mol Neurodegener* **13**, 24 (2018).

843 36. C. J. Garwood, L. E. Ratcliffe, J. E. Simpson, P. R. Heath, P. G. Ince, S. B. Wharton, Review: Astrocytes in Alzheimer's
844 disease and other age-associated dementias: a supporting player with a central role. *Neuropathol Appl Neurobiol* **43**, 281–
845 298 (2017).

846 37. M. Huang, E. Modeste, E. Dammer, P. Merino, G. Taylor, D. M. Duong, Q. Deng, C. J. Holler, M. Gearing, D. Dickson,
847 N. T. Seyfried, T. Kukar, Network analysis of the progranulin-deficient mouse brain proteome reveals pathogenic
848 mechanisms shared in human frontotemporal dementia caused by GRN mutations. *Acta Neuropathol Commun* **8**, 163
849 (2020).

850 38. S. Oh, Y. Jang, C. H. Na, Discovery of Biomarkers for Amyotrophic Lateral Sclerosis from Human Cerebrospinal Fluid
851 Using Mass-Spectrometry-Based Proteomics. *Biomedicines* **11**, 1250 (2023).

852 39. R. Mao, Y. Wang, F. Wang, L. Zhou, S. Yan, S. Lu, W. Shi, Y. Zhang, Identification of Four Biomarkers of Human Skin
853 Aging by Comprehensive Single Cell Transcriptome, Transcriptome, and Proteomics. *Front Genet* **13**, 881051 (2022).

854 40. K. Kawane, H. Fukuyama, G. Kondoh, J. Takeda, Y. Ohsawa, Y. Uchiyama, S. Nagata, Requirement of DNase II for
855 definitive erythropoiesis in the mouse fetal liver. *Science* **292**, 1546–1549 (2001).

856 41. H. D. Shin, B. L. Park, H. S. Cheong, H. S. Lee, J. B. Jun, S. C. Bae, DNase II polymorphisms associated with risk of
857 renal disorder among systemic lupus erythematosus patients. *J Hum Genet* **50**, 107–111 (2005).

858 42. P. A. Keyel, Dnases in health and disease. *Dev Biol* **429**, 1–11 (2017).

859 43. J. Root, P. Merino, A. Nuckols, M. Johnson, T. Kukar, Lysosome dysfunction as a cause of neurodegenerative diseases:
860 Lessons from frontotemporal dementia and amyotrophic lateral sclerosis. *Neurobiol Dis* **154**, 105360 (2021).

861 44. C. J. Holler, G. Taylor, Q. Deng, T. Kukar, Intracellular Proteolysis of Progranulin Generates Stable, Lysosomal
862 Granulins that Are Haploinsufficient in Patients with Frontotemporal Dementia Caused by GRN Mutations. *eNeuro* **4**
863 (2017).

864 45. M. Hutton, C. L. Lendon, P. Rizzu, M. Baker, S. Froelich, H. Houlden, S. Pickering-Brown, S. Chakraverty, A. Isaacs,
865 A. Grover, J. Hackett, J. Adamson, S. Lincoln, D. Dickson, P. Davies, R. C. Petersen, M. Stevens, E. de Graaff, E. Wauters,
866 J. van Baren, M. Hillebrand, M. Joosse, J. M. Kwon, P. Nowotny, L. K. Che, J. Norton, J. C. Morris, L. A. Reed, J.
867 Trojanowski, H. Basun, L. Lannfelt, M. Neystat, S. Fahn, F. Dark, T. Tannenberg, P. R. Dodd, N. Hayward, J. B. Kwok, P.
868 R. Schofield, A. Andreadis, J. Snowden, D. Craufurd, D. Neary, F. Owen, B. A. Oostra, J. Hardy, A. Goate, J. van Swieten,
869 D. Mann, T. Lynch, P. Heutink, Association of missense and 5'-splice-site mutations in tau with the inherited dementia
870 FTDP-17. *Nature* **393**, 702–5 (1998).

871 46. F. Lim, F. Hernández, J. J. Lucas, P. Gómez-Ramos, M. A. Morán, J. Ávila, FTDP-17 mutations in tau transgenic mice
872 provoke lysosomal abnormalities and Tau filaments in forebrain. *Mol Cell Neurosci* **18**, 702–714 (2001).

873 47. C. D. Pacheco, M. J. Elrick, A. P. Lieberman, Tau normal function influences Niemann-Pick type C disease pathogenesis
874 in mice and modulates autophagy in NPC1-deficient cells. *Autophagy* **5**, 548–550 (2009).

875 48. N. Ashtari, X. Jiao, M. Rahimi-Balaei, S. Amiri, S. E. Mehr, B. Yeganeh, H. Marzban, Lysosomal Acid Phosphatase
876 Biosynthesis and Dysfunction: A Mini Review Focused on Lysosomal Enzyme Dysfunction in Brain. *Curr Mol Med* **16**,
877 439–446 (2016).

878 49. Q. Zhang, Y. Meng, L. Zhang, J. Chen, D. Zhu, RNF13: a novel RING-type ubiquitin ligase over-expressed in pancreatic
879 cancer. *Cell Res* **19**, 348–357 (2009).

880 50. J. M. Berg, J. L. Tymoczko, L. Stryer, Biochemistry, Fifth Edition. Freeman W. H. And Company, Ed. (New York, ed.
881 5th, 2002).

882 51. M. L. Gorno-Tempini, A. E. Hillis, S. Weintraub, A. Kertesz, M. Mendez, S. F. Cappa, J. M. Ogar, J. D. Rohrer, S.
883 Black, B. F. Boeve, F. Manes, N. F. Dronkers, R. Vandenberghe, K. Rascovsky, K. Patterson, B. L. Miller, D. S. Knopman,
884 J. R. Hodges, M. M. Mesulam, M. Grossman, Classification of primary progressive aphasia and its variants. *Neurology* **76**,
885 1006–1014 (2011).

886 52. K. Rascovsky, J. R. Hodges, D. Knopman, M. F. Mendez, J. H. Kramer, J. Neuhaus, J. C. Van Swieten, H. Seelaar, E. G.
887 P. Dopper, C. U. Onyike, A. E. Hillis, K. A. Josephs, B. F. Boeve, A. Kertesz, W. W. Seeley, K. P. Rankin, J. K. Johnson,
888 M. L. Gorno-Tempini, H. Rosen, C. E. Prioleau-Latham, A. Lee, C. M. Kipps, P. Lillo, O. Piguet, J. D. Rohrer, M. N.
889 Rossor, J. D. Warren, N. C. Fox, D. Galasko, D. P. Salmon, S. E. Black, M. Mesulam, S. Weintraub, B. C. Dickerson, J.
890 Diehl-Schmid, F. Pasquier, V. Deramecourt, F. Lebert, Y. Pijnenburg, T. W. Chow, F. Manes, J. Grafman, S. F. Cappa, M.
891 Freedman, M. Grossman, B. L. Miller, Sensitivity of revised diagnostic criteria for the behavioural variant of frontotemporal
892 dementia. *Brain* **134**, 2456–2477 (2011).

893 53. M. J. Cardoso, R. Wolz, M. Modat, N. C. Fox, D. Rueckert, S. Ourselin, Geodesic information flows. *Med Image*
894 *Comput Comput Assist Interv* **15**, 262–270 (2012).

895 54. I. B. Malone, K. K. Leung, S. Clegg, J. Barnes, J. L. Whitwell, J. Ashburner, N. C. Fox, G. R. Ridgway, Accurate
896 automatic estimation of total intracranial volume: a nuisance variable with less nuisance. *Neuroimage* **104**, 366–372 (2015).

897 55. P. Langfelder, S. Horvath, WGCNA: An R package for weighted correlation network analysis. *BMC Bioinformatics* **9**,
898 1–13 (2008).

899 56. U. Raudvere, L. Kolberg, I. Kuzmin, T. Arak, P. Adler, H. Peterson, J. Vilo, g:Profiler: a web server for functional
900 enrichment analysis and conversions of gene lists (2019 update). *Nucleic Acids Res* **47**, W191–W198 (2019).
901

902

903

904

905

906

907

908

909

910

911

912

913

914

915

916

917

918

919

920

921

922

Acknowledgments

We thank Ida Pesämaa for discussions around the work with microglial activation-dependent markers, from which the published results were used as an external validation cohort of this study.

Funding

This work is supported by Race Against Dementia fellowship, supported by Alzheimer's Research UK (ARUK-RADF2021A-003 to AS-E). The UK Dementia Research Institute which receives its funding from DRI Ltd, funded by the UK Medical Research Council, Alzheimer's Society and Alzheimer's Research UK to AS-E. The Dementia Research Centre is supported by Alzheimer's Research UK, Alzheimer's Society, Brain Research UK, and The Wolfson Foundation.

Co-authors in the manuscript are supported by the Gothenburg Medical Society (Göteborgs Läkaresällskap, #GLS-988641 to JS). HZ is a Wallenberg Scholar and a Distinguished Professor at the Swedish Research Council supported by grants from the Swedish Research Council (#2023-00356; #2022-01018 and #2019-02397 to HZ), the European Union's Horizon Europe research and innovation programme under grant agreement No 101053962 to HZ, Swedish State Support for Clinical Research (#ALFGBG-71320 to HZ), the Alzheimer Drug Discovery Foundation (ADDF), USA (#201809-2016862 to HZ), the AD Strategic Fund and the Alzheimer's Association (#ADSF-21-831376-C, #ADSF-21-831381-C, #ADSF-21-831377-C, and #ADSF-24-1284328-C to HZ), the European Partnership on Metrology, co-financed from the European Union's Horizon Europe Research and Innovation Programme and by the Participating States (NEuroBioStand, #22HLT07 to HZ), the Bluefield Project, Cure Alzheimer's Fund, the Olav Thon Foundation, the Erling-Persson Family Foundation, Familjen Rönströms Stiftelse, Stiftelsen för Gamla Tjänarinnor, Hjärnfonden, Sweden (#FO2022-0270 to HZ), the European Union's Horizon 2020 research and innovation programme under the Marie Skłodowska-Curie grant agreement No 860197 (MIRIADE), the European Union Joint Programme – Neurodegenerative Disease Research (JPND2021-00694 to HZ), the National Institute for Health and Care Research University College London Hospitals Biomedical Research Centre, and the UK Dementia Research Institute at UCL (UKDRI-1003 to HZ).

950 KB is supported by the Swedish Research Council (#2017-00915 and #2022-00732 to KB), the
 951 Swedish Alzheimer Foundation (#AF-930351, #AF-939721 and #AF-968270 to KB), Hjärnfonden,
 952 Sweden (#FO2017-0243 and #ALZ2022-0006 to KB), the Swedish state under the agreement between
 953 the Swedish government and the County Councils, the ALF-agreement (#ALFGBG-715986 and
 954 #ALFGBG-965240 to KB), the European Union Joint Program for Neurodegenerative Disorders
 955 (JPND2019-466-236 to KB), the Alzheimer's Association 2021 Zenith Award (ZEN-21-848495 to
 956 KB), and the Alzheimer's Association 2022-2025 Grant (SG-23-1038904 QC to KB).
 957 JCVS was supported by the Dioraphte Foundation grant 09-02-03-00, Association for Frontotemporal
 958 Dementias Research Grant 2009, Netherlands Organization for Scientific Research grant HCM1 056-
 959 13-018, ZonMw Memorabel (Deltaplan Dementie, project number 733 051 042 to JCVS), Alzheimer
 960 Nederland and the Bluefield Project. FM received funding from the Tau Consortium and the Center
 961 for Networked Biomedical Research on Neurodegenerative Disease. RS-V is supported by
 962 Alzheimer's Research UK Clinical Research Training Fellowship (ARUK-CRF2017B-2 to RS-V) and
 963 has received funding from Fundació Marató de TV3, Spain (grant no. 20143810 to RS-V). DG
 964 received support from the EU Joint Programme-Neurodegenerative Disease Research and the Italian
 965 Ministry of Health (PreFrontALS) grant 733051042 to DG. CG received funding from EU Joint
 966 Programme-Neurodegenerative Disease Research -Prefrontals VR Dnr 529-2014-7504, VR 2015-
 967 02926 and 2018-02754 to CG, the Swedish FTD Initiative-Schörling Foundation, Alzheimer
 968 Foundation, Brain Foundation and Stockholm County Council ALF. MM has received funding from a
 969 Canadian Institute of Health Research operating grant and the Weston Brain Institute and Ontario
 970 Brain Institute. JBR has received funding from the Wellcome Trust (220258 to JBR), the Bluefield
 971 Project, and is supported by the Cambridge University Centre for Frontotemporal Dementia, the
 972 Medical Research Council (MC_UU_00030/14; MR/T033371/1) and the National Institute for Health
 973 Research Cambridge Biomedical Research Centre (NIHR203312).. EF has received funding from a
 974 Canadian Institute of Health Research grant #327387 to EF. RV has received funding from the Mady
 975 Browaeys Fund for Research into Frontotemporal Dementia. JL received funding for this work by the
 976 Deutsche Forschungsgemeinschaft German Research Foundation under Germany's Excellence
 977 Strategy within the framework of the Munich Cluster for Systems Neurology (EXC 2145 SyNergy—

ID 390857198 to JL). MO has received funding from Germany's Federal Ministry of Education and Research (BMBF). JDR is supported by the Bluefield Project and the National Institute for Health and Care Research University College London Hospitals Biomedical Research Centre and has received funding from an MRC Clinician Scientist Fellowship (MR/M008525/1 to JDR) and a Miriam Marks Brain Research UK Senior Fellowship. DA received funding by the Fondation Recherche Alzheimer, and the Swiss National Science Foundation (project CRSK-3_196354/1 to DA). JG is supported by Alzheimerfonden (AF-980746 to JG) and Stiftelsen för Gamla tjänarinnor (2022-01324 to JG). Several authors of this publication are members of the European Reference Network for Rare Neurological Diseases (ERN-RND) - Project ID No 739510 to JCVS, MS, RV, AdM, MO, RV and JDR. This work was also supported by the EU Joint Programme—Neurodegenerative Disease Research GENFI-PROX grant [2019-02248; to JDR, MO, BB, CG, JCVS and MS], and by the Clinician Scientist programme "PRECISE.net" funded by the Else Kröner-Fresenius-Stiftung (to CW, DM, and MS).

Authors contributions

AS-E, JDR and JG designed the study. SW, AS-E, and JS performed experiments. JG supervised the analytical study. SW analyzed the data, AS-E and JS assisted with data analyses as well as visualisation. AS-E, SW, and JS wrote the manuscript; JG, JDR, KB and HZ revised the manuscript and contributed to data interpretation. The rest of GENFI consortium authors have contributed with the recruitment of participants and processing of samples at their sites, as well as sending the samples and providing corresponding demographic data of their participants. All authors read and approved the final manuscript.

Conflicts of interest

HZ has served at scientific advisory boards and as a consultant for Abbvie, Acumen, Alector, Alzinova, ALZPath, Amylyx, Annexon, Apellis, Artery Therapeutics, AZTherapies, Cognito

1006 Therapeutics, CogRx, Denali, Eisai, LabCorp, Merry Life, Nervgen, Novo Nordisk, Optoceutics,
1007 Passage Bio, Pinteon Therapeutics, Prothena, Red Abbey Labs, reMYND, Roche, Samumed, Siemens
1008 Healthineers, Triplet Therapeutics, and Wave, has given lectures in symposia sponsored by Alzecure,
1009 Biogen, Cellectricon, Fujirebio, Lilly, Novo Nordisk, and Roche, and is a co-founder of Brain
1010 Biomarker Solutions in Gothenburg AB (BBS), which is a part of the GU Ventures Incubator
1011 Program (outside submitted work).
1012 KB has served as a consultant and at advisory boards for Acumen, ALZPath, BioArctic, Biogen,
1013 Eisai, Lilly, Moleac Pte. Ltd, Novartis, Ono Pharma, Prothena, Roche Diagnostics, and Siemens
1014 Healthineers; has served at data monitoring committees for Julius Clinical and Novartis; has given
1015 lectures, produced educational materials and participated in educational programs for AC Immune,
1016 Biogen, Celdara Medical, Eisai and Roche Diagnostics; and is a co-founder of Brain Biomarker
1017 Solutions in Gothenburg AB (BBS), which is a part of the GU Ventures Incubator Program, outside
1018 the work presented in this paper.
1019 MS has received consultancy honoraria from Ionis, UCB, Prevail, Orphazyme, Biogen, Servier,
1020 Reata, GenOrph, AviadoBio, Biohaven, Zevra, Lilly, and Solaxa, all unrelated to the present
1021 manuscript. JBR has provided consultancy or advisory board input to Alector, Asceneuron,
1022 Astronautx, Astex, CumulusNeuro, Cerevance, Clinical Ink, Curasen, Eisai, WAVE, unrelated to the
1023 current work. SD has provided paid consultancy to QuRALIS, Eisai, Eli Lilly and has received
1024 speaker fees from Eisai. SD is a SDMB member of Aviado Bio, IntelGenX. RV's institution has a
1025 clinical trial agreement (RV as PI) with Alector, AviadioBio, Denali, EliLilly, J&J, UCB. RV's
1026 institution has a consultancy agreement (RV as DSMB chair) with AC Immune. LR is a consultant for
1027 Prevail Therapeutics.

1028

1029 **Data and materials availability**

1030 All data associated with this study are present in the paper or supplementary materials. Proteomic data
1031 underlying the results of this study have been deposited in the Dryad repository (DOI:
1032 [10.5061/dryad.r7sqv9snk](https://doi.org/10.5061/dryad.r7sqv9snk)). Individual identifiers have not been included to protect the privacy of
1033 study participants but can be requested from the authors. No custom code was used for data analysis;

1034 respective R packages have been indicated where applicable. The data used for external validation of
 1035 the *GRN* results as well as for AD-FTD comparisons are publicly available in the supplementary
 1036 sections of the respective publications by Pesämaa *et al.*, Tijms *et al.* and Higginbotham *et al.*
 1037
 1038 In addition to members of GENFI who are co-authors, the following members are collaborators who
 1039 have contributed to the study design, data analysis, and interpretation: David L Thomas², Thomas
 1040 Cope⁴¹, Timothy Rittman⁴¹, Alberto Benussi⁴⁶, Enrico Premi⁴⁷, Roberto Gasparotti⁴⁶, Silvana
 1041 Archetti⁴⁷, Stefano Gazzina⁴⁷, Valentina Cantoni⁴⁶, Andrea Arighi^{10, 11}, Chiara Fenoglio^{10, 11}, Elio
 1042 Scarpini^{10, 11}, Giorgio Fumagalli^{10, 11}, Vittoria Borracci^{10, 11}, Giacomina Rossi¹⁶, Giorgio Giaccone¹⁶,
 1043 Giuseppe Di Fede¹⁶, Paola Caroppo¹⁶, Pietro Tiraboschi¹⁶, Sara Prioni¹⁶, Veronica Radaelli¹⁶, David
 1044 Tang-Wai⁵⁴, Ekaterina Rogaeva³⁹, Michel Castelo-Branco¹⁷, Morris Freedman⁵⁵, Ron Keren⁵⁴, Sandra
 1045 Black⁴⁰, Sara Mitchell⁴⁰, Christen Shoesmith³⁸, Robart Bartha^{56, 57}, Rosa Rademakers⁵⁸, Jackie Poos⁵,
 1046 Janne M. Papma⁵, Lucia Giannini⁵, Rick van Minkelen⁵⁹, Yolande Pijnenburg⁶⁰, Benedetta Nacmias⁶¹,
 1047 Camilla Ferrari⁶¹, Cristina Polito⁶², Gemma Lombardi⁶¹, Valentina Bessi⁶¹, Michele Veldsman³³,
 1048 Christin Andersson⁶³, Hakan Thonberg⁸, Linn Öijerstedt^{8, 9}, Vesna Jelic⁶⁴, Paul Thompson¹⁹, Tobias
 1049 Langheinrich^{19, 65}, Abert Lladó⁶, Anna Antonell⁶, Jaume Olives⁶, Mircea Balasa⁶, Nuria Bargalló⁶⁶,
 1050 Sergi Borrego-Écija⁶, Ana Verdelho⁶⁷, Carolina Maruta⁶⁸, Catarina B. Ferreira⁶⁹, Gabriel
 1051 Miltenberger¹⁵, Frederico Simões do Couto⁷⁰, Alazne Gabilondo^{44, 45}, Jorge Villanua⁷¹, Marta
 1052 Cañada⁷², Mikel Tainta⁴⁵, Miren Zulaica⁴⁵, Myriam Barandiaran^{44, 45}, Patricia Alves^{45, 73}, Benjamin
 1053 Bender⁷⁴, Carlo Wilke^{42, 43}, Lisa Graf⁴², Annick Vogels⁷⁵, Mathieu Vandenbulcke^{76, 77}, Philip van
 1054 Damme^{13, 78}, Rose Buffaerts^{79, 80}, Koen Poesen⁸¹, Pedro Rosa-Neto⁸², Serge Gauthier⁸³, Agnès
 1055 Camuzat³⁵, Alexis Brice^{35, 36}, Anne Bertrand^{35, 84, 85}, Aurélie Funkiewicz^{35, 36}, Daisy Rinaldi^{35, 36}, Dario
 1056 Saracino^{35, 36}, Olivier Colliot^{35, 84}, Sabrina Sayah³⁵, Catharina Prix²¹, Elisabeth Wlasich²¹, Olivia
 1057 Wagemann²¹, Sandra Loosli²¹, Sonja Schönecker²¹, Tobias Hoegen²¹, Jolina Lombardi²⁶, Sarah
 1058 Anderl-Straub²⁶, Adeline Rollin³⁰, Gregory Kuchcinski^{28, 30}, Maxime Bertoux^{29, 30}, Thibaud
 1059 Lebouvier^{28, 29, 30}, Vincent Deramecourt^{28, 29, 30}, Beatriz Santiago¹⁷, Diana Duro¹⁷, Maria João Leitão¹⁸,
 1060 Maria Rosario Almeida¹⁷, Miguel Tábuas-Pereira¹⁷, Sónia Afonso⁸⁶.
 1061 Affiliations 1 to 53 can be found on the first page of the paper.

1062 ⁵⁴The University Health Network, Krembil Research Institute, M5T 0S8, Toronto, Canada

1063 ⁵⁵Baycrest Health Sciences, Rotman Research Institute, University of Toronto, M5S 3E6, Toronto,

1064 Canada

1065 ⁵⁶Department of Medical Biophysics, The University of Western Ontario, N6A 5C1, London, Ontario,

1066 Canada

1067 ⁵⁷Centre for Functional and Metabolic Mapping, Robarts Research Institute, The University of

1068 Western Ontario, N6A 5B7, London, Ontario, Canada

1069 ⁵⁸Center for Molecular Neurology, University of Antwerp, 2650, Edegem, Belgium

1070 ⁵⁹Department of Clinical Genetics, Erasmus Medical Center, 3000, Rotterdam, Netherlands

1071 ⁶⁰Amsterdam University Medical Centre, Amsterdam VUmc, 1081 HV, Amsterdam, Netherlands

1072 ⁶¹Department of Neuroscience, Psychology, Drug Research and Child Health, University of Florence,

1073 50139, Florence, Italy

1074 ⁶²Department of Biomedical, Experimental and Clinical Sciences “Mario Serio”, Nuclear Medicine

1075 Unit, University of Florence, 50139, Florence, Italy

1076 ⁶³Department of Clinical Neuroscience, Karolinska Institutet, Stockholm, 171 65, Solna, Sweden

1077 ⁶⁴Division of Clinical Geriatrics, Karolinska Institutet, Stockholm, 171 65, Solna, Sweden

1078 ⁶⁵Manchester Centre for Clinical Neurosciences, Department of Neurology, Salford Royal NHS

1079 Foundation Trust, M6 8HD, Manchester, UK

1080 ⁶⁶Imaging Diagnostic Center, Hospital Clínic, 08036, Barcelona, Spain

1081 ⁶⁷Department of Neurosciences and Mental Health, Centro Hospitalar Lisboa Norte - Hospital de

1082 Santa Maria & Faculty of Medicine, University of Lisbon, 1649-028, Lisbon, Portugal

1083 ⁶⁸Laboratory of Language Research, Centro de Estudos Egas Moniz, Faculty of Medicine, University

1084 of Lisbon, 2829 – 511, Lisbon, Portugal

1085 ⁶⁹Laboratory of Neurosciences, Faculty of Medicine, University of Lisbon, 1649-028, Lisbon,

1086 Portugal

1087 ⁷⁰Faculdade de Medicina, Universidade Católica Portuguesa, 2635-631, Rio de Mouro, Portugal

1088 ⁷¹OSATEK, University of Donostia, San Sebastian, 20014, Gipuzkoa, Spain

1089 ⁷²CITA Alzheimer, San Sebastian, 20009, Gipuzkoa, Spain

1090 ⁷³Department of Educational Psychology and Psychobiology, Faculty of Education, International
1091 University of La Rioja, 26006, Logroño, Spain

1092 ⁷⁴Department of Diagnostic and Interventional Neuroradiology, University of Tübingen, 72074,
1093 Tübingen

1094 ⁷⁵Department of Human Genetics, KU Leuven, 3000, Leuven, Belgium

1095 ⁷⁶Geriatric Psychiatry Service, University Hospitals Leuven, 3000, Leuven, Belgium

1096 ⁷⁷Neuropsychiatry, Department of Neurosciences, KU Leuven, 3000, Leuven, Belgium

1097 ⁷⁸Laboratory for Neurobiology, VIB-KU Leuven Centre for Brain Research, 3000, Leuven, Belgium

1098 ⁷⁹Department of Biomedical Sciences, University of Antwerp, 2000, Antwerp, Belgium

1099 ⁸⁰Biomedical Research Institute, Hasselt University, 3500 Hasselt, Belgium

1100 ⁸¹Laboratory for Molecular Neurobiomarker Research, KU Leuven, 3000, Leuven, Belgium

1101 ⁸²Translational Neuroimaging Laboratory, McGill Centre for Studies in Aging, McGill University,
1102 H3A 2B4, Montreal, Québec, Canada

1103 ⁸³Alzheimer Disease Research Unit, McGill Centre for Studies in Aging, Department of Neurology &
1104 Neurosurgery, McGill University, H4H 1R2, Montreal, Québec, Canada

1105 ⁸⁴Inria, Aramis project-team, 75013, Paris, France

1106 ⁸⁵Centre pour l'Acquisition et le Traitement des Images, Institut du Cerveau et la Moelle, 75013, Paris,
1107 France

1108 ⁸⁶Instituto Ciencias Nucleares Aplicadas a Saude, Universidade de Coimbra, 3000-548, Coimbra,
1109 Portugal

1110

1111

1112

1113

1114

1115

1116

Figures and tables

Tables

Table 1. Baseline demographic characteristics of the GENFI cohort. Abbreviations: MMSE, mini mental state examination; FTLD-CDR-SOB, frontotemporal lobar degeneration national Alzheimer's disease coordinating centre + clinical dementia rating sum of boxes; NfL, neurofilament light.

Characteristic	Overall, N = 238 ¹	Non-carrier, N = 76 ¹	Presymptomatic <i>C9orf72</i> , N = 44 ¹	Presymptomatic <i>GRN</i> , N = 38 ¹	Presymptomatic <i>MAPT</i> , N = 25 ¹	Symptomatic <i>C9orf72</i> , N = 27 ¹	Symptomatic <i>GRN</i> , N = 17 ¹	Symptomatic <i>MAPT</i> , N = 11 ¹	P-value ²
Age, years	48 (38, 58)	43 (38, 53)	43 (33, 50)	50 (37, 56)	42 (33, 46)	58 (55, 70)	64 (58, 67)	63 (59, 66)	<0.001
Sex, male	108 (45%)	33 (43%)	19 (43%)	18 (47%)	9 (36%)	16 (59%)	8 (47%)	5 (45%)	0.8
Education, years	15 (12, 16)	15 (12, 17)	14 (12, 16)	15 (13, 16)	15 (13, 16)	13 (11, 14)	14 (9, 15)	13 (12, 16)	0.019
Plasma NfL, pg/mL	8 (6, 15)	7 (5, 10)	8 (6, 10)	8 (5, 10)	6 (5, 9)	40 (21, 55)	44 (37, 69)	20 (18, 23)	<0.001
MMSE	30.0 (28.0, 30.0)	30.0 (29.0, 30.0)	30.0 (29.0, 30.0)	30.0 (29.0, 30.0)	30.0 (29.0, 30.0)	26.0 (20.3, 28.8)	23.0 (20.5, 28.0)	24.5 (17.8, 27.0)	<0.001
CDR FTLD SOB	0.0 (0.0, 1.0)	0.0 (0.0, 0.0)	0.0 (0.0, 0.5)	0.0 (0.0, 0.0)	0.0 (0.0, 0.5)	11.5 (4.8, 15.5)	10.0 (4.8, 13.0)	7.5 (3.3, 10.6)	<0.001

¹ Median (IQR); n (%)

² Kruskal-Wallis rank sum test; Fisher's exact test

Figure Legends

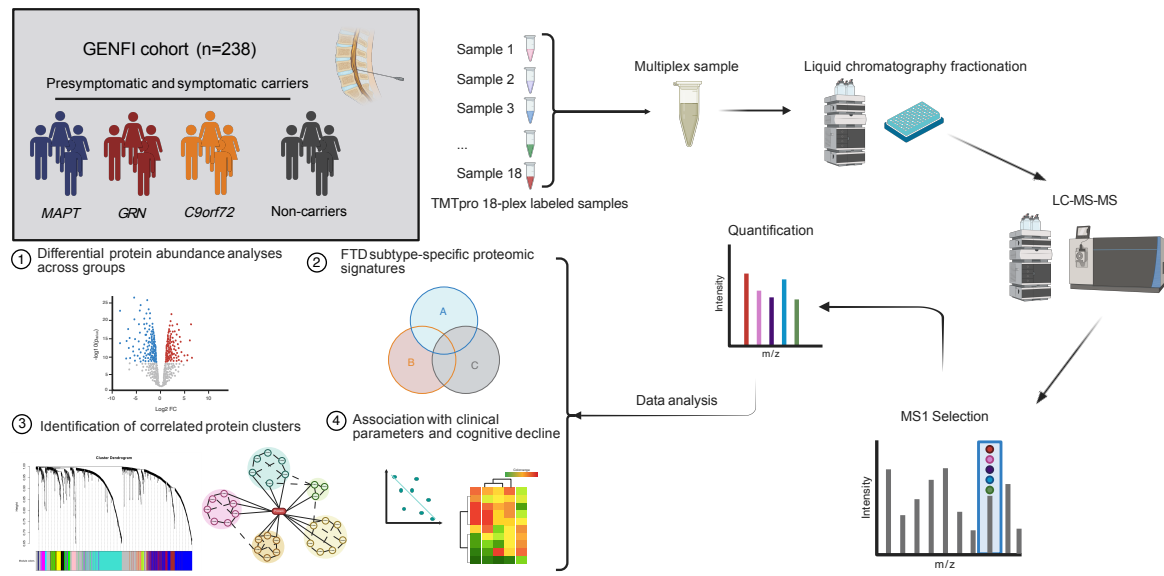


Fig. 1. Key information about participants, proteomics workflow and data analysis.

This figure shows the TMT tandem mass spectrometry (MS/MS) proteomics workflow, in which samples were pre-processed and labelled with 18 different isobaric TMTpro tags (TMTpro 18-plex) and combined into multiplex samples to allow for relative quantification and simultaneous analysis of the 18 individual samples. This process was then repeated until all 238 samples were labelled with isobaric tags. Next, each multiplex sample was fractionated using offline high-pH liquid chromatography (HP-LC) to reduce sample complexity, and each fraction was subsequently analyzed by LC-MS/MS. The data analysis conceptually consisted of four steps: 1) Investigating differences in protein abundances in mutation carriers compared with non-carriers and 2) determining FTD-subtype specific proteomic signatures employing linear models, 3) protein network analysis to investigate mutation and pathology-specific pathophysiological features as well as finally 4) correlating these protein clusters with clinical parameters and cognitive decline to discern clinically relevant changes. Abbreviations: TMT, tandem mass tag; FTD, frontotemporal dementia; MS, mass spectrometry; *MAPT*, microtubule associated protein tau; *GRN*, progranulin; *C9orf72*, chromosome 9 open reading frame 72; GENFI, GENetic Frontotemporal dementia Initiative.

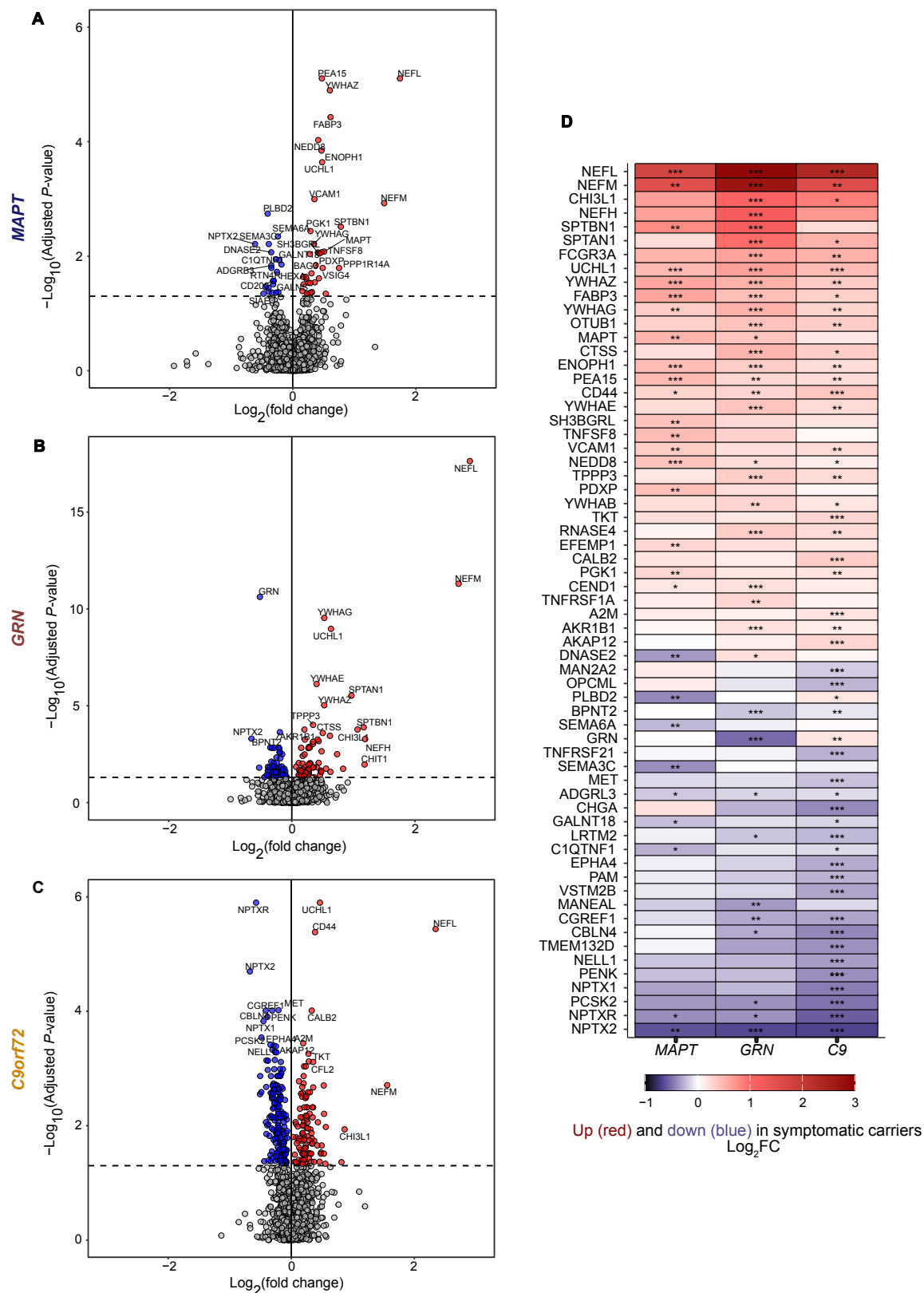


Fig. 2. Volcano plots and heat map displaying top protein hits in symptomatic mutation carriers vs non-carriers.

(A – C) Volcano plots showing proteomic differences in symptomatic *MAPT* (A), *GRN* (B) and *C9orf72* (C) mutation carriers based on linear regression analysis with age and sex as covariates. Differences were considered significant if Benjamini-Hochberg (false discovery rate [FDR]) adjusted *P*-values were <0.05. (D) The heatmap displays the 25 proteins in each group that had the lowest FDR-adjusted *P*-values in linear regression analysis, resulting in 62 proteins when accounting for overlapping proteins among groups. The log₂ fold abundance change between non-carriers and the respective mutation carrier group is colour-coded; proteins higher or lower in abundance in symptomatic mutation carriers vs. non-carriers are shown in red and blue, respectively. Note that not all proteins listed in D were significantly altered in all groups. * $P_{adjust} < 0.05$, ** $P_{adjust} < 0.01$, *** $P_{adjust} < 0.001$. Details on exact *P*-values and log₂ fold change can be found in Table S1A-S1C.

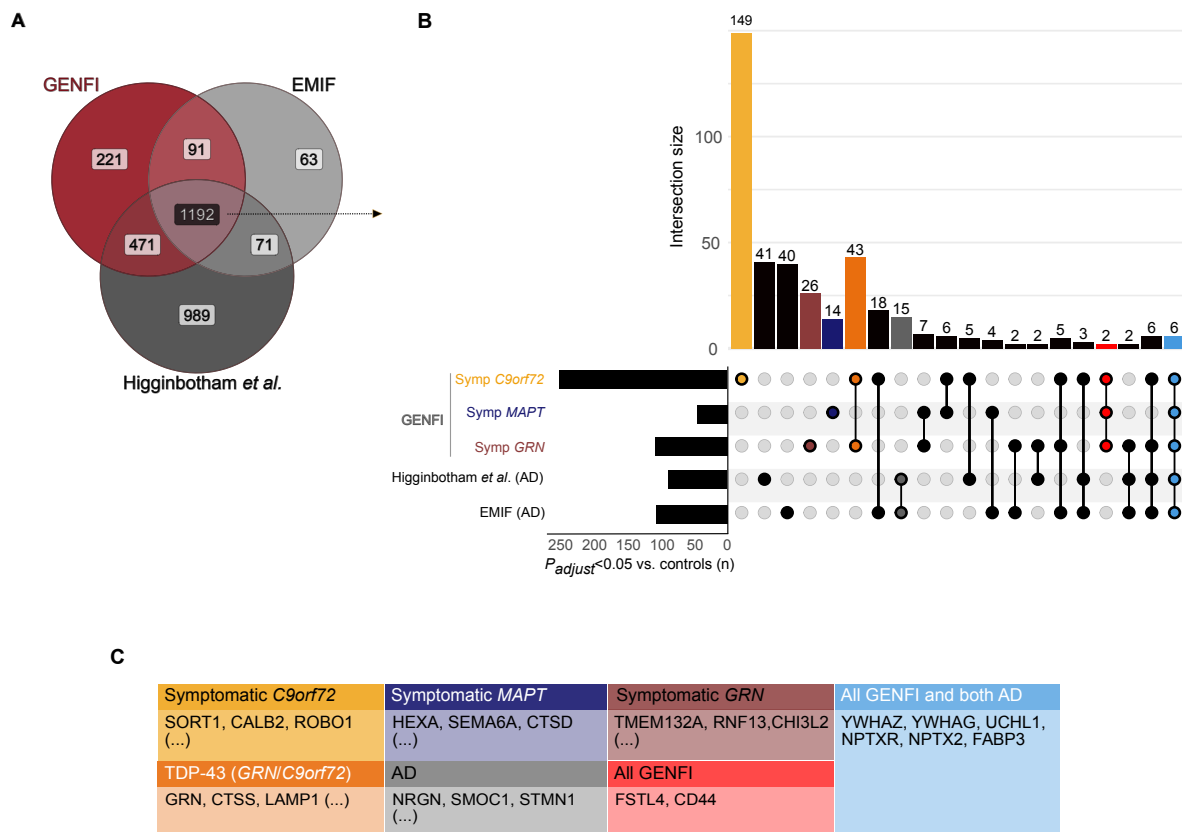


Fig. 3. Cross cohort comparisons of symptomatic genetic FTD with AD.

(A) Venn diagram with proteins measured in GENFI, the EMIF cohort (25) and Higginbotham *et al.* (28). The overlap (n=1192) represents proteins quantified in all studies. (B) Upset plot of differentially expressed proteins (FDR-adjusted $P < 0.05$) for symptomatic *C9orf72*, *MAPT*, *GRN* mutation carriers and for patients with AD from the Higginbotham and EMIF cohort. The upper, vertical bars show the number of differentially expressed proteins exclusive to one patient group or shared between groups. The left horizontal bars represent the total number of proteins with $P_{\text{adjust}} < 0.05$ comparing each group with control individuals. Intersections of clinical interest are color-coded. Intersections only containing 1 protein are not displayed in the figure. (C) Selection of proteins in intersections from the upset plot in panel B that are of clinical interest, as well as proteins specifically altered in one group. Proteins included in each of these intersections, as well as those not displayed, can be found in Table S5. Abbreviations: GENFI, GENetic Frontotemporal dementia Initiative; EMIF, European Medical Information Framework; AD, Alzheimer's disease.

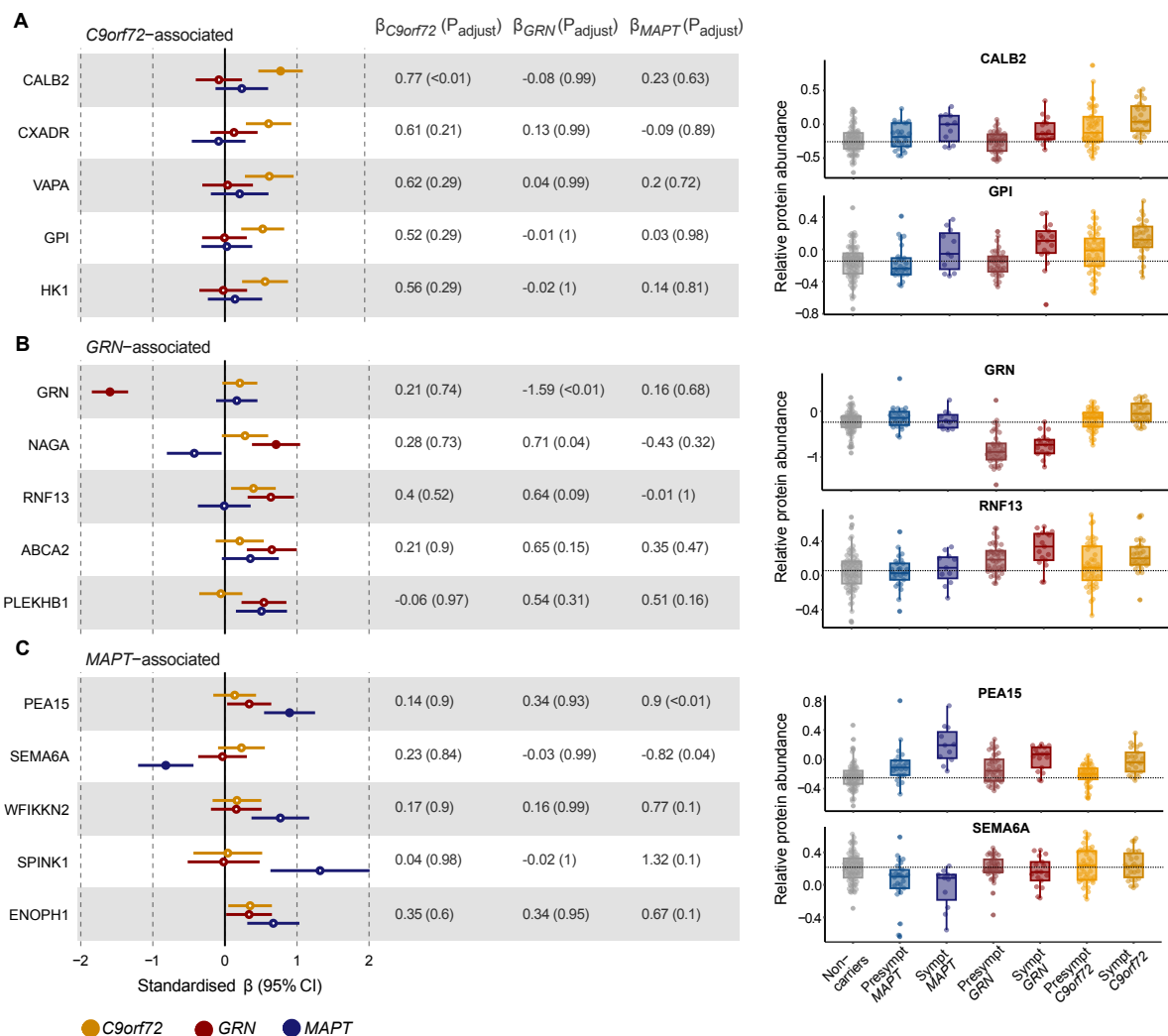
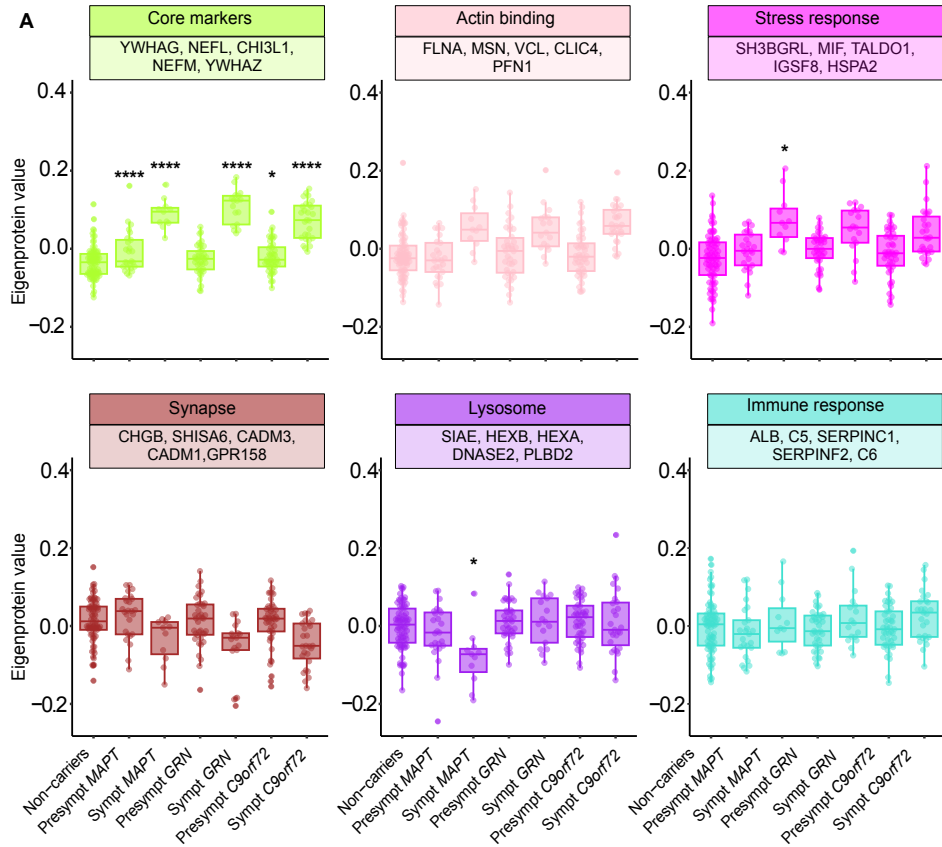


Fig. 4. Identification of mutation-associated proteins. (A to C) Left: Forest plots of the top five proteins most strongly associated with *C9orf72* (A), *GRN* (B), and *MAPT* (C) mutation. For the identification of mutation-associated proteins, linear models were fitted testing the effect of mutation carrier group on protein abundance, including affection (presence/absence of symptoms) as well as age and sex as covariates. Non-carriers served as reference group. Coefficients with an adjusted $P < 0.05$ are depicted as coloured points and 95% CI were added. Standardised β estimates including corresponding Benjamini-Hochberg-adjusted P -values for each association and mutation group were reported. Right: Boxplots of two manually selected proteins across the entire cohort. The dotted line denotes the median log₂-transformed protein abundance value of the non-carrier group. Abbreviations: CI, confidence interval.



B

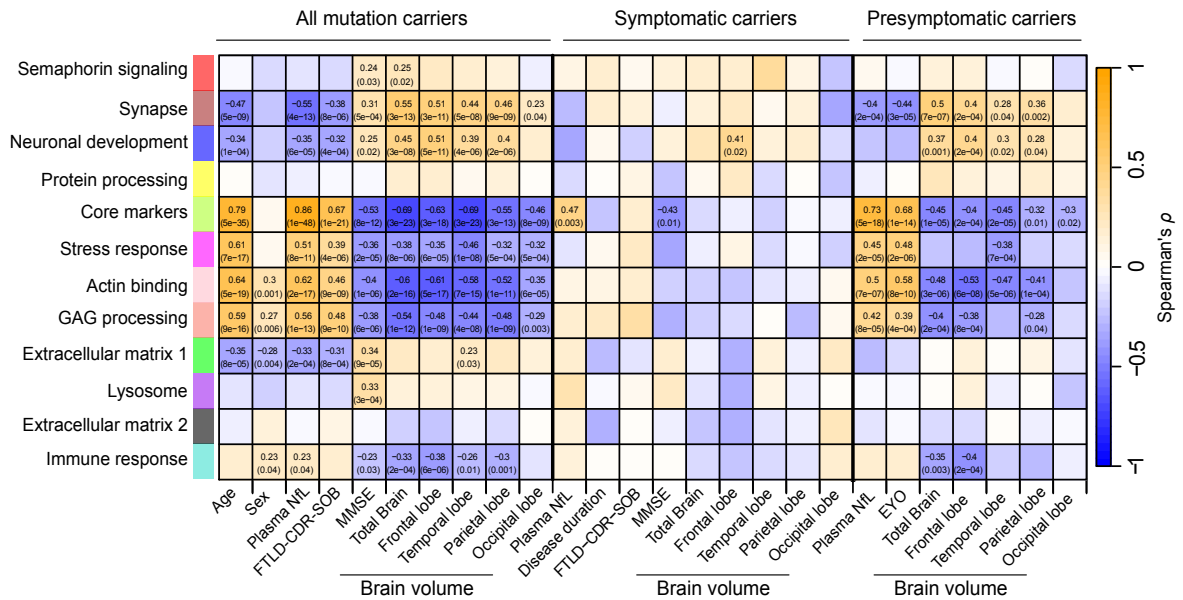


Fig.5. Weighted gene co-expression network modules show mutation/pathology-specific changes and correlate with relevant clinical parameters.

(A) Employing Weighted gene co-expression network analysis (WGCNA), we identified 14 distinct highly correlated modules of proteins. For this figure, six modules of particular interest were selected

and their Eigenprotein values were plotted across the entire cohort: ‘Core markers’, ‘Actin binding’, ‘Stress response’, ‘Synapse’, ‘Lysosome’, ‘Immune response’. Modules were named in accordance with gene ontology (GO) terms mapped to their constituent proteins. Framed boxes contain the names of the top five hub proteins of each module, as determined by having the highest module membership value (kME). *P*-values for respective group comparisons vs. non-carriers are derived from linear regression analyses with post hoc Tukey’s honestly significant difference (HSD) to adjust for multiplicity. Boxplots of the remaining modules can be found in Fig. S24. * $P < 0.05$, ** $P < 0.01$, *** $P < 0.001$, **** $P < 0.0001$. **(B)** Heatmap of correlation parameters of module Eigenproteins with different clinical measures. Spearman’s rho values are colour-coded, and the corresponding Bonferroni-corrected *P*-values are included in parentheses for each tile. To evaluate the association of protein modules with clinical parameters at different time points of the disease continuum, correlations were performed in an indicated subset of individuals only. Abbreviations: FTLD-CDR-SOB, frontotemporal lobar degeneration clinical dementia rating sum of boxes; EYO, estimated years to disease onset; GAG, Glycosaminoglycan; MMSE, Mini Mental State Examination.

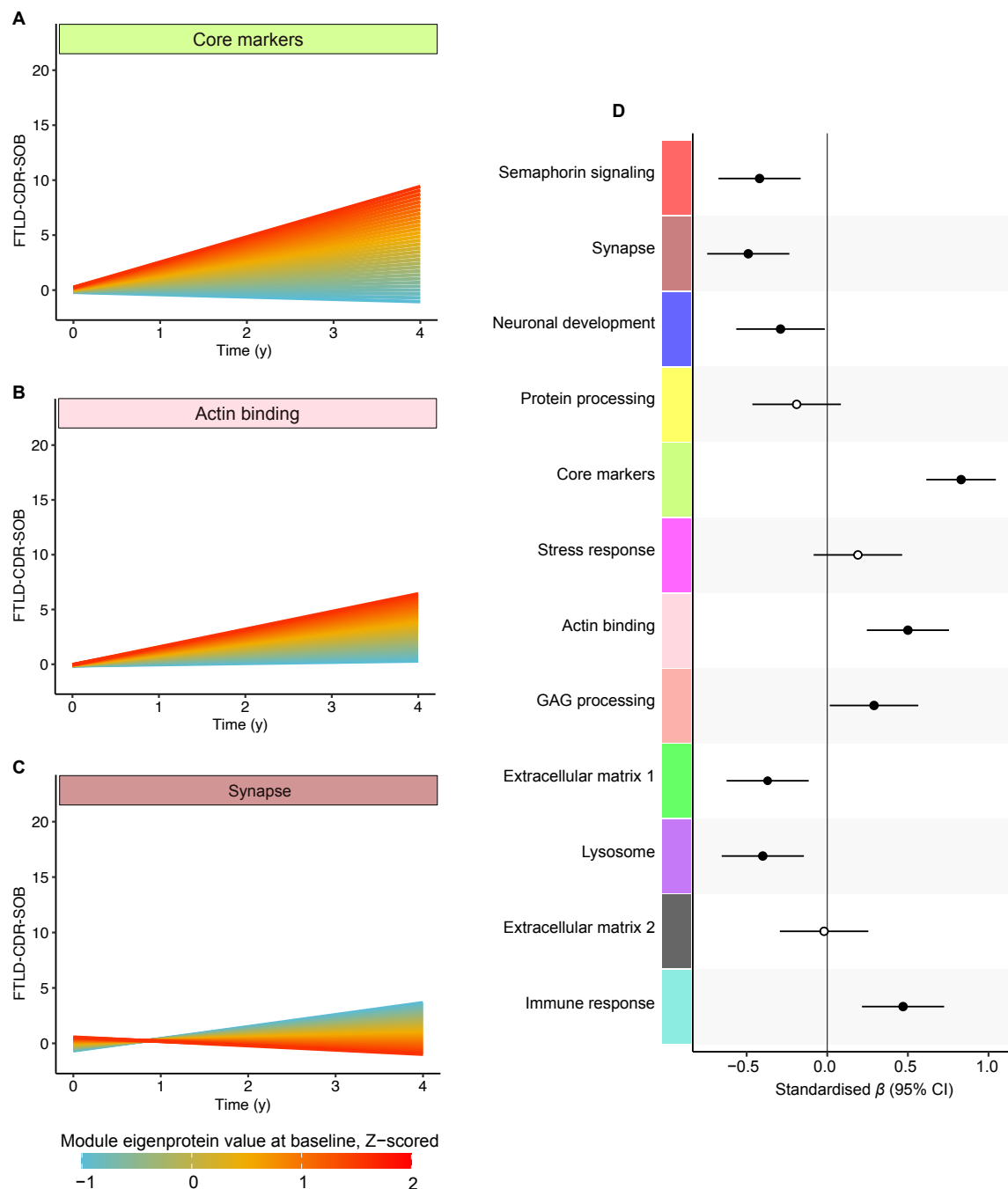


Fig 6. Weighted gene co-expression network modules predict cognitive change in genetic FTD.

The plots show estimates of the fixed effect (standardised module Eigenprotein value*time in years from baseline) of linear mixed effects models with FTL-D-CDR-SOB as dependent variable in mutation carriers (n=146). The models included standardised Eigenprotein values*time, age, sex, years of education and affection at baseline (presymptomatic/symptomatic) as independent variables. Panels (A-C) Estimates of ME values for ‘Core biomarkers’ (A), ‘Actin binding’ (B), and ‘Synapse’ (C)

1246 modules from separate models. The colours visualise the estimated cognitive trajectories at Z-scored
1247 baseline Eigenprotein values ranging from -1 to 2 SD from the mean. (D) Forest plot of the standardised
1248 β estimates and 95% CI of each module Eigenprotein value*time. The filled points denote statistically
1249 significant ($P<0.05$) interaction terms.

1250

1251

1252

1253

1254

1255

1256

1257

1258

1259

1260

1261

1262

1263

1264

1265

1266

1267

1268

1269

1270

1271

1272

Supplementary Materials for

Proteomic analysis reveals distinct cerebrospinal fluid signatures across genetic frontotemporal dementia subtypes

Sogorb-Esteve A, Weiner S and Simrén J *et al.*

The PDF file includes:

Supplementary methods

Supplementary Figures S1-S25

References 53-56

Other Supplementary Material for this manuscript includes the following:

Supplementary data file – Tables S1-S10

Reproducibility checklist

Supplementary Methods

Fluid, imaging and cognitive biomarker collection and processing.

Participants also had plasma samples collected as part of the GENFI protocol. Plasma was collected, processed, and stored in aliquots at -80°C according to standardised procedures. Plasma neurofilament light chain (NfL) levels were correlated (Spearman's correlation) with TMT relative reporter ion intensities of CSF NfL (n=163). Plasma NfL concentration was measured with Single molecule array (Simoa) technology using the Neurology 4-Plex A kit (Quanterix, Billerica, USA) on an HD-X Analyzer following the manufacturer's instructions (Quanterix, Billerica, USA). Measurements were completed in duplicate (all CVs below 15%) over a total of 3 batches, each with an 8-point calibration curve tested in triplicate and 2 controls tested in duplicate, as reported before (7).

In addition, TMT tryptic peptide measurements of the synaptic proteins 14-3-3 epsilon ([R].IISIEQK.[E], n=119), neuronal pentraxin 2 ([K].VAELEDEK.[S], n=181) and neuronal pentraxin receptor ([R].NNYMYAR.[V], n=169) were correlated with corresponding tryptic peptide measurements as performed in the publication Sogorb-Esteve et al, 2020 (26). In brief, to 100 µL of CSF, a mixture of stable-isotope-labeled peptides (internal standard) was added (25 µL, 0.032 pmol/µL, JPT Peptide Technologies, Berlin, Germany; SpikeTides L). This was then followed by a stepwise protocol of reduction, alkylation, and tryptic digestion, and lastly solid-phase extraction for purification purposes. LC-MS/MS analysis was performed using a microflow HPLC, equipped with a Hypersil Gold reversed-phase column (100 × 2.1 mm, particle size 1.9 µm, Thermo Fisher Scientific), and a Triple Quadrupole mass spectrometer (6495 Triple Quadrupole LC/MS system, Agilent Technologies). To monitor the performance of the assay over time, quality control (QC) sample replicates were injected at regular intervals during runs. The panel of synaptic markers included: AP-2 complex subunit beta, complexin-2, beta-synuclein, gamma-

1316 synuclein, 14-3-3 proteins (eta, epsilon, zeta/delta), neurogranin, Rab GDP dissociation
1317 inhibitor alpha (Rab GDI alpha), syntaxin-1B, syntaxin-7, phosphatidylethanolamine-binding
1318 protein 1 (PEBP-1), neuronal pentraxin receptor (NPTXR), neuronal pentraxin 1 (NPTX1),
1319 and neuronal pentraxin 2 (NPTX2).

1320 Volumetric T1-weighted MRI scans were bias field corrected and parcellated using the
1321 geodesic information flow algorithm (53). From this parcellation, the volumes of the bilateral
1322 frontal, temporal, parietal and occipital cortices and of the whole brain were extracted and
1323 expressed as a percentage of the total intracranial volume, which was computed with SMP12
1324 v6470 (Statistical Parametric Mapping, Wellcome Trust Centre for Neuroimaging, London,
1325 UK) running under Matlab R201b (Math Works, Natick, MA, USA) (54).

1326 The standardized GENFI clinical assessment included a history, examination, cognitive
1327 assessment (including Mini-Mental State Examination [MMSE]), FRS, and the CDR plus
1328 NACC FTLD rating scale. Mutation carriers were classified into asymptomatic, prodromal,
1329 or symptomatic if they scored 0, 0.5, or ≥ 1 , respectively, on the CDR plus NACC FTLD
1330 global score. As part of the GENFI clinical assessment, the CDR plus NACC FTLD was
1331 administered as per standard protocol (interviewing both the participant and an informant
1332 separately) including the core cognitive and functional domain items from the CDR
1333 (memory, orientation, judgment and problem solving, community affairs, hobbies, personal
1334 care), and the two-clinician judgment (global) scores from the NACC FTLD for behavior and
1335 language.

1336

1337 *Data processing and normalisation*

1338 All RAW files were processed using Proteome Discoverer Version 2.5.0.400 (Thermo
1339 Scientific). The most confident centroid integration method with an integration tolerance of
1340 20 ppm was employed to perform peak integration for reporter ion quantification. Peptides

1341 were identified searching against the UniProtKB Swiss-Prot (TaxID = 9606, Homo sapiens)
 1342 database utilising the SequestHT search engine with search parameters specified as follows:
 1343 precursor Δm tolerance = 5 ppm, fragment Δm tolerance = 0.02 Da, missed cleavages = 2,
 1344 min. peptide length = 6, fixed modifications = carbamidomethyl, TMTpro (peptide N-
 1345 terminus, K residues). Percolator was used for peptide scoring, filtering peptide spectral
 1346 matches and peptides to a false discovery rate (FDR) of <1%. Peptides were then assembled
 1347 into proteins based on their uniqueness (unique peptides). In the event of redundancy,
 1348 peptides were assigned to a protein sequence in accordance with the principle of parsimony
 1349 (razor peptides).
 1350 For data normalisation, individual protein abundances were divided by their corresponding
 1351 set-wise global internal standard (GIS) protein measurement. Each obtained protein ratio was
 1352 then additionally divided by the respective sample median, accounting for aberrant
 1353 differences in total protein amount. Finally, all data was transformed into a log₂-space.
 1354 Potential batch effects and sample outliers were assessed by performing a principal
 1355 component (PCA) analysis (Fig. S25) and hierarchical clustering considering all sample-wise
 1356 protein abundances.
 1357
 1358 *Weighted gene co-expression network analysis (WGCNA) and correlation with clinical*
 1359 *parameters*
 1360 Weighted gene co-expression networks were constructed using the R package *WGCNA* (55).
 1361 Due to the limited sample sizes of individual diagnostic groups, a network including all
 1362 samples of the present cohort was built. Following the removal of proteins with missing
 1363 values in >50% of all study participants, the optimal soft threshold power was chosen as the
 1364 power at which scale free topology R^2 approached an asymptote at around 0.9 and the mean
 1365 and median connectivity were <100. A signed network was built using the

1366 WGCNA::blockwiseModules function with the following settings: soft threshold power = 14,
1367 deepSplit = 4, corType = bicor, minModuleSize = 10, mergeCutHeight = 0.2,
1368 pamRespectsDendro TRUE, pamStage TRUE, maxPOutliers $p < 0.05$, reassignThreshold =
1369 0.05. In brief, a robust correlation metric insensitive to outliers (bicor) is used to compute the
1370 correlation between all pairs of proteins. Next, the resulting correlation matrix is transformed
1371 into an adjacency matrix raising the co-expression similarities to the determined soft
1372 threshold power. The adjacency matrix is then used to construct a topological overlap matrix
1373 (TOM), reflecting the relative interconnectedness of each protein. Finally, hierarchical
1374 protein clustering is performed on the corresponding topological overlap dissimilarity
1375 measure (1-TOM), resulting in module construction via dynamic tree cutting. A total of 14
1376 modules could be identified, including a grey module (645 proteins) containing proteins that
1377 could not be assigned to any of the modules and a module containing contaminants from the
1378 laboratory environment (tan module). In a next step, module Eigenproteins corresponding to
1379 the module's first principal component were identified. Protein module membership kME
1380 was determined by performing Pearson correlation of each protein with each module
1381 Eigenprotein. Proteins with a kME > 0.7 were considered as the module's respective hub
1382 proteins. Module Eigenproteins of different subsets of the cohort (presymptomatic and/or
1383 symptomatic mutation carriers) were correlated (Spearman rank-order correlation) with
1384 clinical parameters. Significance levels were adjusted with Bonferroni correction to account
1385 for multiple testing. To investigate the prognostic properties of module Eigenprotein values
1386 in mutation carriers, separate linear mixed effects models for each module Eigenprotein value
1387 were fitted including only mutation carriers (both symptomatic and presymptomatic carriers)
1388 with cognitive score (FTLD-NACC+CDR-SOB) as dependent variable. Fixed effects
1389 included the interaction of module Eigenprotein value*time (years since baseline), with age,
1390 sex, years of education and cognitive status (symptomatic or presymptomatic) as covariates.

1391 All models included random intercepts and slopes for each participant. To enable
1392 comparability between models, module Eigenprotein values were standardised. These
1393 analyses were performed using the *lme4* package in R.

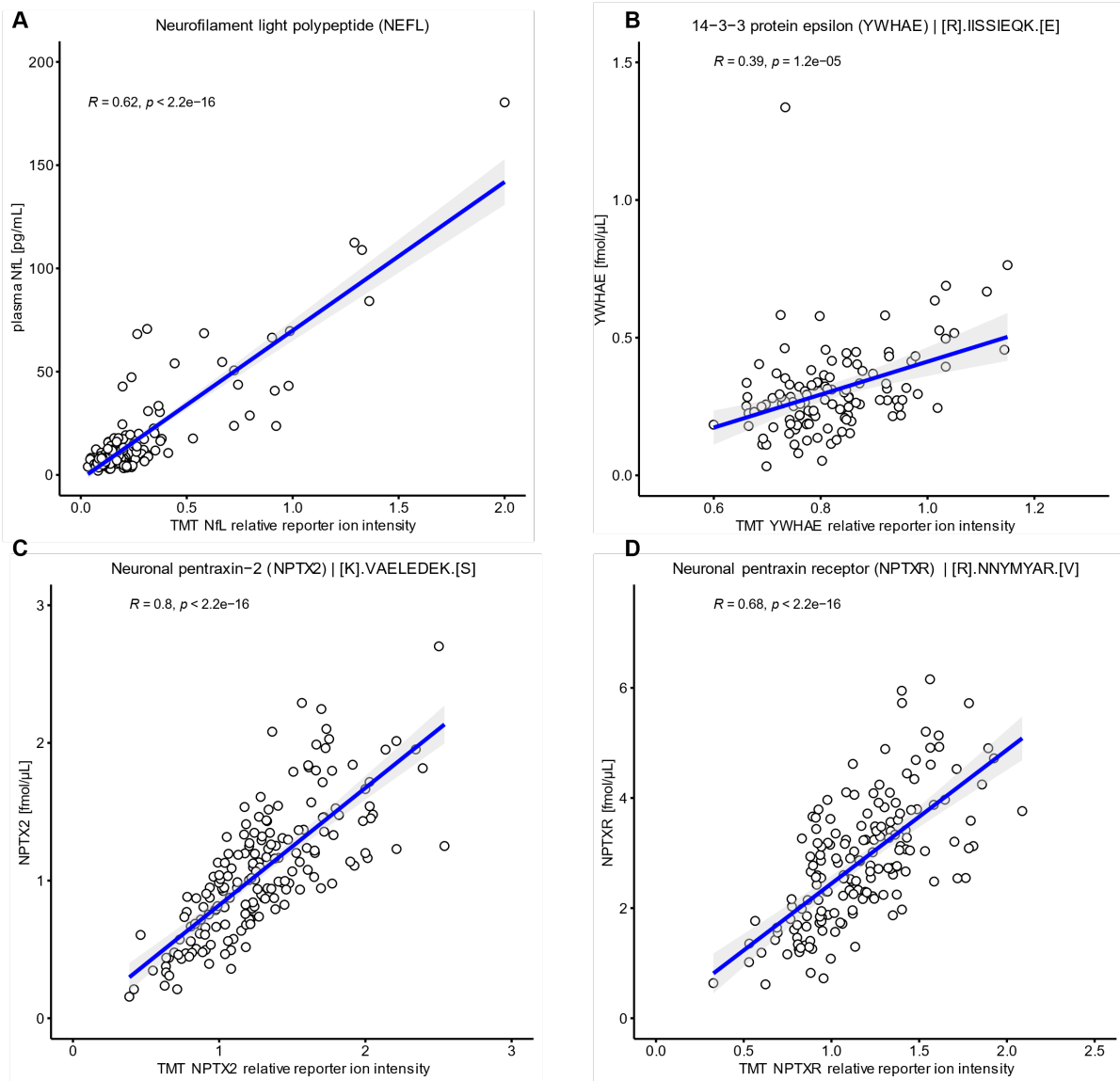
1394

1395 *Gene ontology analysis of WGCNA modules*

1396 Gene ontology (GO) analysis of WGCNA modules was conducted with g:Profiler, a web
1397 server for functional enrichment analysis (56). g:Profiler performs statistical
1398 overrepresentation analysis utilising cumulative hypergeometric probability, also known as
1399 Fisher's one-tailed test, to calculate the significance of functional terms in the input protein
1400 list. Calculated *P*-values represent the probability of randomly drawing *n* or more proteins in
1401 a subset of proteins (WGCNA modules) annotating to a specific GO term from the total
1402 number of proteins identified in the study. Multiple testing correction was performed with the
1403 method of Benjamini and Hochberg with a threshold of <0.05 to apply a less stringent
1404 approach for obtaining corrected *P*-values. GO results were then filtered to reduce
1405 redundancy and highlight driver terms, i.e. representative GO terms for a larger group of
1406 terms, as described in (56). Terms best representing the proteins in a respective module were
1407 chosen for module annotation.

1408

1409



1410

1411 **Figure S1.** Correlation between biomarkers when measured with TMT-based proteome-wide
 1412 quantification and targeted techniques. (A to D) Correlations between Neurofilament light
 1413 (A), 14-3-3 protein epsilon (B), Neuronal pentraxin-2 (C) and Neuronal pentraxin receptor
 1414 (D) abundances measured in the same samples with tandem mass tag (TMT)-based
 1415 quantification on the x-axis and single molecule array (Simoa) (A) or multiple reaction
 1416 monitoring (MRM)-based (B-D) quantification on the y-axis. All measurements except for
 1417 Simoa Neurofilament light, which was carried out in plasma, were made in cerebrospinal
 1418 fluid using mass spectrometric methods.

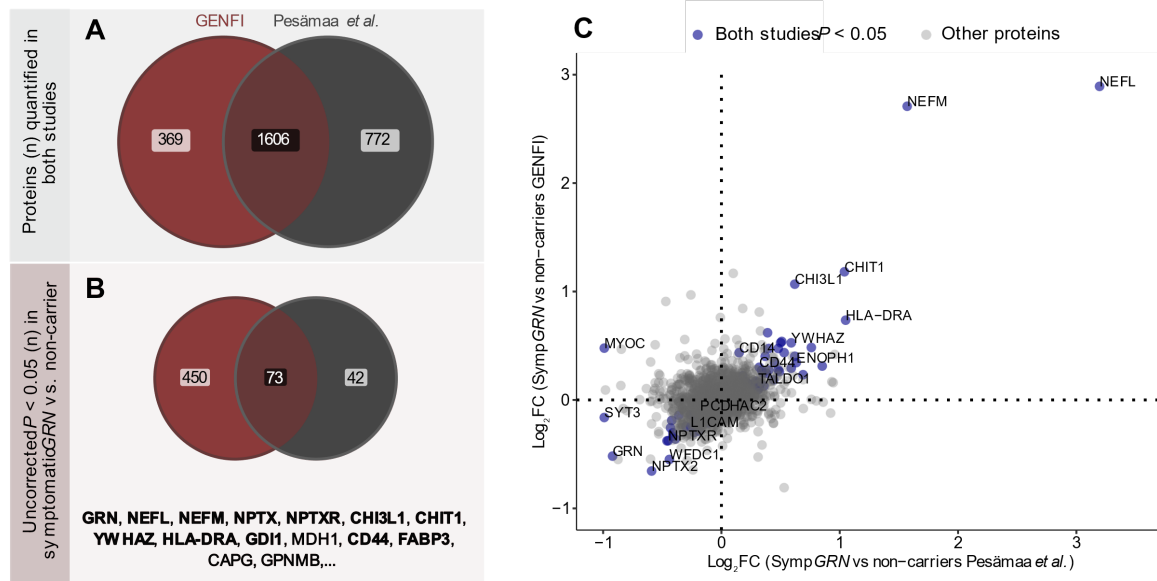


Figure S2. (A) Cross-cohort comparisons of CSF proteomic changes in symptomatic *GRN* carriers. Venn diagram showing the number of proteins quantified in the current study (red), a published label-free mass spectrometry dataset of symptomatic *GRN* carriers and non-carriers from the ALLFTD cohort (grey), with the number of proteins quantified in both studies being shown in grey/red. (B) Number of proteins significantly changed in unadjusted ANOVA analysis in the same studies. At the bottom of the panel, a selection of proteins changed in both studies are shown. Gene names highlighted in bold denote proteins with false discovery rate (FDR)-corrected *P*-values < 0.05 in linear regression analyses with age and sex as covariates in the GENFI cohort. (C) Correlation between log₂ fold changes between symptomatic *GRN* carriers of proteins in GENFI and ALLFTD cohorts (Spearman *R* = 0.87, *P* < 0.0001). Proteins with ANOVA *P*-values < 0.05 in both studies are shown in blue, whereas proteins not matching this criterion are shown in grey. Spearman correlation was performed in this subset of proteins. Abbreviations; GENetic Frontotemporal dementia Initiative, GENFI; European Medical Information Framework.

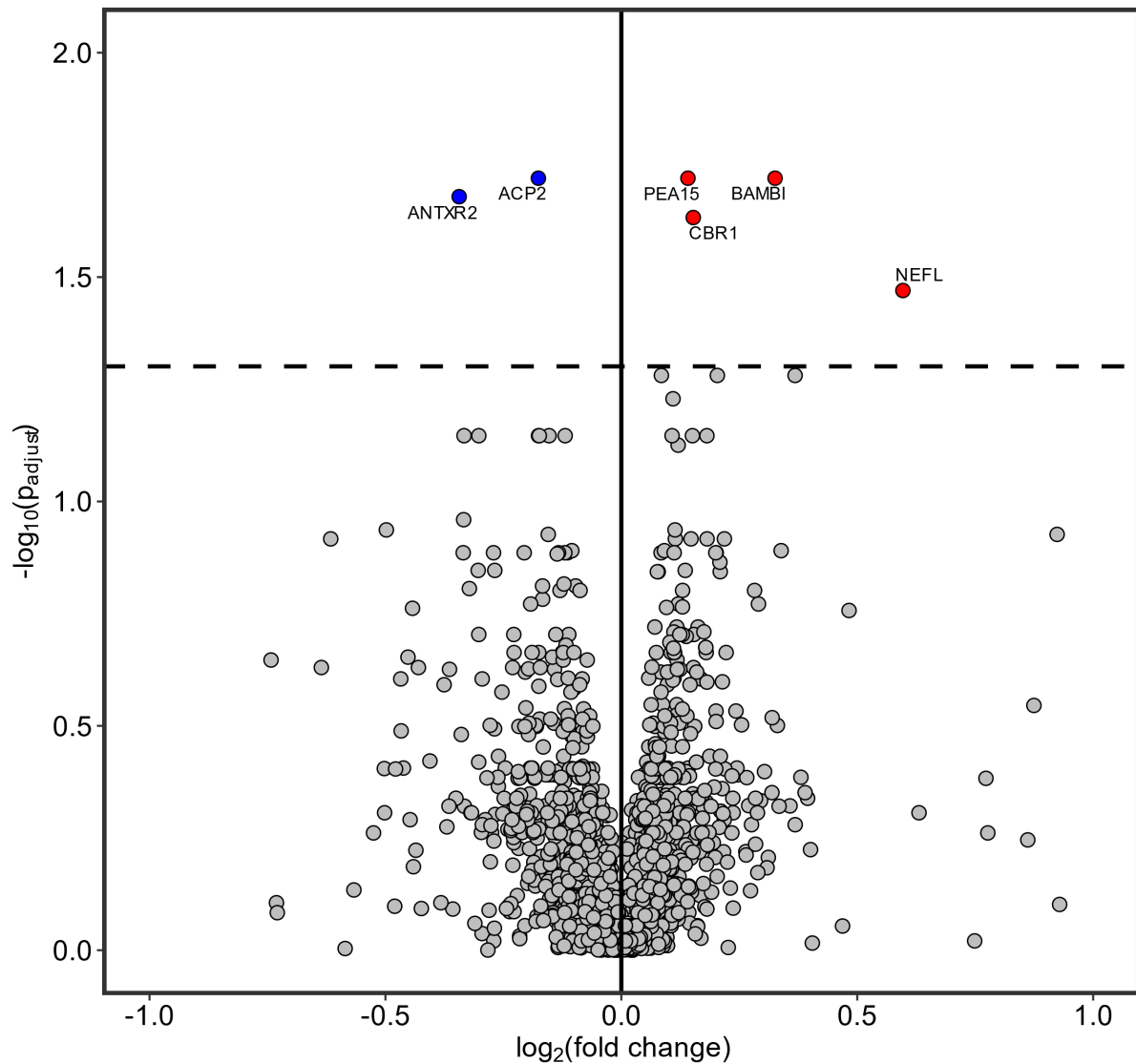


Figure S3. Volcano plot showing proteins changed in presymptomatic *MAPT* carriers vs. non-carriers. The volcano plot displays an overview of the altered proteins in presymptomatic *MAPT* mutation carriers when compared with non-carriers based on an analysis of covariance (ANCOVA) with age and sex as covariates. *P*-values were corrected for multiple testing according to the Benjamini-Hochberg method. *P*_{adjust} cut-off: 0.05. Abbreviations: neurofilament light, NEFL; ACP2, Acid Phosphatase 2, Lysosomal; PEA15, Astrocytic phosphoprotein PEA-15; ANTXR2, ANTXR Cell Adhesion Molecule 2; CBR1, Carbonyl reductase 1; BAMBI, BMP And Activin Membrane Bound Inhibitor.

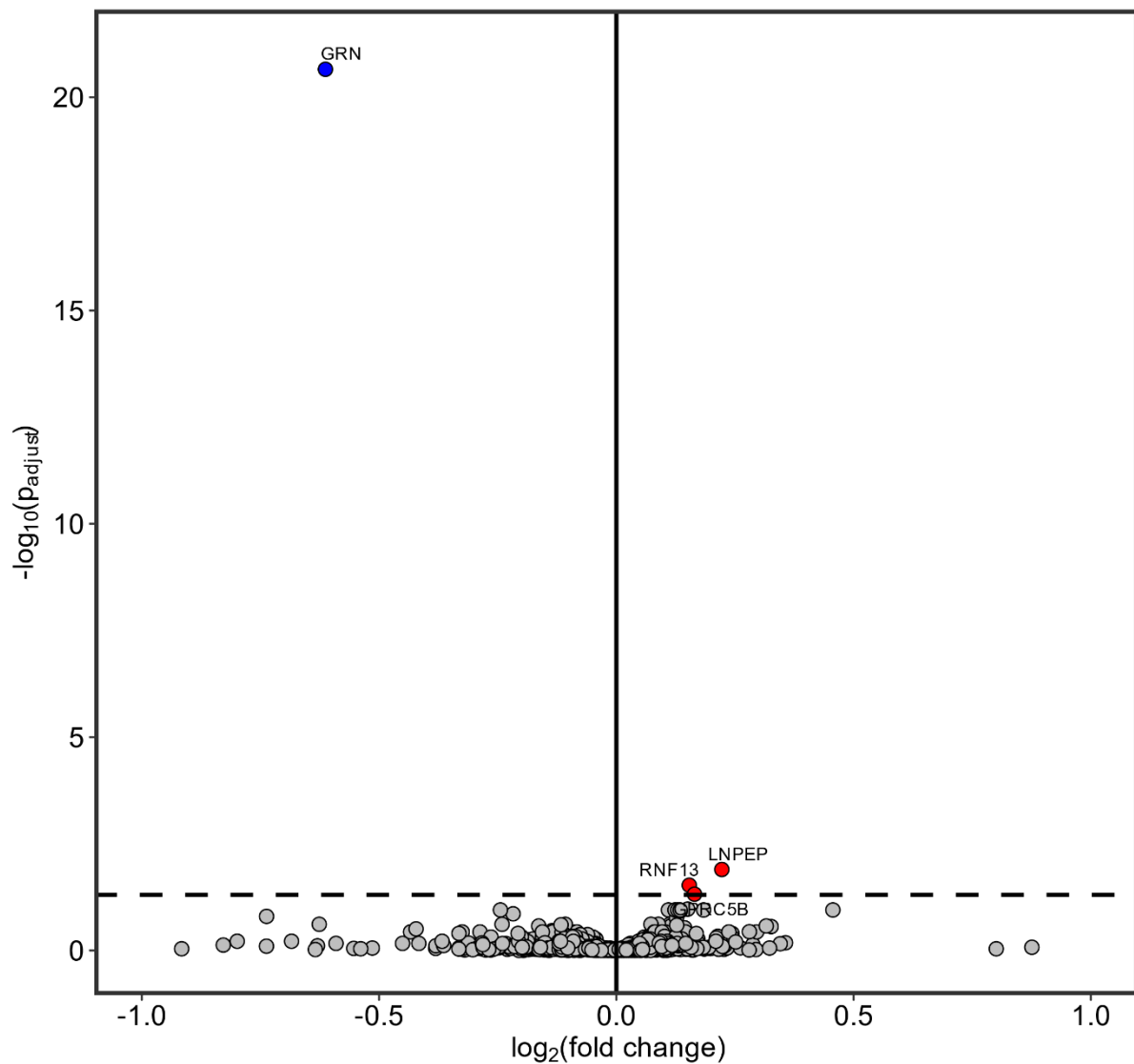


Figure S4. Volcano plot showing proteins changed in presymptomatic *GRN* carriers vs. non-carriers. The volcano plot displays an overview of the altered proteins in presymptomatic *GRN* mutation carriers when compared with non-carriers based on an analysis of covariance (ANCOVA) with age and sex as covariates. *P*-values were corrected for multiple testing according to the Benjamini-Hochberg method. P_{adjust} cut-off: 0.05. Abbreviations: Progranulin, GRN; LNPEP, Leucyl and Cystinyl Aminopeptidase; RNF13, Ring Finger Protein 13; GPRC5B, G Protein-Coupled Receptor Class C Group 5 Member B.

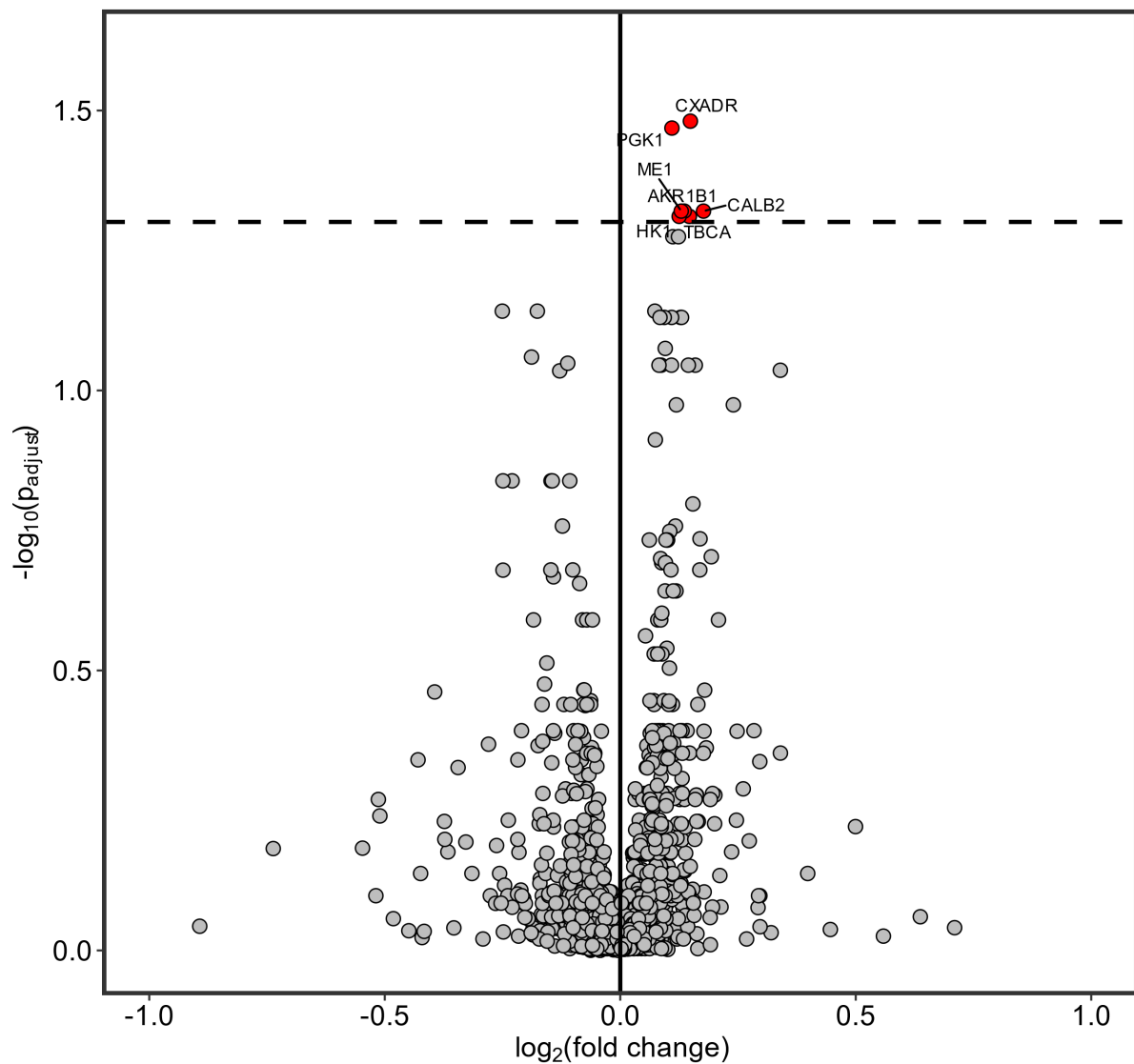


Figure S5. Volcano plot showing proteins changed in presymptomatic *C9orf72* carriers vs. non-carriers. The volcano plot displays an overview of the altered proteins in presymptomatic *C9orf72* mutation carriers when compared with non-carriers based on an analysis of covariance (ANCOVA) with age and sex as covariates *P*-values were corrected for multiple testing according to the Benjamini-Hochberg method. *P*_{adjust} cut-off: 0.05. Abbreviations: CXADR Ig-Like Cell Adhesion Molecule, CXADR; Phosphoglycerate Kinase 1, PGK1; Malic enzyme 1, ME1; Calretinin, CALB2; Aldo-keto reductase family 1, AKR1B1; Tubulin-specific chaperone A, TBCA; Hexokinase 1; HK1.

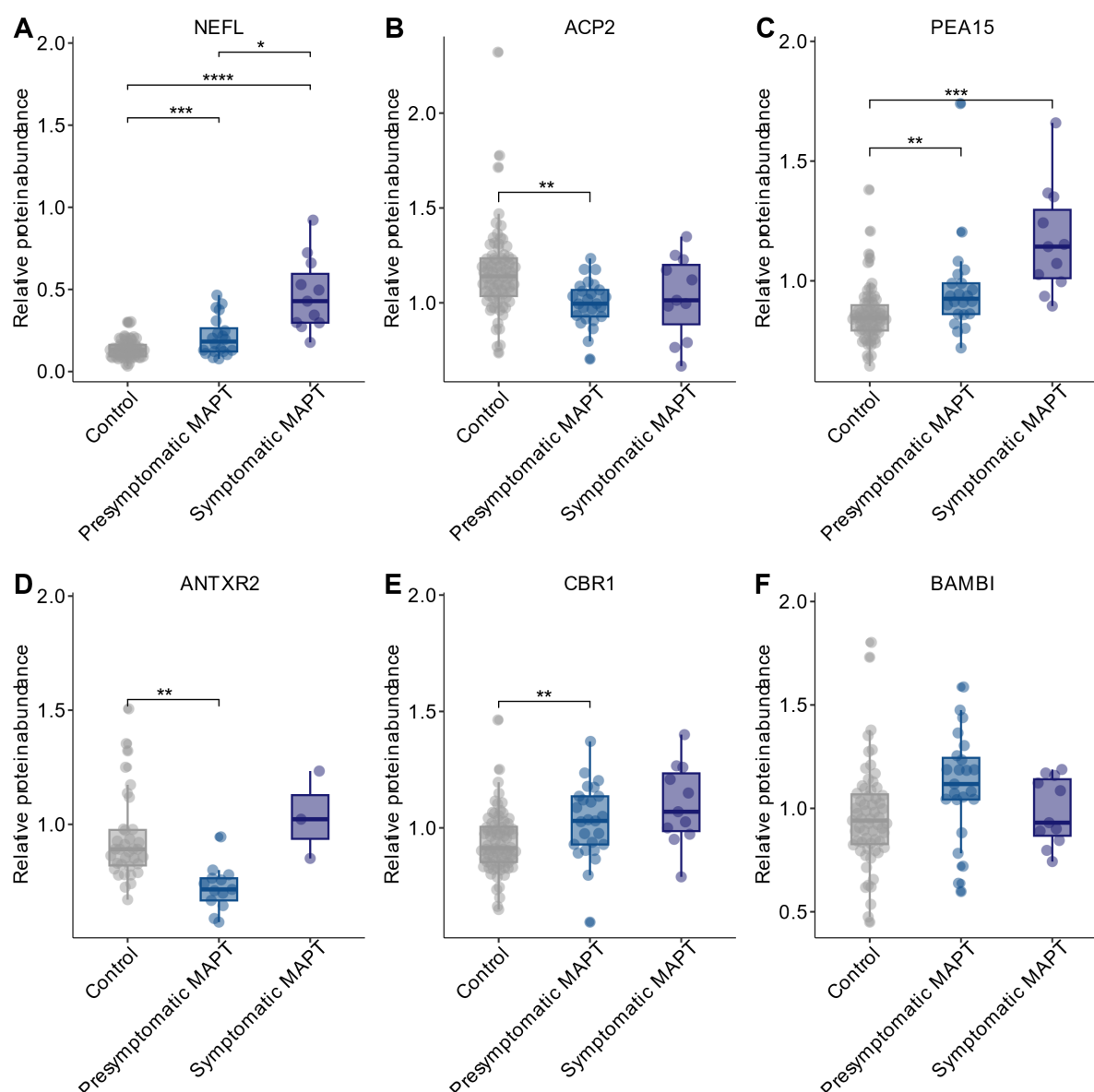


Figure S6. Proteins changed in presymptomatic *MAPT* carriers vs. non-carriers extracted from Figure S3. Overview of the altered proteins in presymptomatic *MAPT* mutation carriers when compared with controls based on an analysis of covariance (ANCOVA) with age and sex as covariates and post hoc Tukey's honest significant difference (HSD). (A) NEFL; (B) ACP2; (C) PEA15; (D) ANTXR2; (E) CBR1, and (F) BAMBI in non-carriers, presymptomatic and symptomatic *MAPT* carriers. Abbreviations: neurofilament light, NEFL; ACP2, Acid Phosphatase 2, Lysosomal; PEA15, Astrocytic phosphoprotein PEA-15; ANTXR2, ANTXR Cell Adhesion Molecule 2; CBR1, Carbonyl reductase 1; BAMBI, BMP And Activin Membrane Bound Inhibitor. * $p < 0.05$, ** $p < 0.01$, *** $p < 0.001$, **** $p < 0.0001$. Note: Non-significant comparison in tile F is due to the presence of outliers which were removed for analyses performed for Figure S3.

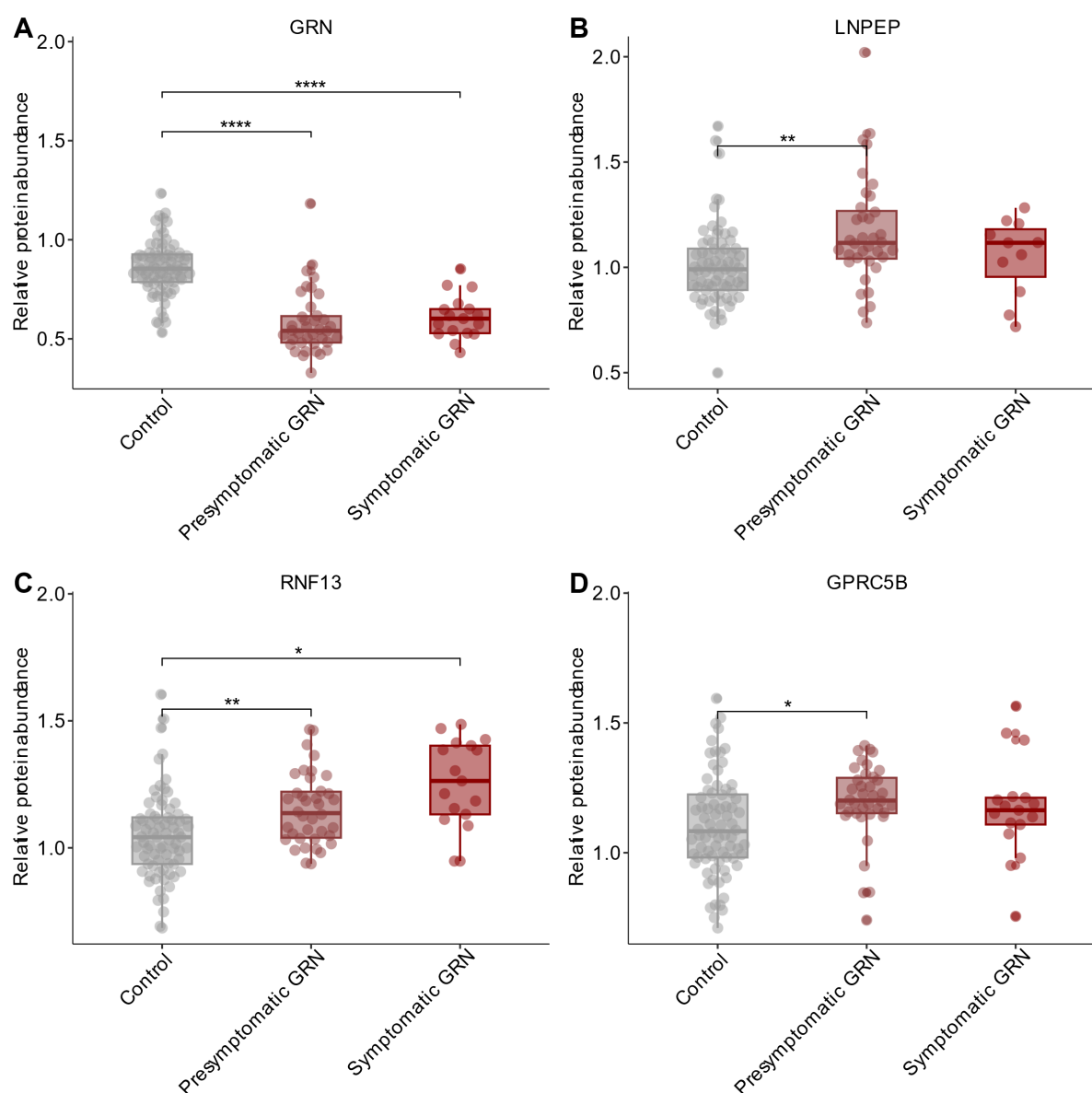


Figure S7. Proteins changed in presymptomatic *GRN* carriers vs. non-carriers extracted from Figure S4. Overview of the altered proteins in presymptomatic *GRN* mutation carriers when compared with controls based on an analysis of covariance (ANCOVA) with age and sex as covariates and post hoc Tukey's honest significant difference (HSD). Panels show (A) GRN, (B) LNPEP, (C) RNF13, and (D) GPRC5B in non-carriers, presymptomatic and symptomatic *GRN* carriers. Abbreviations: Progranulin, GRN; LNPEP, Leucyl and Cystinyl Aminopeptidase; RNF13, Ring Finger Protein 13; GPRC5B, G Protein-Coupled Receptor Class C Group 5 Member B. * $p < 0.05$, ** $p < 0.01$, *** $p < 0.001$, **** $p < 0.0001$.

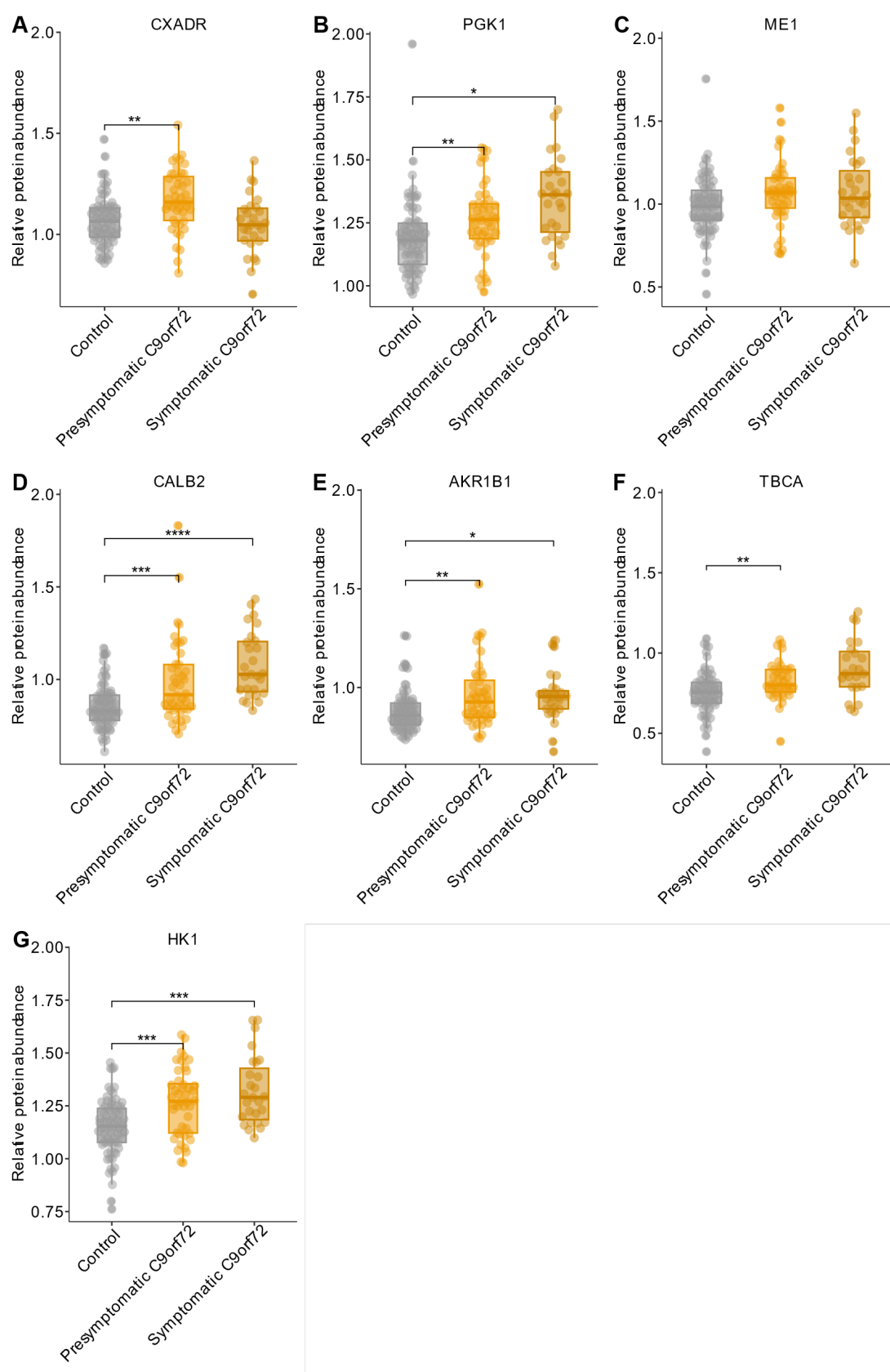
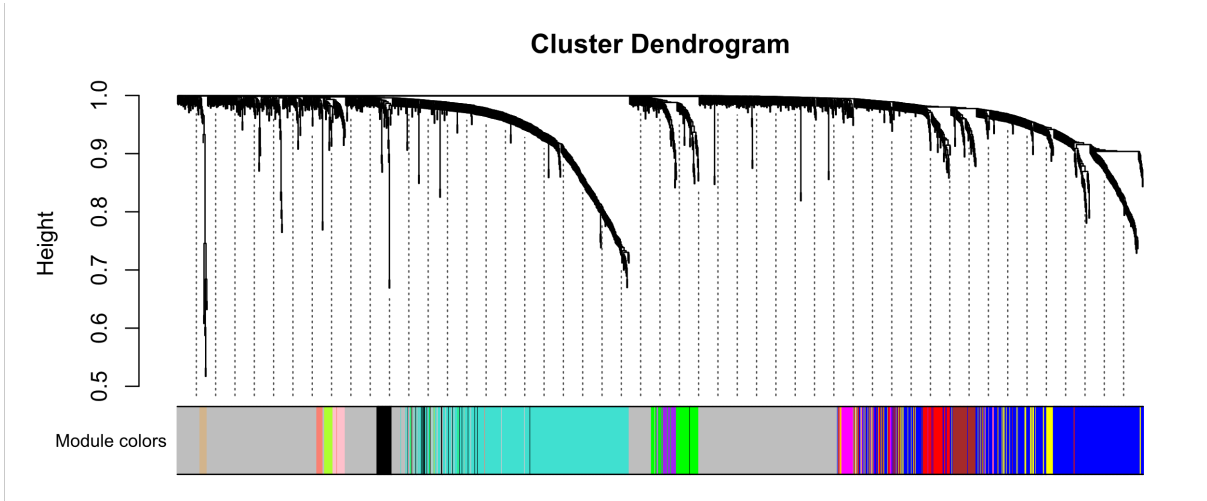


Figure S8. Proteins changed in presymptomatic *C9orf72* carriers vs. non-carriers extracted from Figure S5. Overview of the altered proteins in presymptomatic *C9orf72* mutation carriers when compared with controls based on an analysis of covariance (ANCOVA) with

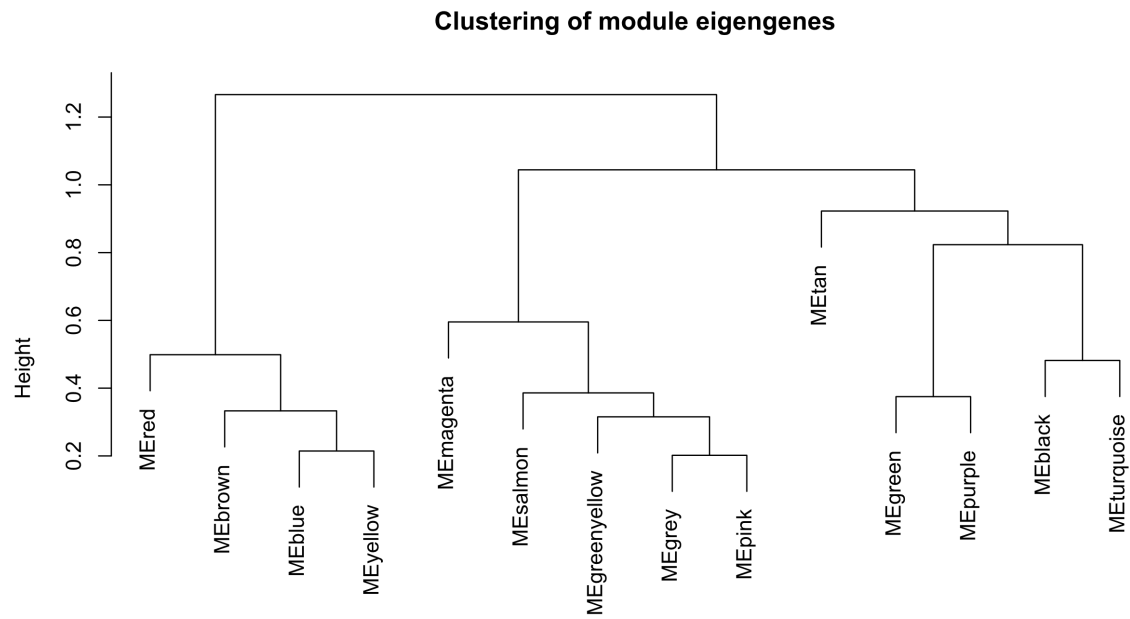
age and sex as covariates and post hoc Tukey's honest significant difference (HSD). Panels show (A) CXADR; (B) PGK1, (C) ME1, (D) CALB2, (E) AKR1B1, (F) TBCA and (G) HK1 in non-carriers, presymptomatic and symptomatic *C9orf72* carriers. Abbreviations: CXADR Ig-Like Cell Adhesion Molecule, CXADR; Phosphoglycerate Kinase 1, PGK1; Malic enzyme 1, ME1; Calretinin, CALB2; Aldo-keto reductase family 1, AKR1B1; Tubulin-specific chaperone A, TBCA; Hexokinase 1; HK1. * $p<0.05$, ** $p<0.01$, *** $p<0.001$, **** $p<0.0001$. Note: Non-significant comparison in tile C is due to the presence of outliers which were removed for analyses performed for Figure S5.

1537



1538

1539 **Figure S9.** Cluster dendrogram of the weighted gene co-expression network analysis
1540 (WGCNA). Cluster dendrogram and color representation of the network modules produced
1541 by average linkage hierarchical clustering of proteins based on their topological overlaps.
1542



1543

1544 **Figure S10.** Clustering of module Eigenproteins of the weighted gene co-expression network
 1545 analysis (WGCNA). Hierarchical clustering of module Eigenproteins identified in the
 1546 WGCNA.

1547

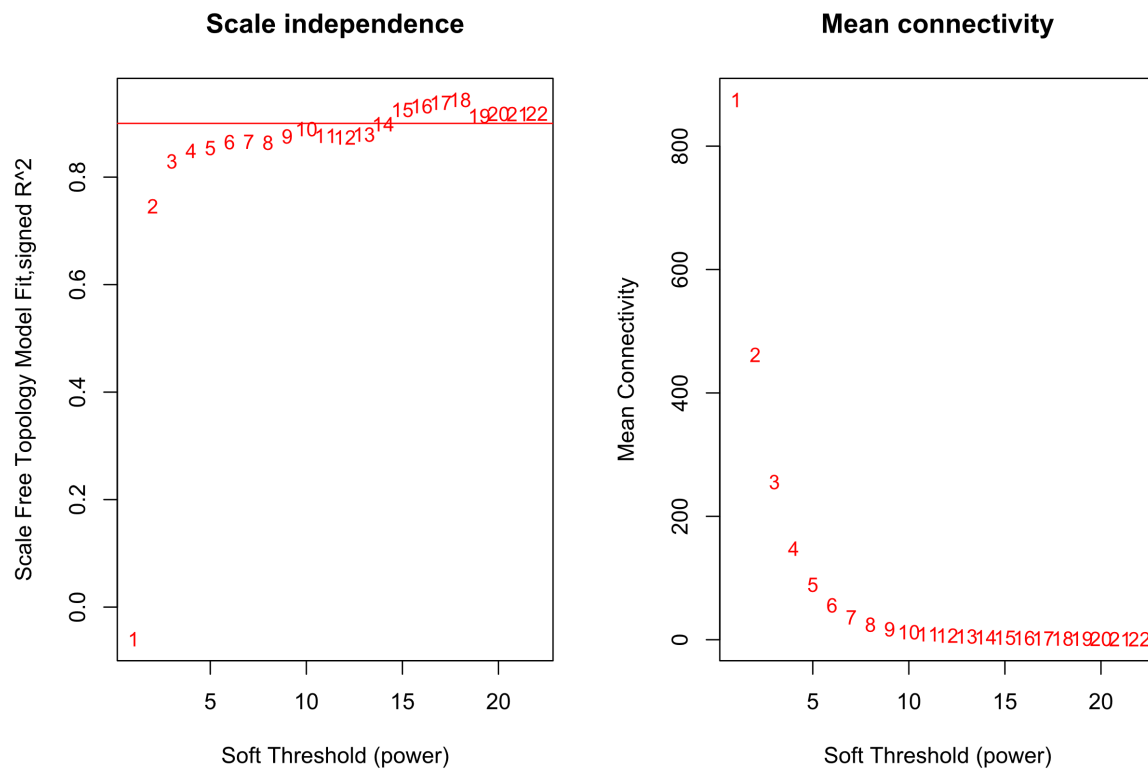


Figure S11. Determination of soft-threshold power in weighted gene co-expression network analysis (WGCNA). This figure shows the scale-free topology index (A) and mean connectivity (B) for each power value between 1 and 22. The R^2 cut-off was drawn at 0.875.

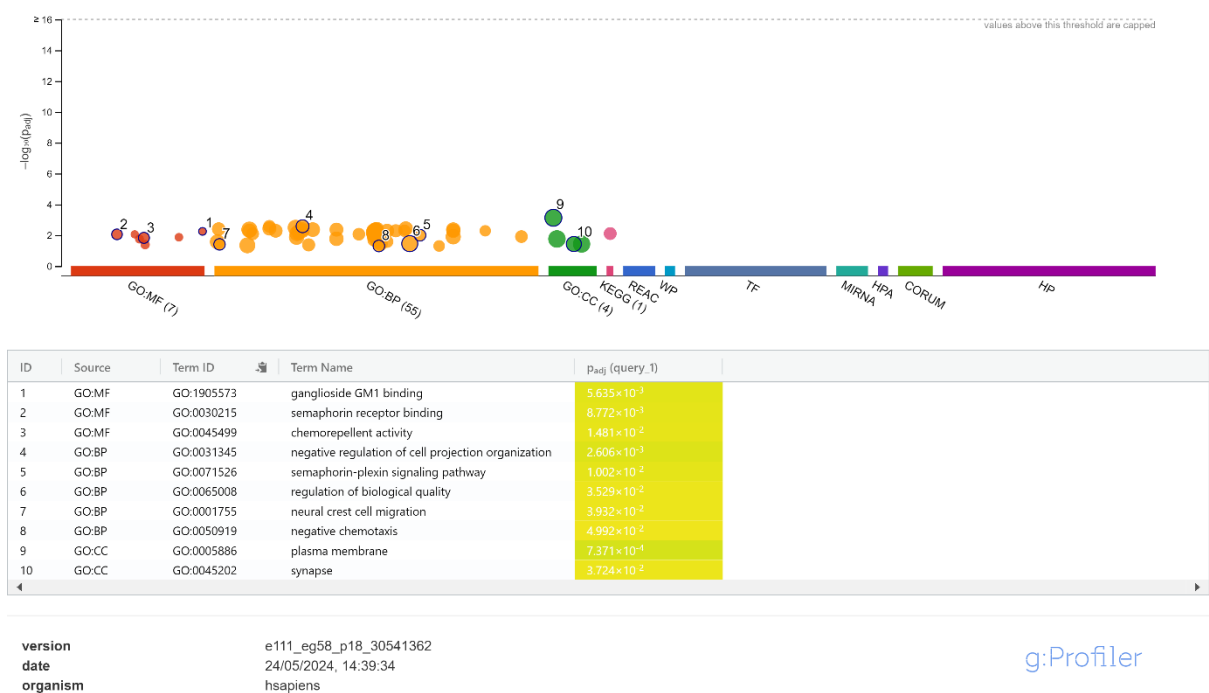


Figure S12. Gene ontology terms associated with the ‘Semaphorin signaling’ (red) module. Gene ontology (GO) analysis of WGCNA modules was conducted with g:Profiler, a web server for functional enrichment analysis. g:Profiler performs statistical overrepresentation analysis utilising cumulative hypergeometric probability, also known as Fisher’s one-tailed test, to calculate the significance of functional terms in the input protein list. Multiple testing correction was performed with the method of Benjamini and Hochberg with a threshold of <0.05 . The y-axis of the plot displays the negative decadic logarithm of the adjusted p -value while the x-axis highlights the category of all corresponding GO terms. GO results were then filtered to reduce redundancy and highlight driver terms, i.e. representative GO terms for a larger group of terms (displayed in the list below the plot).

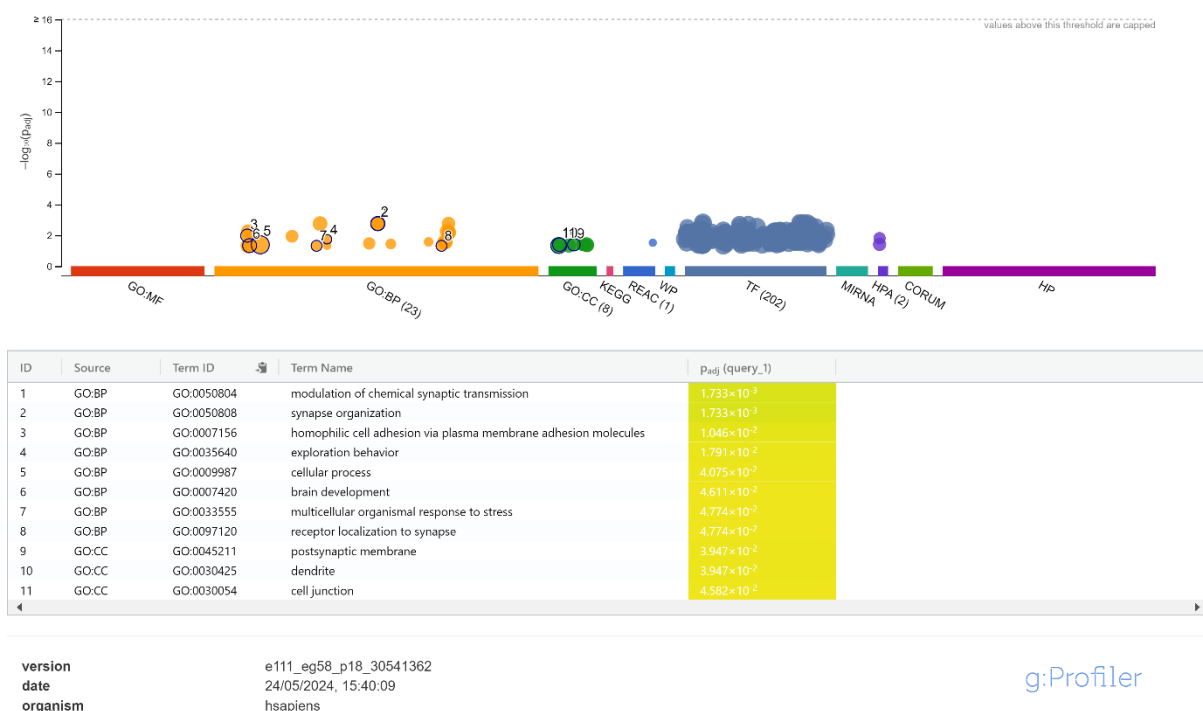


Figure S13. Gene ontology terms associated with the 'Synapse' (brown) module. Gene ontology (GO) analysis of WGCNA modules was conducted with g:Profiler, a web server for functional enrichment analysis. g:Profiler performs statistical overrepresentation analysis utilising cumulative hypergeometric probability, also known as Fisher's one-tailed test, to calculate the significance of functional terms in the input protein list. Multiple testing correction was performed with the method of Benjamini and Hochberg with a threshold of <0.05 . The y-axis of the plot displays the negative decadic logarithm of the adjusted p -value while the x-axis highlights the category of all corresponding GO terms. GO results were then filtered to reduce redundancy and highlight driver terms, i.e. representative GO terms for a larger group of terms (displayed in the list below the plot).

1577



1578

1579 **Figure S14.** Gene ontology terms associated with the ‘Neuronal development’ (blue) module.

1580 Gene ontology (GO) analysis of WGCNA modules was conducted with g:Profiler, a web
1581 server for functional enrichment analysis. g:Profiler performs statistical overrepresentation
1582 analysis utilising cumulative hypergeometric probability, also known as Fisher’s one-tailed
1583 test, to calculate the significance of functional terms in the input protein list. Multiple testing
1584 correction was performed with the method of Benjamini and Hochberg with a threshold of
1585 <0.05 . The y-axis of the plot displays the negative decadic logarithm of the adjusted p -value
1586 while the x-axis highlights the category of all corresponding GO terms. GO results were then
1587 filtered to reduce redundancy and highlight driver terms, i.e. representative GO terms for a
1588 larger group of terms (displayed in the list below the plot).

1589

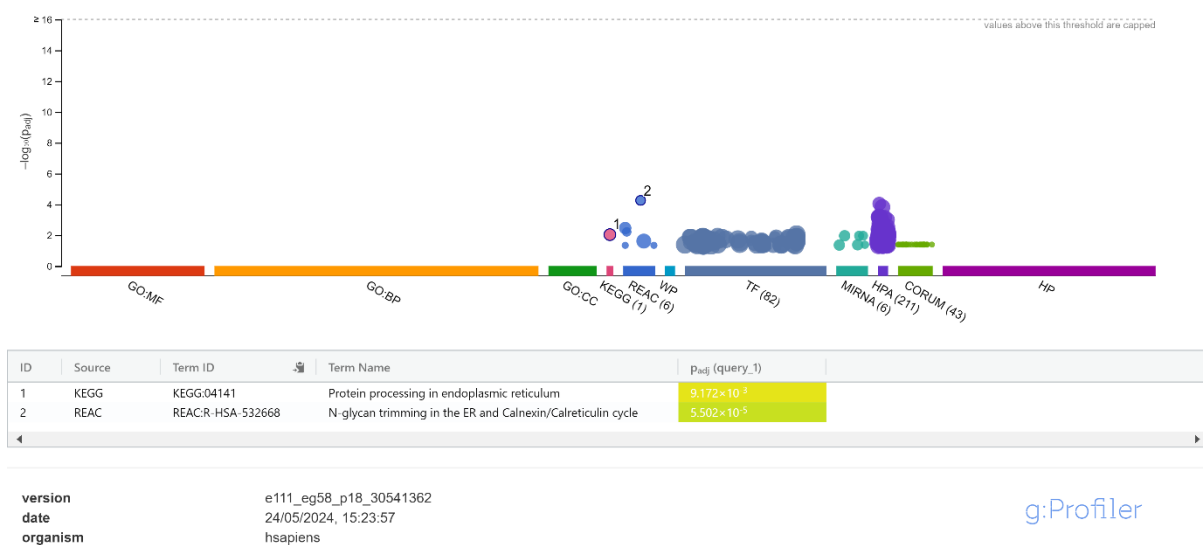


Figure S15. Gene ontology terms associated with the ‘Protein processing’ (yellow) module. Gene ontology (GO) analysis of WGCNA modules was conducted with g:Profiler, a web server for functional enrichment analysis. g:Profiler performs statistical overrepresentation analysis utilising cumulative hypergeometric probability, also known as Fisher’s one-tailed test, to calculate the significance of functional terms in the input protein list. Multiple testing correction was performed with the method of Benjamini and Hochberg with a threshold of <0.05 . The y-axis of the plot displays the negative decadic logarithm of the adjusted p -value while the x-axis highlights the category of all corresponding GO terms. GO results were then filtered to reduce redundancy and highlight driver terms, i.e. representative GO terms for a larger group of terms (displayed in the list below the plot).



Figure S16. Gene ontology terms associated with the ‘Core markers’ (greenyellow) module. Gene ontology (GO) analysis of WGCNA modules was conducted with g:Profiler, a web server for functional enrichment analysis. g:Profiler performs statistical overrepresentation analysis utilising cumulative hypergeometric probability, also known as Fisher’s one-tailed test, to calculate the significance of functional terms in the input protein list. Multiple testing correction was performed with the method of Benjamini and Hochberg with a threshold of <0.05 . The y-axis of the plot displays the negative decadic logarithm of the adjusted p -value while the x-axis highlights the category of all corresponding GO terms. GO results were then filtered to reduce redundancy and highlight driver terms, i.e. representative GO terms for a larger group of terms (displayed in the list below the plot).

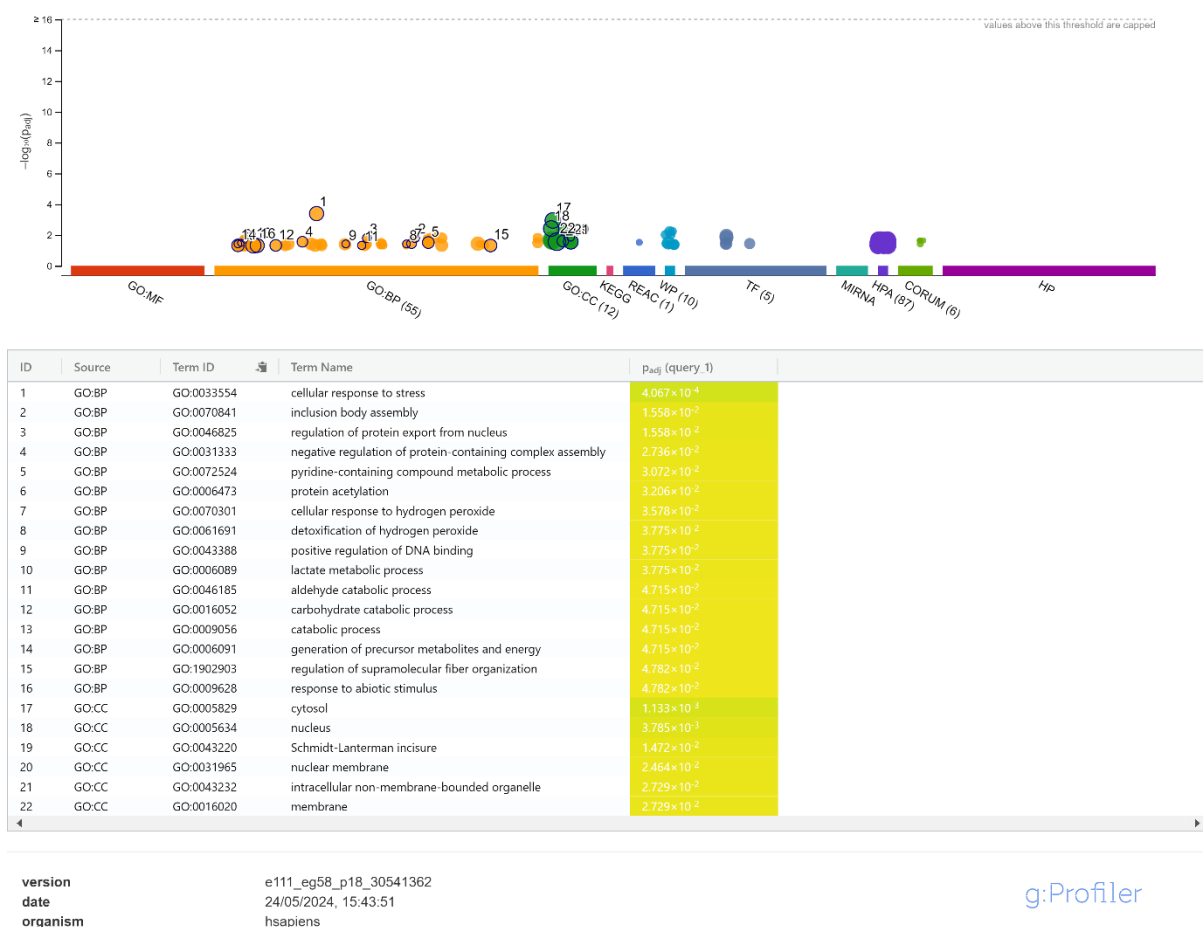


Figure S17. Gene ontology terms associated with the ‘Stress response’ (magenta) module. Gene ontology (GO) analysis of WGCNA modules was conducted with g:Profiler, a web server for functional enrichment analysis. g:Profiler performs statistical overrepresentation analysis utilising cumulative hypergeometric probability, also known as Fisher’s one-tailed test, to calculate the significance of functional terms in the input protein list. Multiple testing correction was performed with the method of Benjamini and Hochberg with a threshold of <0.05 . The y-axis of the plot displays the negative decadic logarithm of the adjusted p -value while the x-axis highlights the category of all corresponding GO terms. GO results were then filtered to reduce redundancy and highlight driver terms, i.e. representative GO terms for a larger group of terms (displayed in the list below the plot).

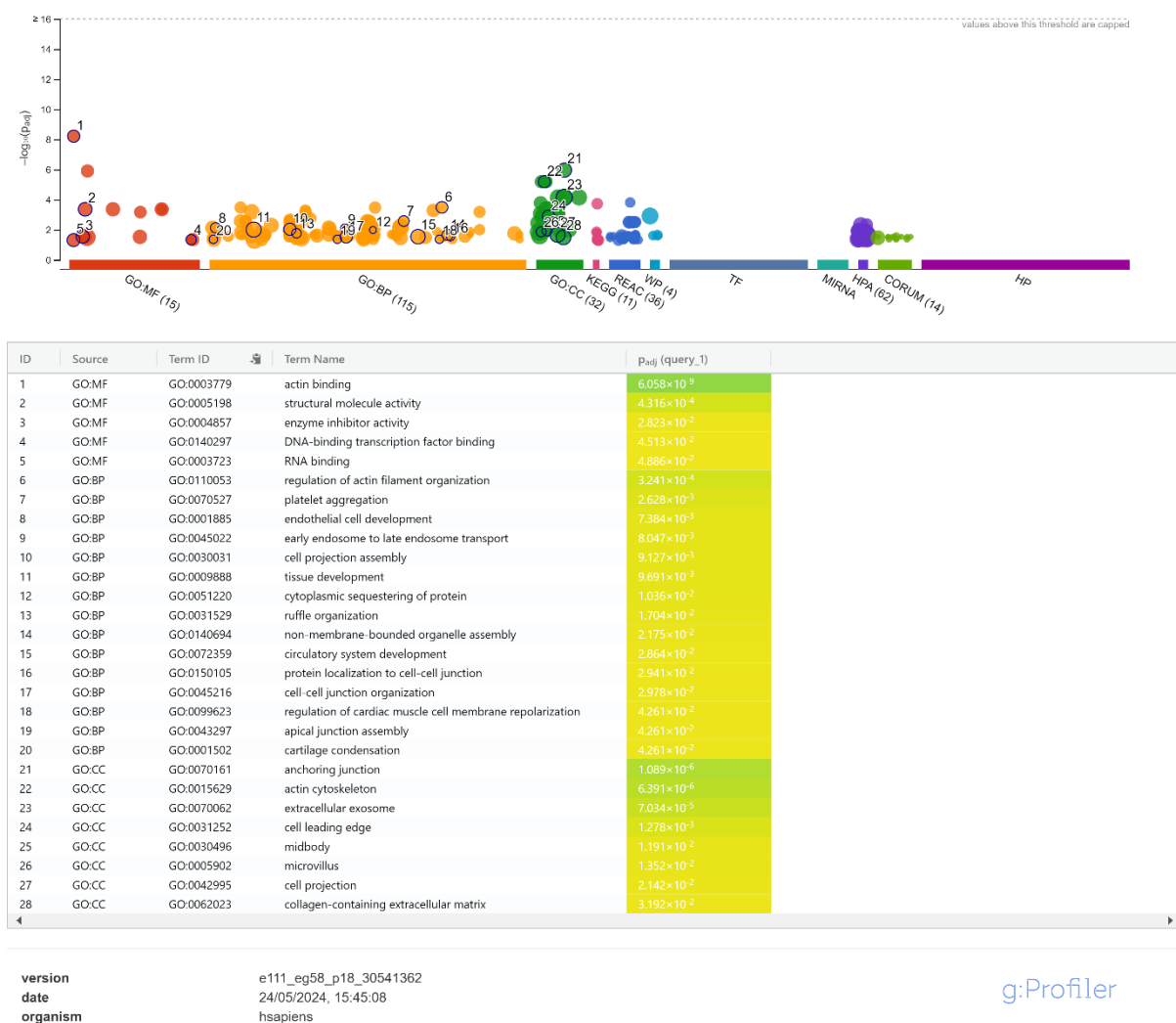


Figure S18. Gene ontology terms associated with the ‘Actin binding’ (pink) module. Gene ontology (GO) analysis of WGCNA modules was conducted with g:Profiler, a web server for functional enrichment analysis. g:Profiler performs statistical overrepresentation analysis utilising cumulative hypergeometric probability, also known as Fisher’s one-tailed test, to calculate the significance of functional terms in the input protein list. Multiple testing correction was performed with the method of Benjamini and Hochberg with a threshold of <0.05 . The y-axis of the plot displays the negative decadic logarithm of the adjusted p -value while the x-axis highlights the category of all corresponding GO terms. GO results were then filtered to reduce redundancy and highlight driver terms, i.e. representative GO terms for a larger group of terms (displayed in the list below the plot).



Figure S19. Gene ontology terms associated with the ‘GAG processing’ (salmon) module. Gene ontology (GO) analysis of WGCNA modules was conducted with g:Profiler, a web server for functional enrichment analysis. g:Profiler performs statistical overrepresentation analysis utilising cumulative hypergeometric probability, also known as Fisher’s one-tailed test, to calculate the significance of functional terms in the input protein list. Multiple testing correction was performed with the method of Benjamini and Hochberg with a threshold of <0.05 . The y-axis of the plot displays the negative decadic logarithm of the adjusted p -value while the x-axis highlights the category of all corresponding GO terms. GO results were then filtered to reduce redundancy and highlight driver terms, i.e. representative GO terms for a larger group of terms (displayed in the list below the plot).

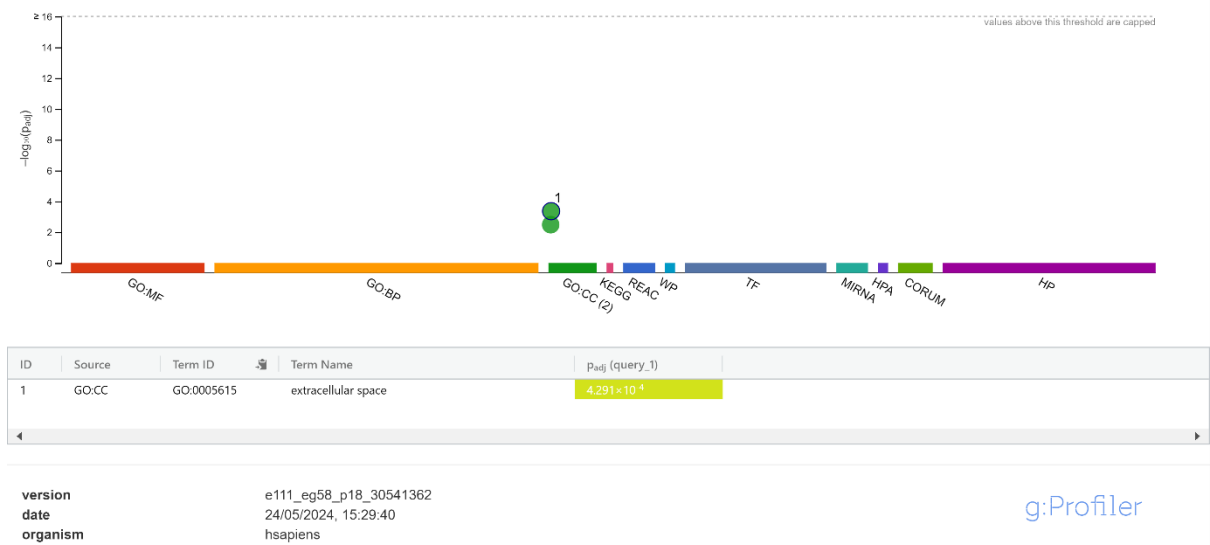


Figure S20. Gene ontology terms associated with the 'Extracellular matrix 1' (green) module. Gene ontology (GO) analysis of WGCNA modules was conducted with g:Profiler, a web server for functional enrichment analysis. g:Profiler performs statistical overrepresentation analysis utilising cumulative hypergeometric probability, also known as Fisher's one-tailed test, to calculate the significance of functional terms in the input protein list. Multiple testing correction was performed with the method of Benjamini and Hochberg with a threshold of <0.05 . The y-axis of the plot displays the negative decadic logarithm of the adjusted p -value while the x-axis highlights the category of all corresponding GO terms. GO results were then filtered to reduce redundancy and highlight driver terms, i.e. representative GO terms for a larger group of terms (displayed in the list below the plot).



Figure S21. Gene ontology terms associated with the ‘Lysosome’ (purple) module. Gene ontology (GO) analysis of WGCNA modules was conducted with g:Profiler, a web server for functional enrichment analysis. g:Profiler performs statistical overrepresentation analysis utilising cumulative hypergeometric probability, also known as Fisher’s one-tailed test, to calculate the significance of functional terms in the input protein list. Multiple testing correction was performed with the method of Benjamini and Hochberg with a threshold of <0.05 . The y-axis of the plot displays the negative decadic logarithm of the adjusted p -value while the x-axis highlights the category of all corresponding GO terms. GO results were then filtered to reduce redundancy and highlight driver terms, i.e. representative GO terms for a larger group of terms (displayed in the list below the plot).



Figure S22. Gene ontology terms associated with the ‘Extracellular matrix 2’ (black) module. Gene ontology (GO) analysis of WGCNA modules was conducted with g:Profiler, a web server for functional enrichment analysis. g:Profiler performs statistical overrepresentation analysis utilising cumulative hypergeometric probability, also known as Fisher’s one-tailed test, to calculate the significance of functional terms in the input protein list. Multiple testing correction was performed with the method of Benjamini and Hochberg with a threshold of <0.05 . The y-axis of the plot displays the negative decadic logarithm of the adjusted p -value while the x-axis highlights the category of all corresponding GO terms. GO results were then filtered to reduce redundancy and highlight driver terms, i.e. representative GO terms for a larger group of terms (displayed in the list below the plot).

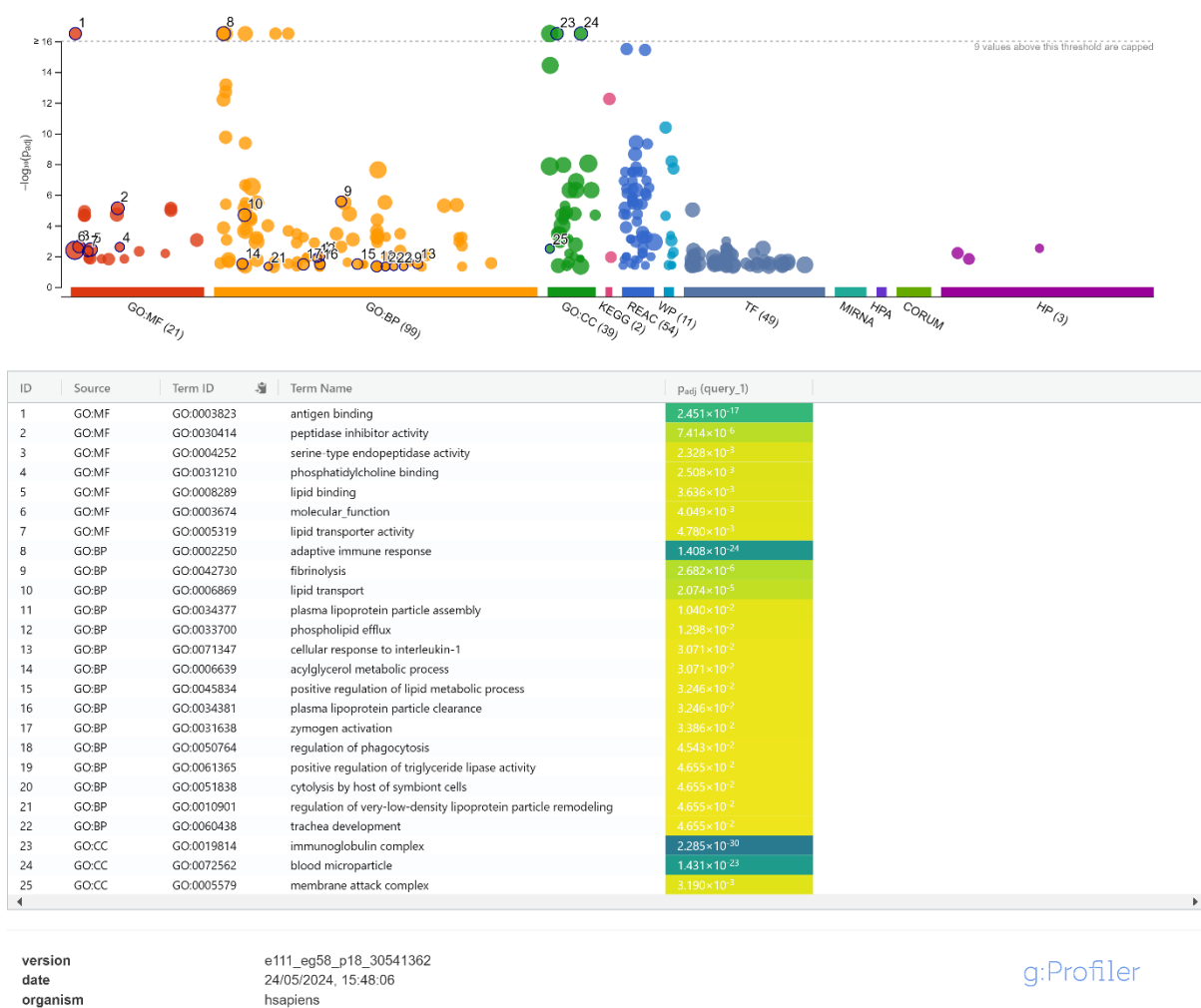


Figure S23. Gene ontology terms associated with the ‘Immune response’ (turquoise) module. Gene ontology (GO) analysis of WGCNA modules was conducted with g:Profiler, a web server for functional enrichment analysis. g:Profiler performs statistical overrepresentation analysis utilising cumulative hypergeometric probability, also known as Fisher’s one-tailed test, to calculate the significance of functional terms in the input protein list. Multiple testing correction was performed with the method of Benjamini and Hochberg with a threshold of <0.05 . The y-axis of the plot displays the negative decadic logarithm of the adjusted p -value while the x-axis highlights the category of all corresponding GO terms. GO results were then filtered to reduce redundancy and highlight driver terms, i.e. representative GO terms for a larger group of terms (displayed in the list below the plot).

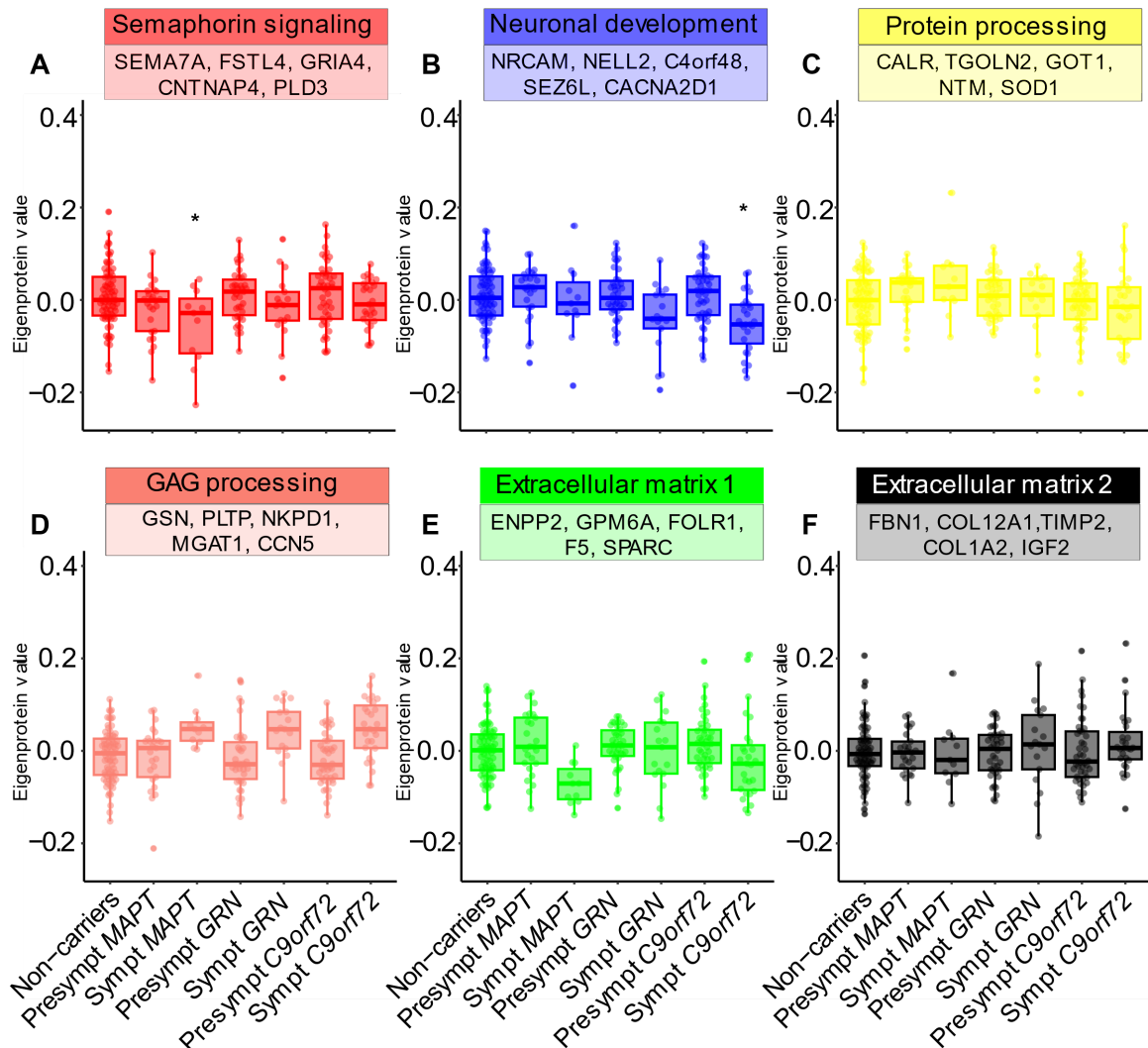


Figure S24. Remaining WGCNA modules that are not depicted in the main body of the manuscript. Eigenprotein values obtained through weighted gene co-expression network analysis (WGCNA), plotted across the continuum of controls as well as presymptomatic and symptomatic mutation carriers. The plots represent Eigenprotein values for (A) ‘Semaphorin signaling’, (B) ‘Neuronal development’, (C) ‘Protein processing’, (D) ‘GAG processing’, (E) ‘Extracellular matrix 1’, and (F) ‘Extracellular matrix 2’ modules. Hub proteins are displayed in boxes. $*P < 0.05$ compared with non-carriers.

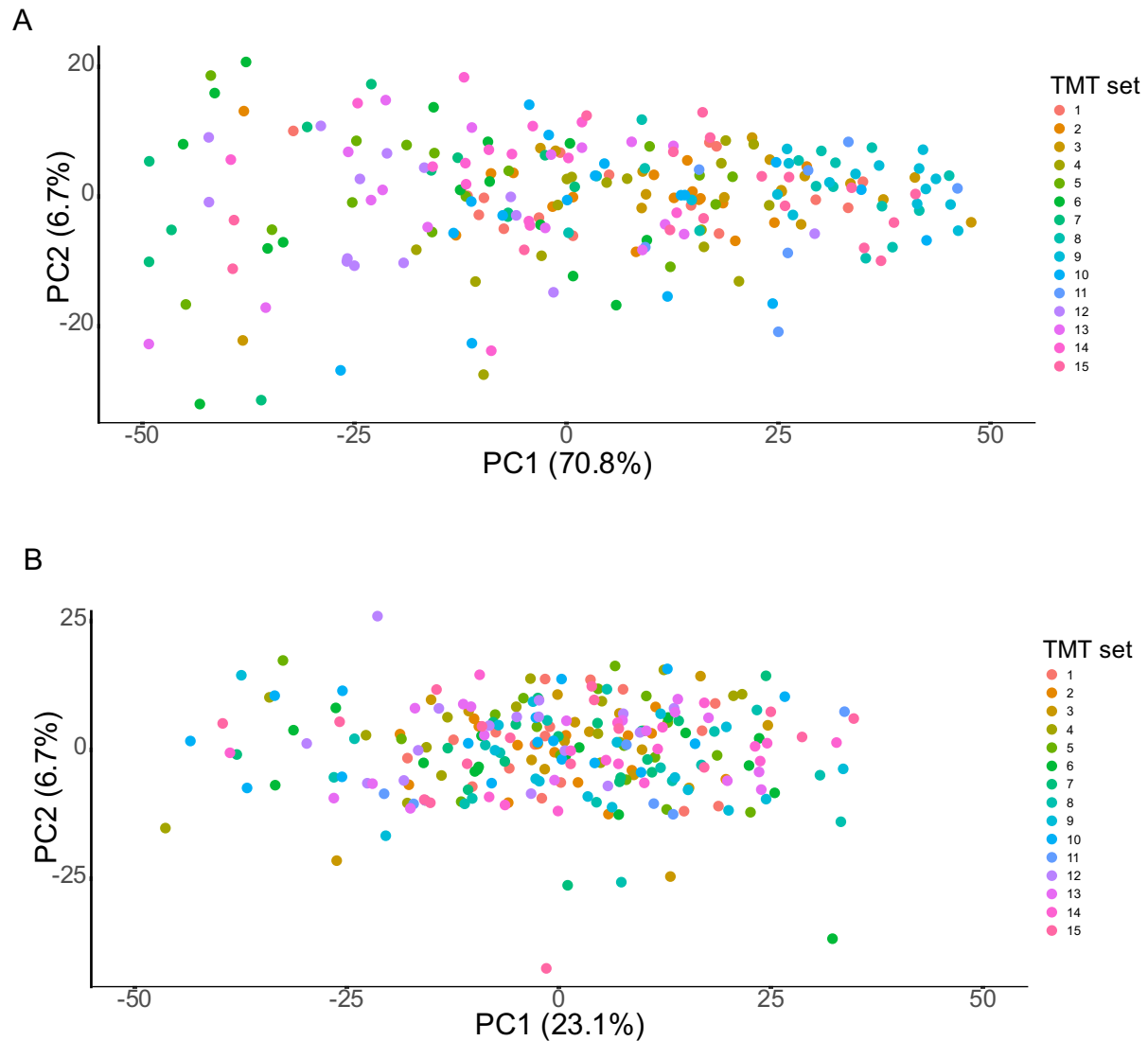


Figure S25. Evaluation of TMT batch effect and sample outliers prior to (A) and after normalization (B) via PCA. PCA was performed on all participants (n=238) of the GENFI cohort including proteins without missingness. (A) Before normalisation, inter-sample variance was high: Most samples separated along PC 1, which accounted for 70% of the total variance. Moreover, batches clustered together. (B) Upon normalisation, overall sample variance (PC1=23% and PC2=6%) and clustering of batches were reduced.